Effect of Corrosive Environment on Fatigue Behavior of Nickel - Based Alloys

By

Aezeden Omar Mohamed

A Thesis submitted to the Faculty of Graduate Studies of

The University of Manitoba

In partial fulfillment of the requirements of the degree of

Doctor of Philosophy

Department of Mechanical and Manufacturing Engineering

University of Manitoba

Winnipeg

Table of Contents

List of Figures

List of Tables

Abstract

Nickel based alloys have been developed as a material offering superior general and localized corrosion resistance compared to the more traditionally used in chemical and oil plant in the most aggressive environment such as hydrochloric acid and ferric chloride. Hence the addition of Cr and Mo to Ni creates alloys with exceptional corrosion resistance in a diverse range of environments. This study examines the roles of Cr and Mo in the corrosion behavior of Ni alloys. The performance of three nickel-base alloys IN600, IN601 and C22 was examined in increasing saline solution severity of sodium chloride, concentrated hydrochloric acid and ferric chloride solution at pH = 0.0. The passive corrosion and breakdown behavior of these alloys suggests that Cr is the primary element influencing general corrosion resistance, while the repassivation potential is strongly dependent on the Mo content. This indicates that Cr plays a strong role in maintaining the passivity of the alloy, while Mo acts to stabilize the passive film after a localized breakdown event.

Corrosion fatigue test results indicate that fatigue life of IN600, IN601 and C22 specimens tested in 3.5 % sodium chloride solution are essentially the same as for specimens tested in air. Test results also showed that for IN600, IN601 and C22 alloys, the number of cycles to failure was highest in air and sodium chloride solution, followed by specimens fatigued in hydrochloric acid, and was least in specimens fatigued in ferric chloride solution. No evidence of surface pitting was found on C22 specimens in all three solutions whereas IN600 and IN601 were both pitted. However, pits were generally larger in IN600 likely due to lower Cr content than in IN601.

Acknowledgments

I would like to express my sincere and heartfelt gratitude to my supervisor, Dr. J.R. Cahoon for his guidance and encouragement throughout this project. I wish also to express my thanks to my co advisor to Dr. W.F. Caley, and Dr. Dimos Polyzois and Dr. C. Ravindran the examiners for their valuable feedback.

I would like to thank all members of my family for their support and encouragements. Special thanks go to my mother and father for their patience, understanding and support during the course of this work. Finally, I'm grateful for the financial support provided by the University of Manitoba.

1 Introduction

Nickel-based alloys can be used in a wide variety of corrosive media and the amount of Cr and Mo present in these alloys has a significant effect on their corrosion properties [1-4]. The current study was undertaken to determine the effect of the Cr and Mo content on the corrosive and corrosion fatigue behavior of three nickel-based alloys, IN600, IN601 and C22. The corrosive environments were 3.5%NaCl solution, concentrated HCl and 10%$FeCl_3$ solution. The addition of Cr to Ni-based alloys changes the nature of the surface from nickel oxide to a more corrosive resistant one comprised largely of chromium oxide thus reducing the corrosion rate. The addition of Mo to nickel-based chromium alloys increases the corrosion resistance and often increases the resistance to pitting and crevice corrosion. The three alloys have similar yield and ultimate tensile strengths [3,4].

Fatigue crack initiation in corrosive media has generally been attributed to various factors such as pitting corrosion sites. More corrosion fatigue enhanced deformation was proposed to explain the apparent intensification of intrusions and extrusions in materials [1-6]. These mechanisms and their interaction with fundamental fatigue processes have recently become of interest to many researchers since little actually is known about the fundamentals of environment/cyclic loading interactions.

Fatigue is the time-dependent growth of subcritical cracks under cyclic (repeated) loading [6]. Fatigue cracking is one of the most common causes of failure of engineering structures and is often undetected, unexpected and could be catastrophic. Considerable engineering efforts over the past century have been devoted to the characterization and understanding of the mechanisms of fatigue. Such understanding is essential to service

life prediction, planning of in-service inspections, development of better fatigue resistant materials, better component design, improved manufacturing processes, and optimum material selection. Fatigue failures have been the subject of engineering studies for more than 150 years [7].

Simultaneous exposure of metals and alloys to aggressive environments and cyclic stresses often results in a degradation of fatigue resistance. Even laboratory air containing some moisture has been shown to influence crack propagation rates of materials when compared with those obtained from tests in vacuum or in dehumidified inert gases. Measures to avoid such corrosion cracking include careful materials selection, heat treatment, and modifications of material/environment interactions through coating, controlled solution chemistry, inhibition, and applied potentials. This is of extreme importance in several industries such as aerospace and power generation.

Extensive studies are necessary to characterize the corrosion fatigue of materials in aqueous environments. Corrosion studies alone have proven that the interaction of materials in different environments is complex and sometimes confusing. The process of corrosion fatigue is even more complex since there are at a least twenty five mechanical, environmental and metallurgical variables that contribute to the process of corrosion fatigue [8]. Many mechanisms have been proposed in the literature based primarily on the individual roles of anodic dissolution and of hydrogen embrittlement. Complexity is further increased when hydrogen embrittlement and dissolution mechanisms operate in parallel. Separation of these two mechanisms in some systems is almost impossible. This frustrates attempts to develop a reasonable understanding of the individual contributions of each mechanism to the corrosion fatigue cracking process.

Electrochemical polarization studies provide a rapid method for predicting the corrosion behavior of metals and alloys in various corrosive aqueous solutions. Such studies can predict long-term corrosion rates and tendencies towards crevice and pitting corrosion in any particular aqueous environment. It is not the intent of the present research to examine in detail the exact fracture mechanisms involved in the corrosion fatigue of the alloys studied or to determine which of the twenty five or so mechanisms may be operative. Rather, the purpose of the research is to determine the overall effect of electrochemical polarization behavior on the corrosion fatigue lives of three high strength and corrosion resistant alloys. The information presented in this research can then be utilized in future investigations to examine the exact fracture mechanisms in greater detail.

The objectives of this study are as follows:

1. To relate the electrochemical behavior of an alloy in a particular corrosive environment to its corrosion fatigue behavior in that environment;
2. To determine the tendency of an alloy to degrade due to crevice and pitting corrosion in a particular environment and to determine the effect of such tendencies on corrosion fatigue in that environment.
3. To determine the effect of alloy composition on the corrosion behavior of each alloy on its electrochemical behavior in various corrosive environments and thus on its high cycle corrosion fatigue characteristics in these environments.

The results of this study should prove valuable in providing a better understanding of the nature of corrosion fatigue and in developing techniques for improving the resistance of alloys to catastrophic corrosion fatigue failure.

2 Literature Review

Corrosion fatigue is defined as the reduction in fatigue strength of a material due to the presence of a corrosive medium [1]. Therefore, the effects of corrosion and fatigue will be addressed both individually and together.

2.1 Fatigue

Fatigue is defined as "The process of progressive localized permanent structural changes occurring in a material subjected to conditions which produce fluctuating stresses and strains at some point or points and which may culminate in cracks or complete fracture after a sufficient number of fluctuations" [2]. A requirement of fatigue is that the cyclic stresses have a tensile component. Fatigue can be viewed as a three-stage process involving crack initiation, crack propagation and final fracture. Initiation is defined by localized microscopic changes usually on the material surface that produce a crack of sufficient size to act as a stress raiser. The second stage corresponds to the portion of the cyclic lifetime involving growth of the crack to a macroscopic critical size at which time, the third stage rapid catastrophic failure, occurs.

2.1.1 Low Cycle Fatigue

Where significant plastic straining occurs, low-cycle fatigue involves large stress magnitudes with significant amounts of plastic deformation and relatively short life ($N<10^4$ cycles). The analytical procedure used to address strain-controlled fatigue is commonly referred to as the Strain-Life. Low cycle fatigue tests are conducted with controlled cycles of elastic plus plastic strain instead of controlled load or stress cycles [3].

2.1.2 High Cycle Fatigue

High cycle fatigue is usually associated with lower loads than low cycle fatigue, and longer life, generally greater than 10^4 cycles. High cycle fatigue is characterized by stress cycles to fracture (S-N) curve. High cycle fatigue failures almost always initiate on a free surface and therefore surface corrosion will likely affect the fatigue life of the material [3].

2.1.3 Effect of Slip

It is widely believed in the fatigue literature that the variation of the fundamental threshold curves of some materials is dependent on the mode of slip deformation, i.e., wavy or planar slip [4]. The perception in the literature is that planar slip materials have always shown higher fatigue resistance than the wavy slip materials [5]. This perception has been based on the observation of a more tortuous crack path and more cracks branching in the case of planar slip alloys which reduce the load value. A common example in the literature is the behavior of precipitation-hardened aluminum 7075 alloy. The microstructure of this alloy is greatly influenced by the ageing conditions and yet the Young's modulus remains almost unchanged. When fundamental threshold curves in air for the underaged (planar slip) and overage (wavy slip) microstructures are compared, the threshold curve of the underaged alloy is always above that of the overaged alloy [6].

Strain hardening during uniaxial tensile deformation of several alloys has been investigated previously [7-9]. Results have been interpreted in terms of the evolution of dislocation structure. The consequences of slip evolution in the amount of strain hardening have not been taken into consideration. Slip within an individual grain of a nickel-base alloy meets several constraints from the neighboring grains. Incompatible

deformations of neighboring grains must be accommodated by elastic or plastic deformation in order to ensure strain hardening continuity [8-13].

Slip bands are very common features in cyclically deformed solid solutions of aluminum, copper and iron alloys [14-17]. The formation of slip bands in these alloys has been attributed to their low stacking-fault energy which leads to the formation of wider extended dislocations, with reduced ability of screw dislocations cross-banding onto other band planes. However, several authors [18-21] have demonstrated that reduced stacking-fault energy may not be the reason for the manifestation of deformation as slip banding in some solid solutions. They have suggested that carbon content plays a decisive role in determining the nature of banding in nickel alloys [22] and other precipitation hardened alloys. The precipitate phases that are in the matrix such that are coherent or semi-coherent can be cut by moving dislocations [23]. Normally, precipitation-hardened alloys show wavy banding in a way similar to that exhibited by single-phase alloys with high stacking-fault energy. It has been suggested that the formation of slip bands is the major factor causing crack nucleation as well as premature failure in nickel-base alloys. Studies on cyclic deformation of IN718 showed slip band shear the precipitates during cyclic deformation followed by the propagation of slip bands [24]. Also, sets of groups of deformation bands were observed during cyclic deformation [25].

2.1.4 Effect of Surface Finish on Fatigue Life

Fatigue failure generally initiates at the surface and since the maximum stress often occurs at the surface, particularly for bending and torsional loadings, it is logical that failure should start there. In axial loading the fatigue failure nearly always begins at the

surface as well, likely due to surface abnormalities. There is evidence that fatigue properties are very sensitive to surface condition. Factors which affect conditions surface of a fatigue specimen [26] can be divided roughly into three categories; 1) surface roughness or stress raisers at the surface; 2) changes in the fatigue strength of the surface metal; and, 3) changes in the residual stress condition of the surface. It has been recognized that surface finishes produced by different machining procedures can appreciably affect fatigue performance. Figure 2.1 and Figure 2.2 show the influence of various surface finishes on steel in reducing the fatigue limit of carefully polished material [26]. The surface finish is characterized by the process used to form the surface. The extreme sensitivity of high strength steel to surface condition is well illustrated. Further corrosion would cause a deterioration of the surface finish and ultimately lead to reduce the fatigue life of the material.

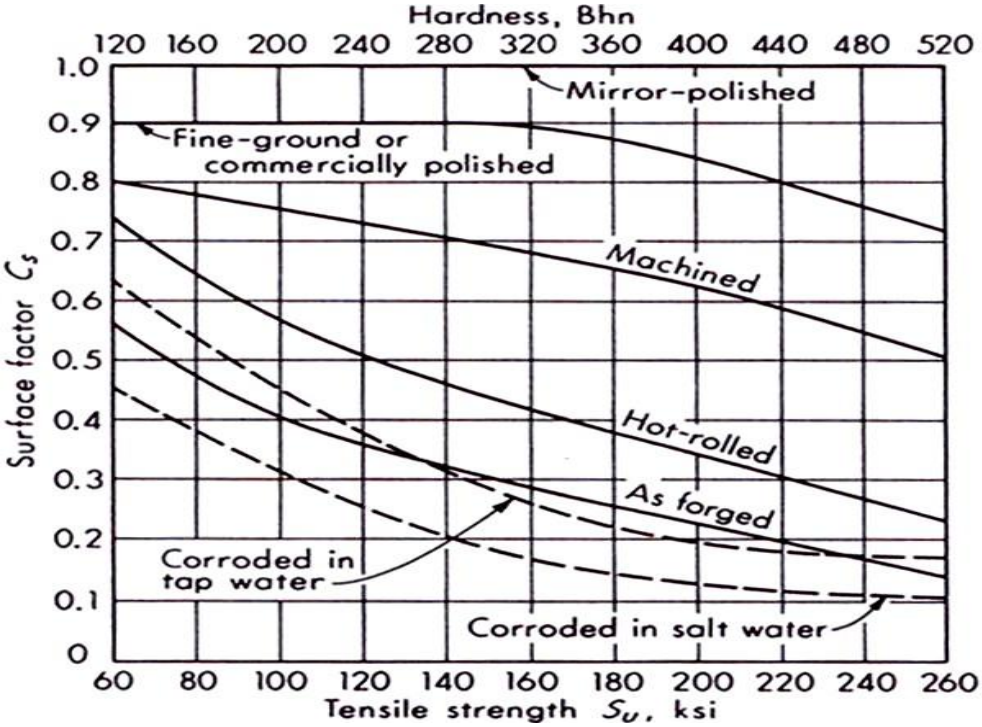

Figure 2.1 Surface factor for fatigue limit of steel due to various surface treatments [26]

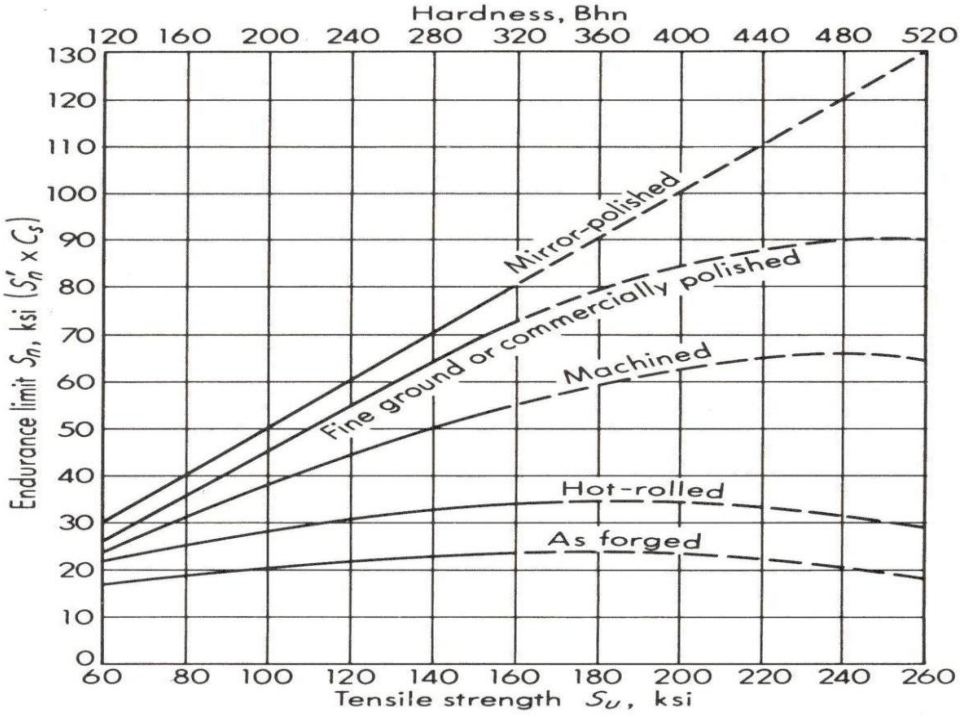

Figure 2.2 Effect of surface finish on endurance limit values for steels [26]

2.2 Corrosion

2.2.1 Electrochemistry of Corrosion

Marcel Pourbaix demonstrated that material could react in one of three ways when exposed to an aqueous corrosive medium; these are immunity, corrosion, and passivity [27]. By varying the electrode potential of the material and the pH of the corrosive medium he designed diagrams to demonstrate the corrosive activity thermodynamically favored for given values of potential and pH. These are now known as Pourbaix diagrams and one for Ni is shown in Figure 2.3. A Pourbaix diagram is divided into areas that predict the three ways a metal will react to a corrosive aqueous medium.

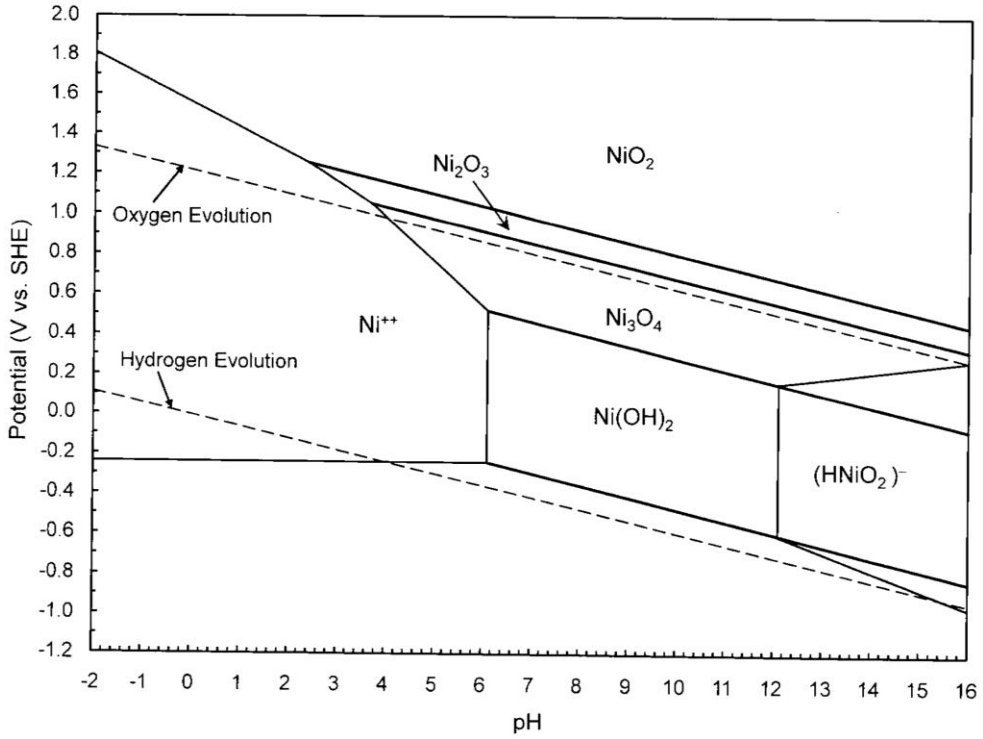

Figure 2.3 Pourbaix diagram for Nickel [27]

While the basic trend of the Pourbaix diagram is the same for all metals, each is specific to the particular metal-aqueous system. For Ni-based alloys, the three regions are shown in Figure 2..

If a metal is not immune to a given aqueous environment, the governing chemistry dictates that the metal is dissolved as a positive ion in an anodic reaction. For Ni, this reaction is $2\ Ni \rightarrow 2Ni^{2+} + 4e$. The freed electrons are consumed by one of four corresponding cathodic reactions, the two most common being the formation of hydroxyl ion, $O_2 + 2H_2O + 4e \rightarrow 4(OH)^{-1}$ and the liberation of hydrogen gas, $2H^{+} + 2e \rightarrow H_2\uparrow$. According to Pourbaix [27], these chemical reactions result in one of three reaction possibilities (immunity, corrosion, or passivation).

Other corrosion related phenomena can also cause failure in metals. The term environment induced cracking is used to characterize some of these. Environment induced cracking includes stress corrosion cracking, hydrogen induced cracking, and corrosion fatigue cracking.

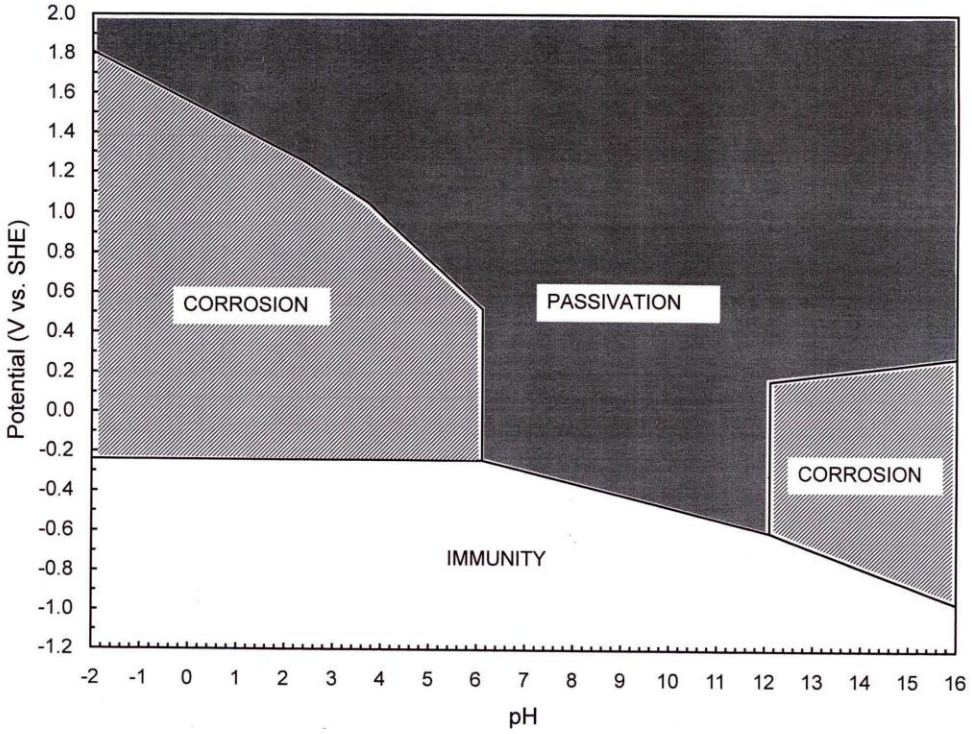

Figure 2.4 Pourbaix diagrams for Nickel indicate three regions [27]

2.2.2 Forms of Corrosion

Various forms of corrosion are pictured schematically in Figure 2.4. The most important with respect to fatigue life are described below [28].

2.2.2.1 Uniform Corrosion

Uniform, regular removal of metal from the surface is the usually expected mode of corrosion as shown in Figure 2.4. For uniform corrosion, the corrosive environment must be metallurgically and composionally uniform. Atmospheric corrosion is probably the most prevalent example of uniform corrosion at a visually apparent rate. The other example is uniform corrosion of steel in an acid solution [28]. As indicated earlier, any surface analyzes associated with corrosion will likely affect the fatigue life.

2.2.2.2 Pitting Corrosion

Localized attack in an otherwise resistant surface produces pitting corrosion. The pits may be deep, shallow, or undercut, as shown in Figure 2.4. A stainless steel and Ni alloys with Cr depend on a passive film for corrosion resistance and are especially susceptible to pitting by local breakdown of the film at isolated sites. Obviously, surface pitting, particularly deep pitting, will have a detrimental effect on fatigue life.

Nickel-based alloys depend on a thin metal oxide surface region to impart corrosion resistance to the bulk material. This region is often called a "passive film". Alloys are not homogeneous and as well the surface region is not homogeneous. Commercial alloys contain numerous inclusions, second phases, and regions of composition-based heterogeneities. These regions are believed to provide initiation points for pitting in alloys. In addition, pitting can occur in homogeneous alloys depending on the presence of certain species in the environment, e.g. chloride ions [28].

2.2.2.3 Crevice Corrosion

Corrosion of an alloy is often greater in the small sheltered volume of the crevice created by contact with another material, as shown in Figure 2.4. The second material may be part of fasteners of the same or different alloy, a deposit of mud, sand or insoluble solid. Corrosion within a crevice maybe caused in atmospheric exposure by retention of water, while the outer surfaces can drain and dry [28]. Crevice corrosion occurs via the same mechanism as pitting corrosion described earlier [28], since a crevice can be considered to be a formed pit.

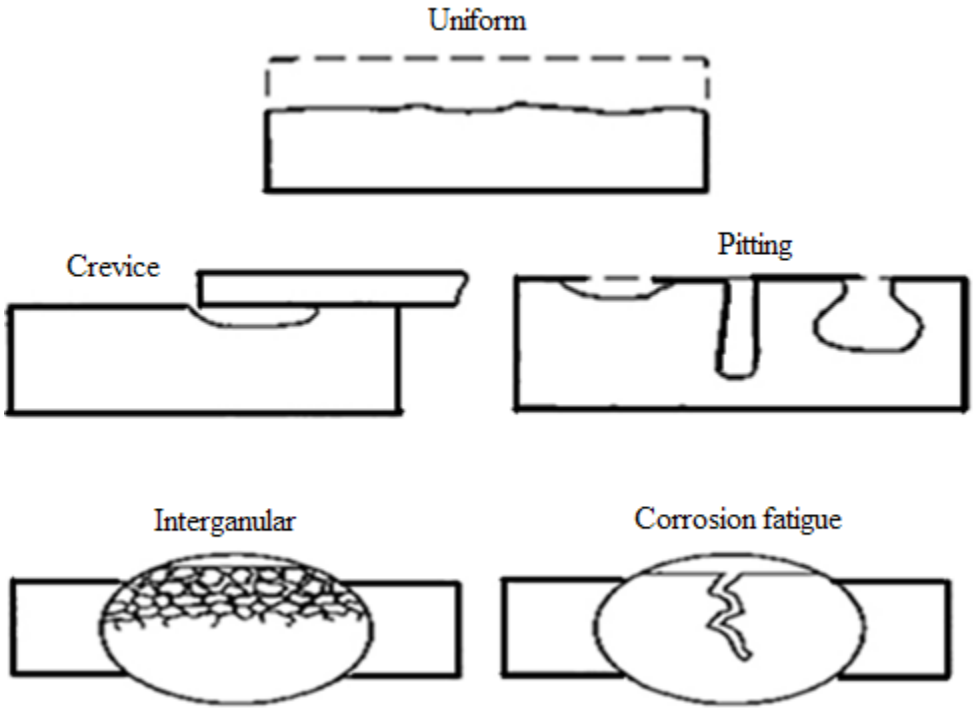

Figure 2.4 Schematic views of various forms of corrosion (modified from [28])

2.2.3 Effect of Alloy Composition on Corrosion Behavior

In nickel-based alloys, the chromium and nickel contents make these alloys superior in withstanding severe corrosive environment conditions. IN600, for example, has been widely used in the nuclear industry. Ni base alloys are used in petrochemical and other chemical process equipment and gas turbine components. They have excellent mechanical properties and have widespread application as key construction materials in industrial furnaces, heat treating equipment such as muffles and retorts, energy production, chemical engineering process equipment, and incinerators.

A few studies of passivation and corrosion of Ni-base alloys have been reported [29-31]. Corrosion behavior of IN600 and IN601 tested in sulphuric acid has been reported and it was found that IN601 has better corrosion resistance than IN600 [32]. The anodic

dissolution of metal is governed by diffusion controlled kinetics in the passivation region. The passivation behavior for IN601 in different concentrations of H_2SO_4 and the passivation potential has been found to be in the range of + 100 mV to + 120 mV [30-34]. The corrosion behavior of IN600 and IN601 in 0.5M H_2SO_4 and in Dead Sea water has shown that IN601 has better corrosion resistance than IN600 [35].

Ni-based alloys can be used in wide varieties of corrosive media. The amount of chromium and molybdenum present in the alloy has a significant effect on the corrosion properties of this alloy. Several studies have been conducted by researchers on Ni-base alloys [27]. Alloys like C276, C4, and IN625 were tested in various corrosive media. These have exhibited corrosion and pitting attack resistance in Cl^- containing solutions and excellent corrosion and oxidation resistance in hydrochloric acid solution. For potentiodynamic tests on pure Ni and IN600 in 0.5M H_2SO_4, the potential of each alloy was within the passive region (+600 mV vs SHE in the case of pure Ni). Results showed that the breakdown of passivity occurred at a critical NaCl concentration.

The addition of Mo to Ni-base alloys decreased corrosion rates [36,37]. Studies performed to understand the role of Mo additions on corrosion resistance showed that the effect of Mo was to stabilize the passive film and thus delay passive film breakdown and the onset and propagation of localized corrosion [36] and [38]. The effect of Cr and Mo Ni-base alloys was to change the behavior of the passive film and Mo was found to prevent pitting and further corrosion [36,37].

2.2.4 Electrochemical Behavior

Ni base alloys have a wide range of application because of their excellent corrosion resistance in aggressive environments [27,28]. Such applications include chemical and

pollution control equipment, heat exchangers, fuel nozzles and the outer wall of nuclear waste containers. Intergranular corrosion [26,33], localized corrosion [31-34], stress corrosion cracking [2,38,39] and passivation behaviors of nickel base alloys have been investigated using conventional electrochemical methods. Often, the most effective method of preventing corrosion failure is by selecting materials that are resistant to specific corrosive service environments. Thus, in order to avoid a costly and unexpected failure during service, the selection of proper materials of construction and attention to corrosion prevention methods have become an integral part of process design. Designers are not only required to have a working knowledge of mechanical and physical properties of materials, but also have a good understanding of their corrosion behavior. These are juxtaposed with cost considerations in order to select the right materials for the application. In view of this, candidate materials are usually tested in simulated or actual service corrosive environments to evaluate their corrosion behavior and determine the best material for the specific application under consideration. Corrosion testing has also been useful for research and development purposes. It has been a significant tool for understanding various mechanisms of corrosion, and developing new corrosion resistant alloys.

Several corrosion testing techniques that exploit the electrochemical nature of corrosion have evolved over the past decade. Such techniques include galvanostatic, galvanodynamic, corrosion potential, polarization resistance, Tafel, cyclic polarization measurements and potentiodynamic [1].

Nickel-base alloys are a candidate material for construction of the inner wall of nuclear waste containers whose life expectancy is more than 10,000 years [1,2]. A study by

Abdallah [38] focused on a number of metal alloys such as stainless steel 316L, IN600 and C22 (Figure 2.5 to Figure 2.7) respectively. Tests which were performed include electrochemical corrosion testing, accelerated corrosion testing in sodium chloride solution and long term exposure. Based on the results of these tests, the most corrosion resistant alloys were found to be, in decreasing order, C22 (Figure 2.7), IN600 (Figure 2.6), and stainless steel 316L (Figure 2.5). Of the top three alloys, the C22 (Figure 2.7) stands out as being the best of the alloys tested, for this application. On the basis of corrosion resistance, combined with weld and mechanical properties, C22 (Figure 2.7) was determined to be the best material for construction of flexible hoses for use at the Space Shuttle launch site [40,41].

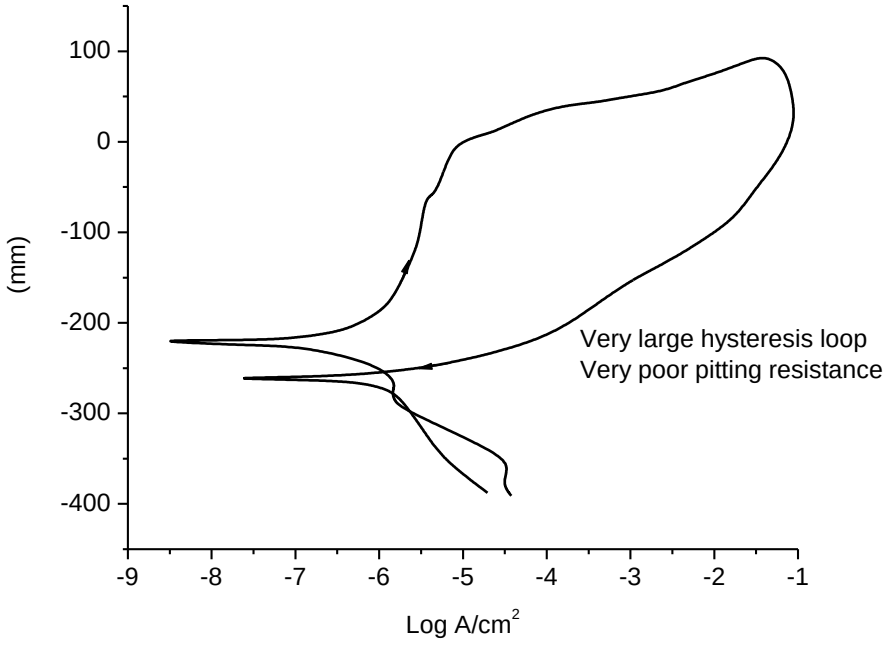

Figure 2.5 Stainless steel 316L cyclic polarization in aerated NaCl and HCl [40]

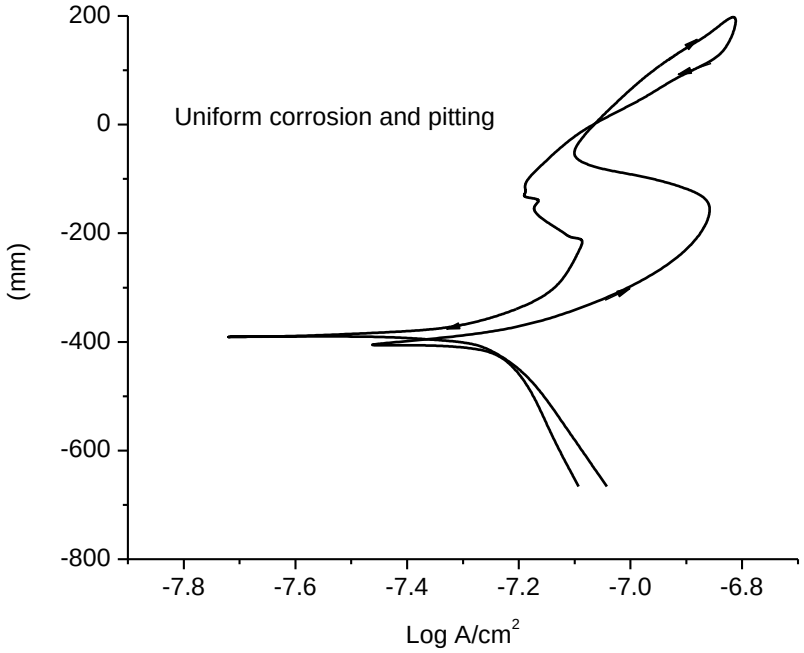

Figure 2.6 IN600 cyclic polarization in aerated NaCl and HCl [40]

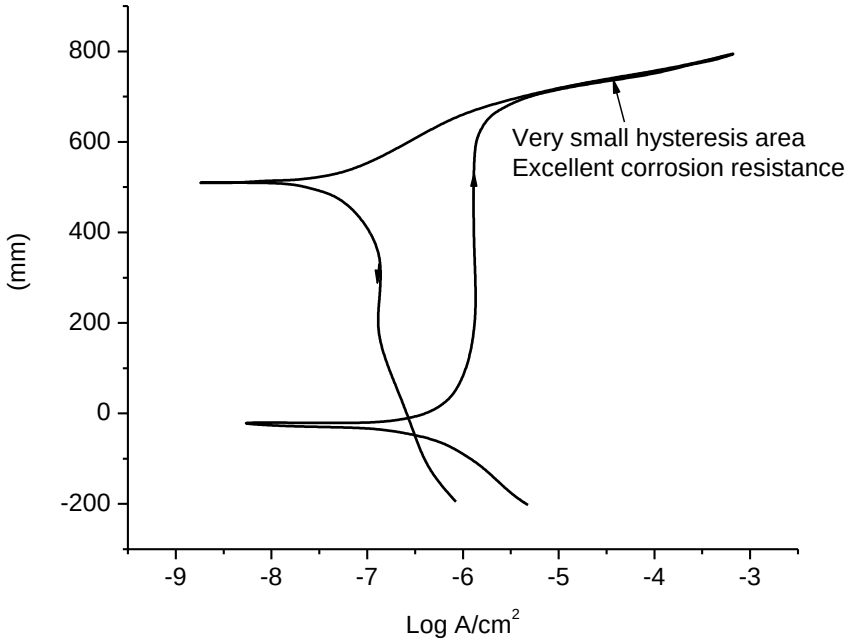

Figure 2.7 C22 cyclic polarization in aerated NaCl and HCl [40]

2.3 Combined Effect of Fatigue and Corrosion

2.3.1 Effect of Frequency

In general, the higher the frequency of stressing, the longer the fatigue life is. But, at high frequencies, e.g., above 1kc/sec., there are difficulties in the interpretation of some results, because considerable heating can occur at such high frequencies.

2.3.1.1 High Cycle Fatigue

For high cycle fatigue, the effect of frequency on the fatigue life, measured in cycles to failure is important. At low frequencies, the effect of the environment rather than high frequencies, and therefore the effect of the environment on the fatigue strength, is more pronounced.

Figure 2. shows that for a 13% Cr steel tested at a frequency of 50Hz, the fatigue strength for smooth specimens tested in 1% NaCl solution after 115 days ($5x10^8$ seconds) is only about 1/3 that of fatigue strength of specimens tested in air [42]. The same trend is observed for notched specimens, as shown in Figure 2.. However, there is also an effect of the environment on low cycle fatigue, as described below.

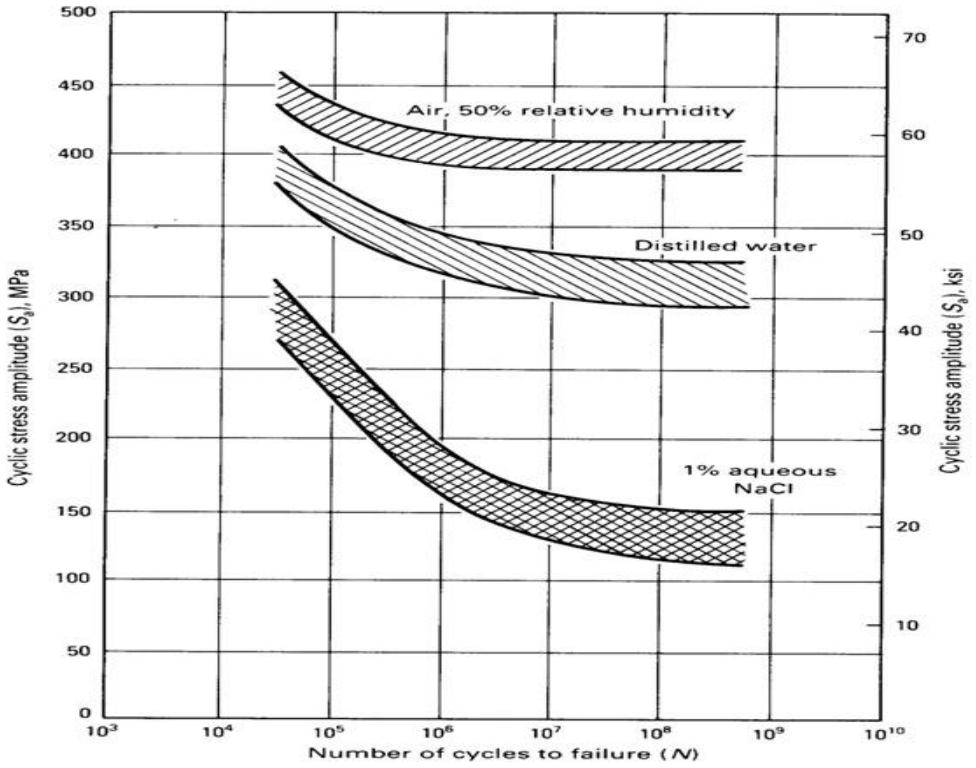

Figure 2.9 Corrosion fatigue endurance data for smooth specimens of 13%Cr at 50Hz and at 23^{o}C [43]

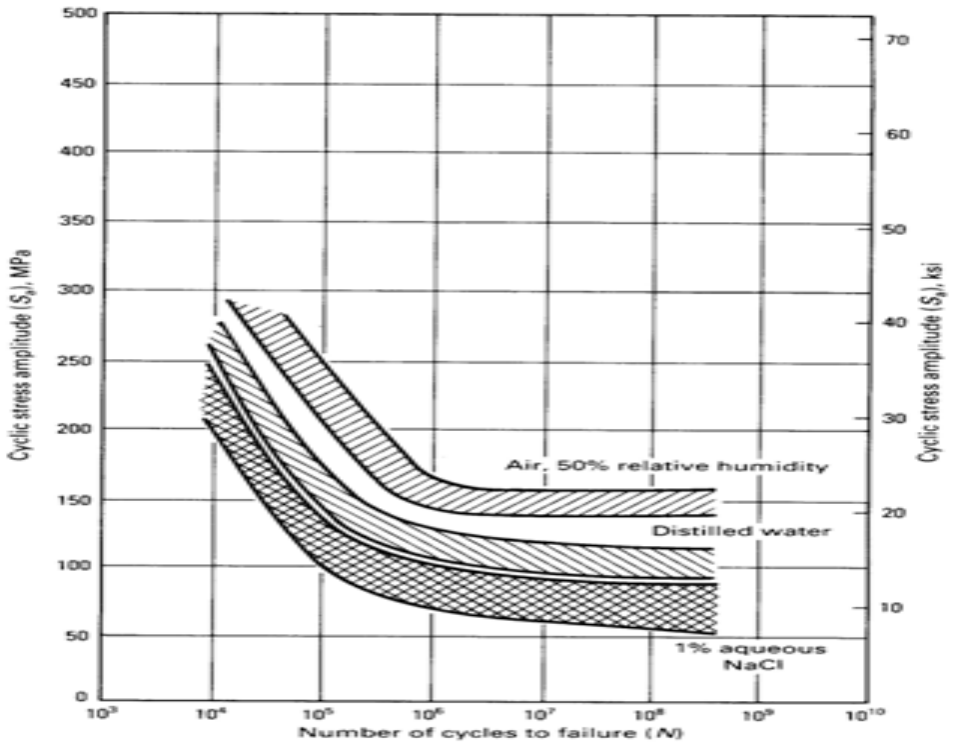

Figure 2.10 Corrosion fatigue endurance data for notched specimens of 13%Cr at 50Hz and at 23^{o}C [43]

2.3.1.2 Low Cycle Fatigue

It has often been observed that the crack growth per cycle is dependent on the frequency in the presence of air or corrosive environments. The general trend has been that the cyclic fatigue crack growth decreases with increasing frequency [43]. In the frequency range of 0.01-100Hz, the effect of environment peaks at moderate levels (0.1-1Hz) while decreasing at frequencies outside this range. In the frequency range of 0.1-10Hz, no frequency effects were observed in alloy steel tested in air and in 3.5%NaCl [44]. The influence of loading cycle waveform on fatigue behavior was used [42]. Other researchers argued that the dependence of fatigue crack growth on frequency in some materials is due to strain rate sensitivity at the crack tip [42]. It was found that fatigue data in vacuum show a slope lower between 0.1 and 0.01 Hz and the fatigue crack growth

at 0.01 Hz in vacuum is markedly greater than the creep crack growth rate in an argon environment [45]. Different fracture mechanisms were observed in specimens fatigue tested in vacuum at 0.01 Hz and in specimens creep tested in argon at the same temperatures. The fracture surface of fatigue tested specimens was transgranular with ductile striations and some intergranular regions were apparent. The transition frequency in vacuum is estimated to be more than two orders of magnitude lower than in air. The creep effects become significant at lower frequencies. The effect of frequency on the low cycle fatigue strength for 13%Cr steel specimens is shown in Figure 2.9 and Figure 2.. These Figures show that samples tested in 1%NaCl solution exhibit a 30% decrease in fatigue strength after only 10 minutes in solution for smooth specimens and a similar decrease after only three minutes in solution for notched specimens [43].

2.3.2 Effect of Aqueous Environment

A comprehensive understanding of corrosion fatigue requires defining the processes involved and their interdependence. In aqueous solutions, crack tip reactions can significantly alter the local environment chemistry relative to the bulk solution chemistry due to limited mass transport. Major progress has been made in experimental measurements of the local solution chemistry despite the technical difficulties associated with the restricted geometries and small solution volume within the crack enclave.

Mass transport of dissolved species in a corrosion fatigue crack can occur due to advection, diffusion, and ion migration [46]. Advection arises from the solution motion induced by the cyclic displacement of the crack faces. Studies show that the mixing effect inside the crack increases as the cyclic frequency is raised. It was suggested that the rate of transport of hydroxyl ions from the crack mouth to the tip may be raised by

more than three orders of magnitude at high loading frequency [47]. It is therefore advantageous to use high cyclic frequency so the difference in solution composition between the bulk and crack solutions is minimized. It is believed that crack electrolyte chemistry may be different, not only for one type of specimen or test procedure compared with another, but also for different stages of the same test upon a single specimen [40].

Solution chemistries exhibited lower pH levels in cracks than that of the bulk solution when tensile steel specimens were tested in seawater, and the potential at the crack was less than the applied anodic potential [44]. This was attributed to the cation hydrolysis reaction associated with metal dissolution at the cracks. This significant variation in local solution chemistry may lead to confusion in interpretation of fatigue behavior, especially when this behavior is judged on the basis of the bulk solution chemistry.

Electrochemical conditions within pits and cracks have been investigated for a wide range of alloys using microelectrodes in order to evaluate the impact of limited mass transport. Results of these studies were reviewed by Turnbull [48], who was concerned with the considerable variation in the experimental results.

Other experimental evidence for effective mixing between the crack solution and the bulk solution during high frequency testing was obtained by examining changes in the applied currents that were required to maintain potentiostatic control [45]. Applied anodic currents required to maintain anodic potential of 0 V_{SCE} during cyclic loading were much less than those required after cycling was stopped for a period of time. The increase in anodic current after cessation of cycling was consistent with polarization behavior at lower pH.

2.4 Surface Analysis

Numerous analyses of surface composition of passive oxide films have been reported for Ni–Cr-Mo based alloys [49-51]. Techniques include Auger Electron Spectroscopy (AES) and Secondary Ion Mass Spectrometry (SIMS). These showed that the presence of an inner oxide layer rich in Cr (barrier layer) is a primary factor in enforcing passivity, as shown in Figure 2.8. The main effect of Mo content is to enhance the corrosion resistance of Ni-Cr-Mo based alloys but its mechanism is less well understood. A variety of possible mechanisms has been suggested. It has been postulated that Mo on the alloy surface preferentially locates at local defects, which otherwise would act as dissolution sites [52], and slows anodic dissolution because of its higher metal–metal bond strength [36]. An alternative hypothesis is that MoO_4 is formed in the solid state in the exterior regions of the film. This MoO_4 layer is cation selective, and resists the incorporation of anions, such as Cl^- and OH^-, and allows for the growth of a CrO inner barrier layer. The resulting bipolar film stabilizes the oxide phase [53]. The passive corrosion properties of a series of Ni–Cr–Mo alloys were investigated. In this study alloys were C22, C2000, C276, C4 and IN625 [53]. The surface analyses showed that the high-Cr alloys were able to build thicker oxides with a layered structure consisting of an inner Cr–Ni oxide layer and an outer Mo/Cr oxide. By contrast, such a high-Cr content inner layer and structured elemental distribution were not achieved with alloys having lower bulk Cr content. Cr dissolution can only occur as Cr (III), additional alloying elements, specifically Mo and W, exert little influence on passive current densities [53].

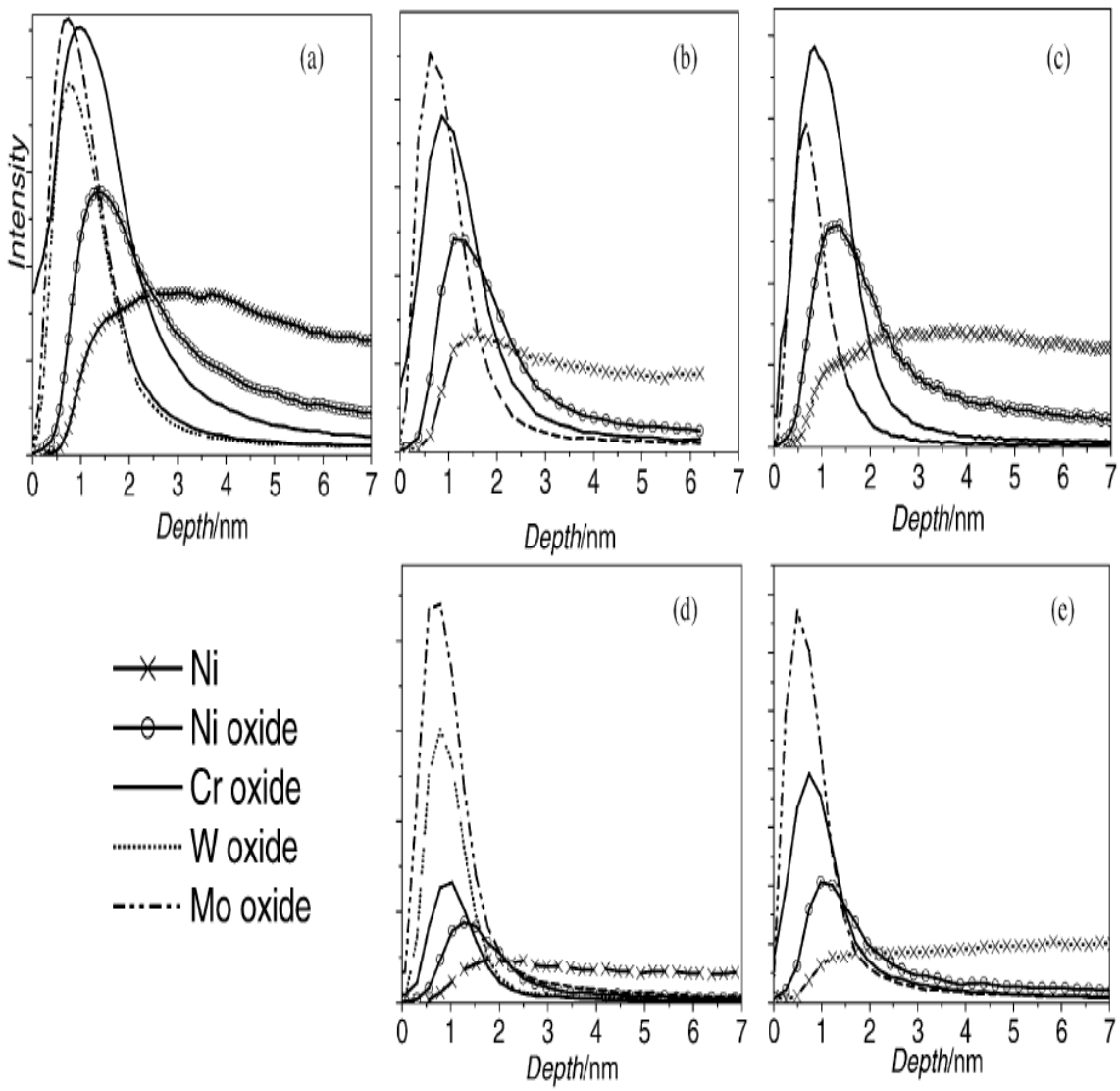

Figure 2.8 SIMS depth profiles after treatment at 200mV for (a) C22, (b) C2000, (c) IN625, (d) C276 and (e) C4 [53]

3 Experimental Program

The investigation of the complex and interdependent nature of the various processes during fatigue and corrosion fatigue requires the knowledge of several subject areas, including fracture analysis, electrochemistry, and microstructural characterization. Fracture surface morphology can provide quantitative information regarding the dependence of crack initiation in the presence of different aggressive solutions. A microstructural characterization is important to identify the crack path and assess the effect of an alloy's mechanical properties, composition, and microstructure. The general characteristics of these alloys, test specimen geometry, and heat treatment procedures are detailed in the following sections.

3.1 Materials

As stated in chapter one, the materials of interest in this research study are three Ni-base alloys: IN600, IN601 and C22. These alloys were chosen because we need to study the effect of Cr and Mo on these alloys. The chemical composition (wt. %) of these alloys is given in Table 3.1 Nominal composition (wt.%) of alloys [43]. The three alloys were supplied as cold worked rods with a diameter of 12.7 mm.

Table 3.1 Nominal composition (wt.%) of alloys [43]

Alloy	Ni	Cr	Fe	Mo	C	Al	W	Co	Si	P	Cu	Ti
IN600	Bal.	15.77	8.58	-	.05	.267	-	.015	.19	.001	.01	.3
IN601	Bal.	22.14	16.09	-	.3	1.59	-	-	.27	.007	.06	.36
C22	Bal.	21.42	2.95	13.67	.003	-	.291	.11	.03	.004	-	-

Figure 3.1, Figure 3.3 and Figure 3.5 show the as-received scanning electron microscope (SEM) micrographs of IN600, IN601 and C22 respectively. The as-received alloys were

annealed for 1 hour at 1000ºC to ensure an equiaxed microstructure and therefore reproducible mechanical properties as shown in Figure 3.2, Figure 3.4 and Figure 3.6.

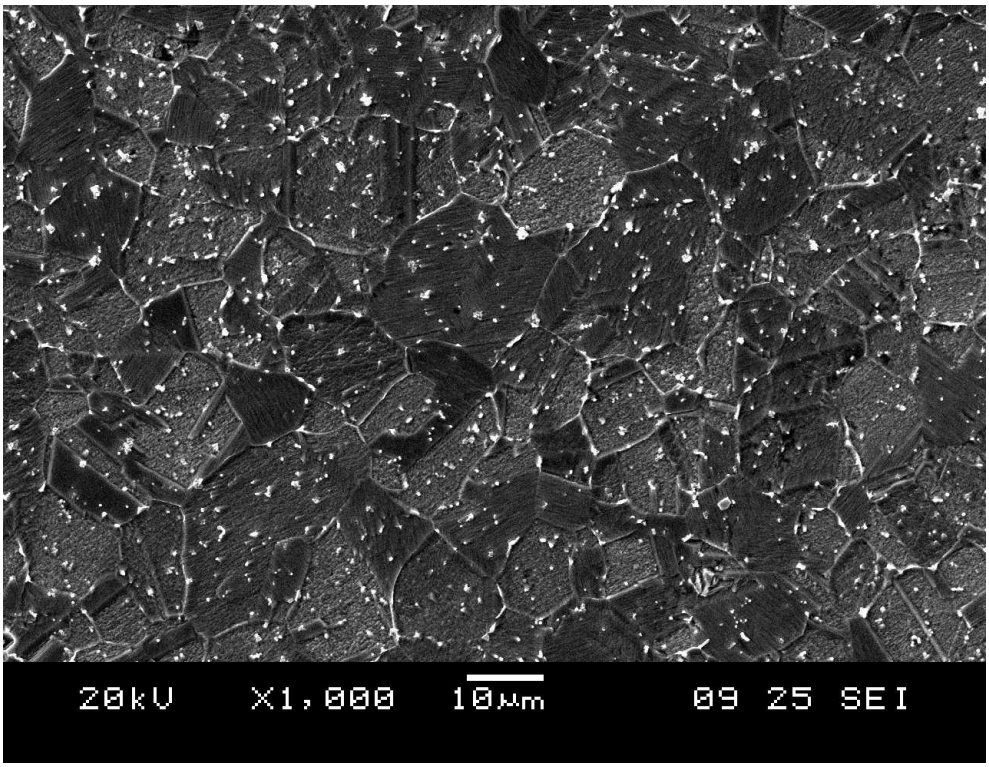

Figure 3.1 SEM micrograph of as-received alloy IN600

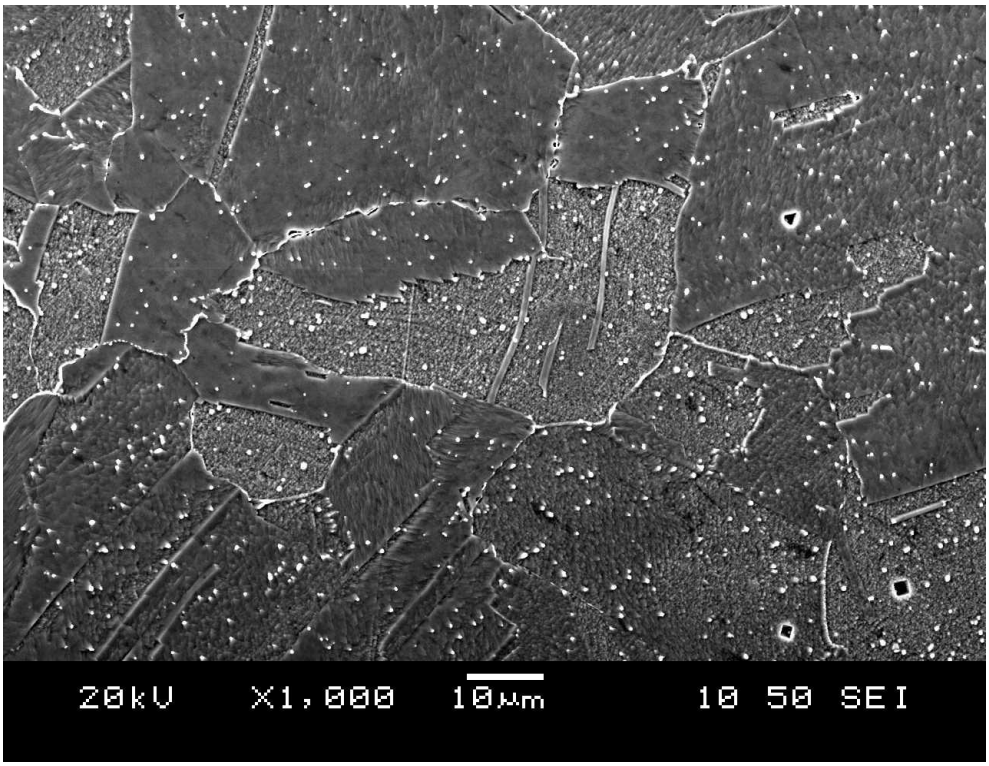

Figure 3.2 SEM micrograph of annealed alloy IN600

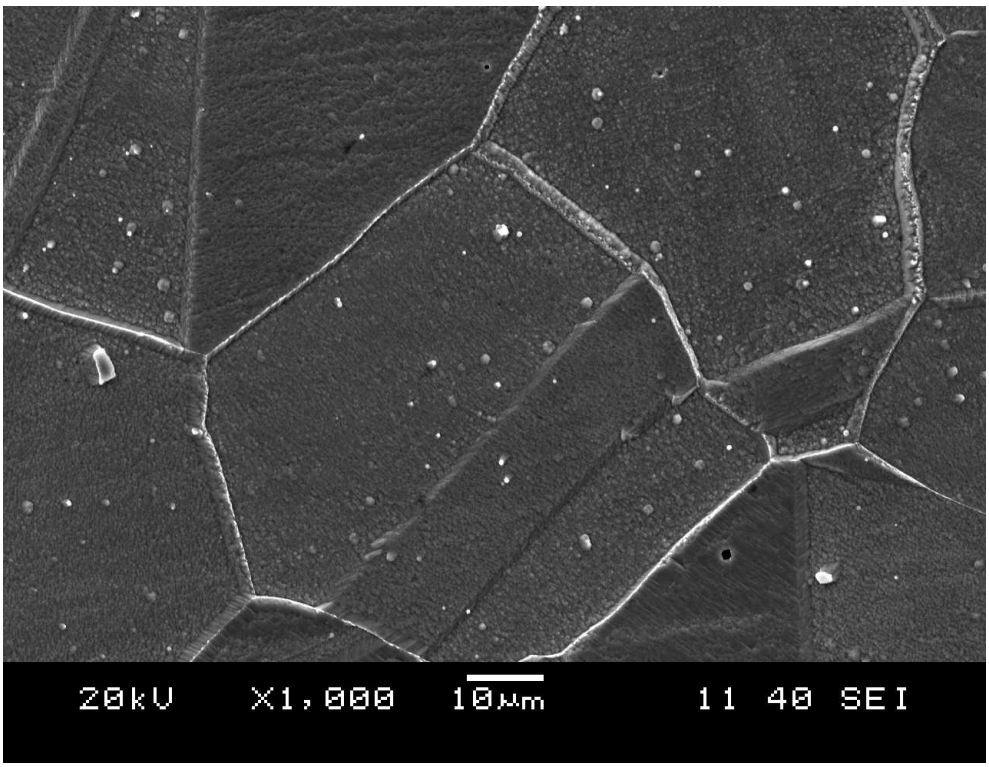

Figure 3.3 SEM micrograph of as-received alloy IN601

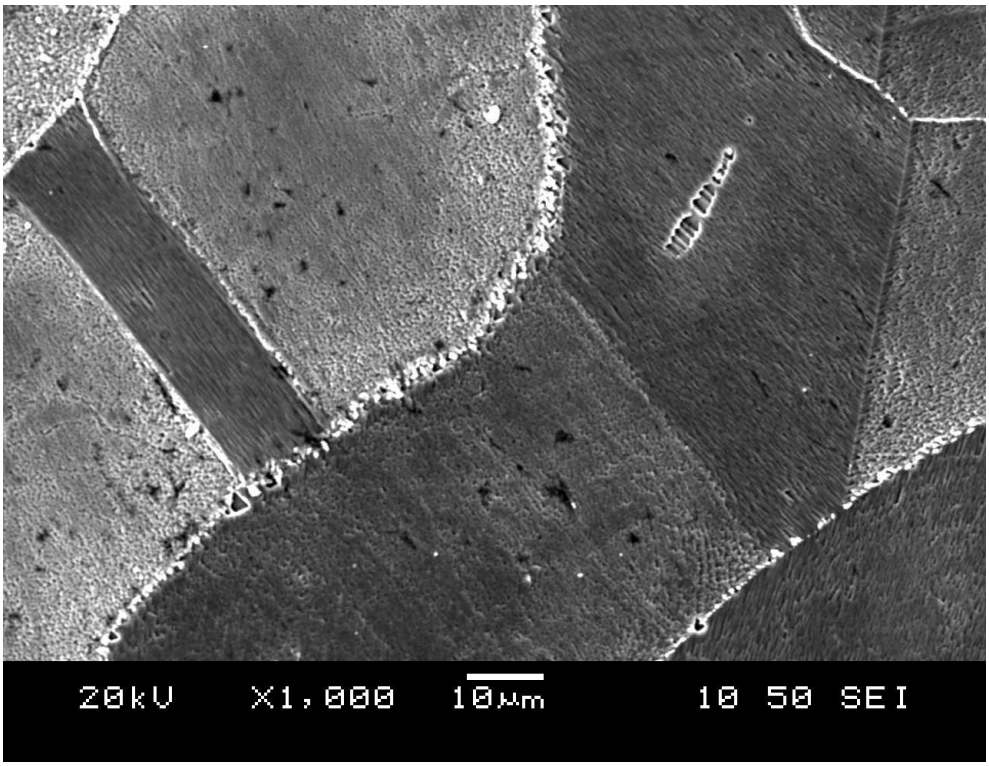

Figure 3.4 SEM micrograph of annealed alloy IN601

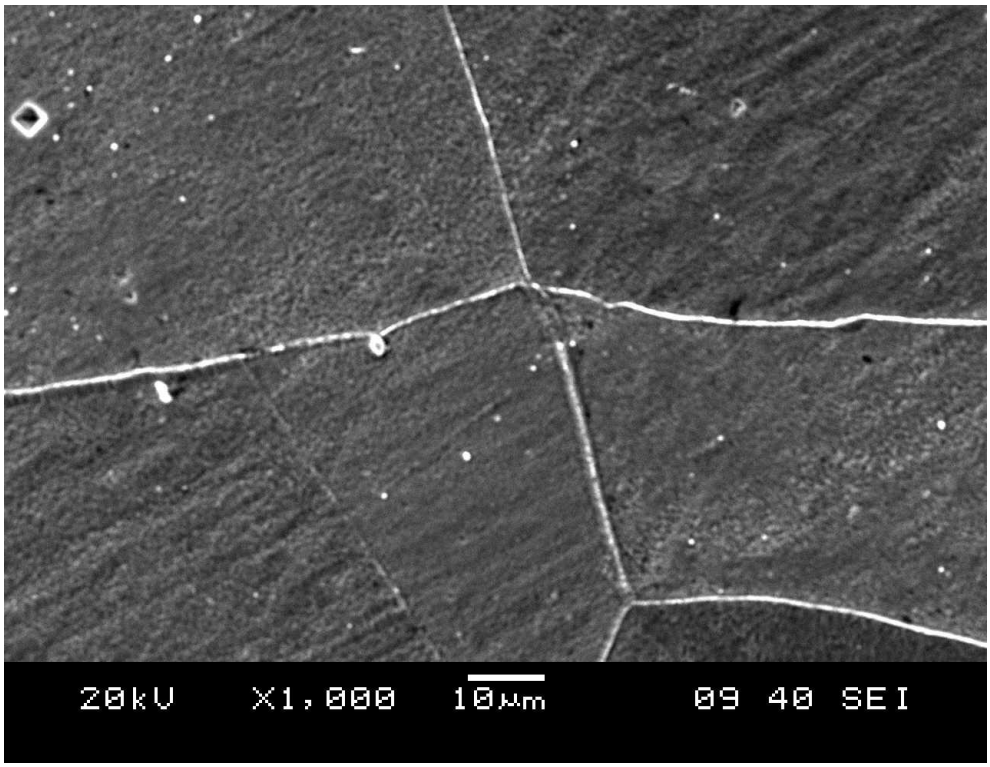

Figure 3.5 SEM micrograph of as-received alloy C22

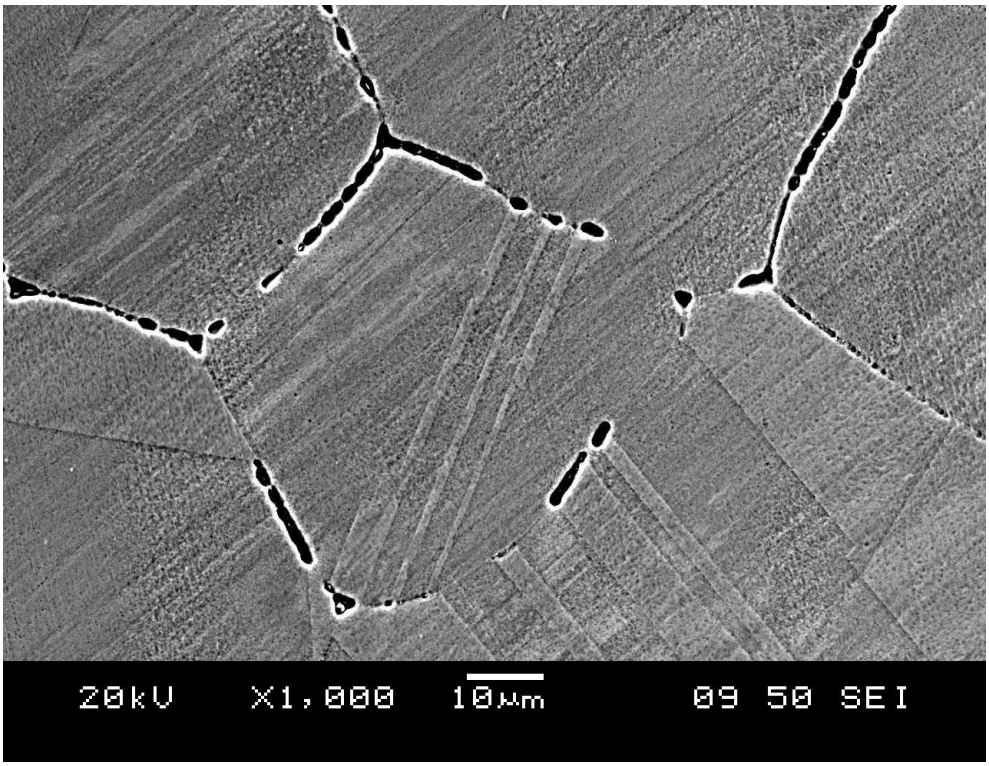

Figure 3.6 SEM micrograph of annealed alloy C22

3.2 Tensile Tests

Tensile tests were conducted to determine the mechanical properties of the three Ni based alloys. Smooth cylindrical specimens with reduced gage sections were machined from as-received material and then annealed. Specimens were fine polished with diamond paste and specimen dimensions are shown in Figure 3.7 and Figure 3.8.

An INSTRON 1337 testing machine with load capability up to 10,000 kg was used. Tests were carried out in air at room temperature with the crosshead speed set at 1 mm/min. Load and displacement values were collected via a chart recorder and converted to stresses and strains. The yield stress, σ_{YS}, was determined using the 0.2% offset method. Table 3.2 lists the mechanical properties, including ultimate tensile strength, σ_{UTS}, for the

three tested alloys. These data are the average values from three tensile tests conducted on each alloy.

Figure 3.7 Photograph of tensile test specimen before and after fracture.

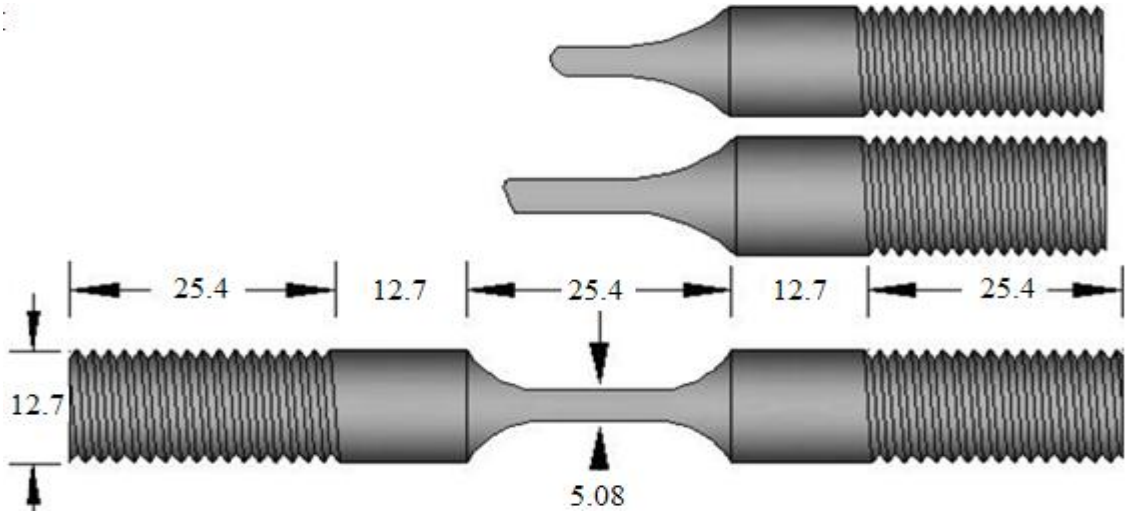

Figure 3.8 Dimensions of tensile test specimen before and after fracture [mm]

3.3 Hardness Test

In addition to tensile tests, Rockwell hardness tests were carried out to further characterize the mechanical properties of the materials. Rockwell hardness numbers, scale B (HRB) are shown in Table 3.2.

3.4 Electrochemical Tests

The present study focuses mainly on uniform and localized corrosion rates of IN600, IN601 and C22 in 3.5 wt. % sodium chloride (NaCl) solution at pH = 7.0, concentrated hydrochloric (HCl) acid at pH = 0.0, and 10 wt. % ferric chloride ($FeCl_3$) solution at pH = 0.0 as evaluated through potentiodynamic measurements. A potentiodynamic polarization test is one of the electrochemical techniques used to determine the aqueous corrosion behavior of a metal or an alloy. The procedures for conducting this test are described in the following section.

Table 3.2 Mechanical properties of the three alloys as received

Alloy	σ_{YS} MPa	σ_{UTS} MPa	% Elongation	Hardness HRB
IN600	700	900	14	90
IN601	450	725	17	92
C22	450	850	22	90

3.4.1 Specimen Preparation

Three nickel-base alloys used for this study were IN600, IN601, and C22 supplied as rod stock. Flat coupons samples, 12.7 mm in diameter and 12.7 mm long were cut from each alloy. All samples were annealed in an argon atmosphere for one hour at 1000°C. The specimen holder was designed such that the exposed metal flat surface area was 1.27 cm^2. Preparation of each test specimen, shown in Figure 3.9, involved mounting and polishing

with 600 grit paper, ultrasonically degreasing each in a detergent solution and then drying before immersion in the electrolyte.

3.4.2 Procedure

A Model 350A corrosion measurement apparatus, manufactured by EG & G Princeton Applied Research, as shown in

Figure 3.10 was used for potentiodynamic measurements.

The potentiodynamic cell included a saturated calomel reference electrode (SCE), a graphite counter electrode, a test specimen which was the working electrode and a saturated reference electrode. The electrolytes were 3.5 wt. % NaCl solution at pH = 7.0, concentrated HCl at pH = 0.0, and 10 wt. % $FeCl_3$ solution at pH = 0.0. A 500 ml beaker was used to hold the test solution. The potentiodynamic cell was designed to measure and analyze corrosion data. The data were transferred to a computer system for further analysis. The scan started at 250 mV relative to the corrosion potential (E_{corr}) of the three alloys tested.

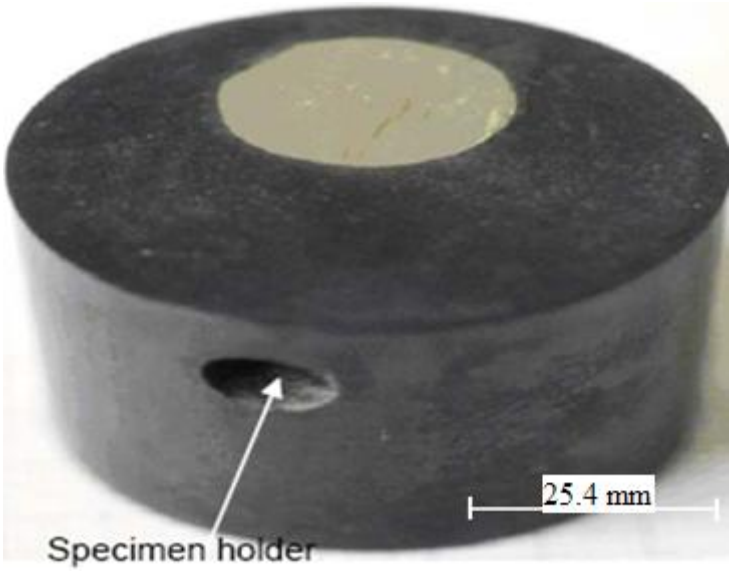

Figure 3.9 Potentiodynamic test specimen

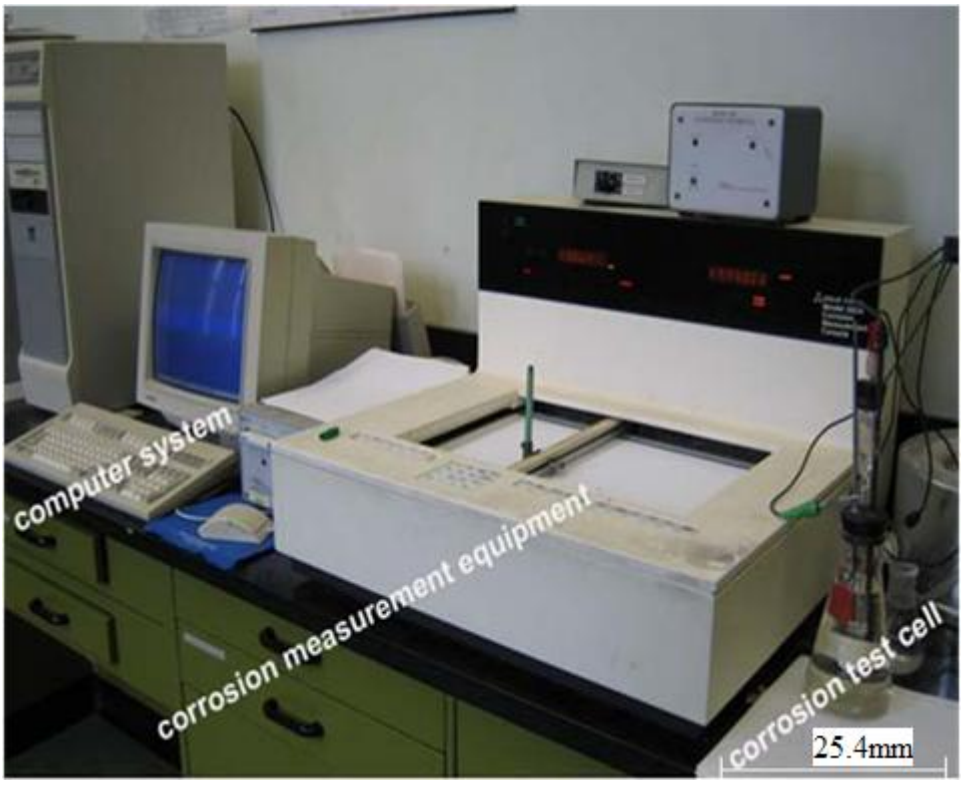

Figure 3.10 Corrosion test measurements setup

The scan rate was 1 mV/sec and the scan was reversed when the current density reached a threshold value of $5x10^6$ nA/cm^2. The reverse potential scan continued until the potential returned to the starting potential of approximately -250 mV relative to E_{corr}. A graph of applied potential versus measured current density was plotted for each alloy. All tests were carried out at room temperature.

3.5 Fatigue Tests

3.5.1 Specimen Preparation

Standard specimens with dimensions shown in Figure 3.11 and Figure 3.12 were machined from the as-received material.

Figure 3.11 Fatigue test specimen before testing

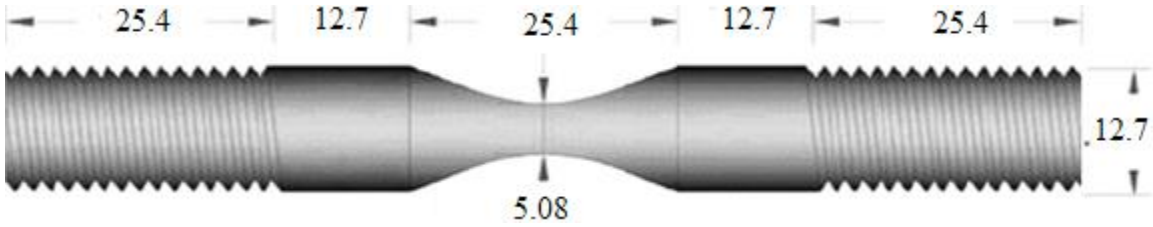

Figure 3.12 Dimensions of fatigue test specimen [mm]

3.5.2 Fatigue Testing

Fatigue tests were performed in four environments, air, 3.5%NaCl solution, concentrated HCl and 10%$FeCl_3$ solution.

3.5.2.1 Fatigue Test Equipment

Fatigue testing was conducted using an INSTRON 1337 Testing Machine, connected to an INSTRON 8500 programmable control unit. The INSTRON 1337 unit has a load cell with a full load scale of 1000 kg/1V. The servo-hydraulic test unit applies a load with a hydraulic actuator, while a computer-controlled servomechanism controls the oil flow to the actuator. The specimen is mounted on the test unit between the actuator and the load cell by screwing it into the test fixture. Figure 3.13 shown the test unit and the testing setup. Testing was conducted at a rate of 10 cycles per second.

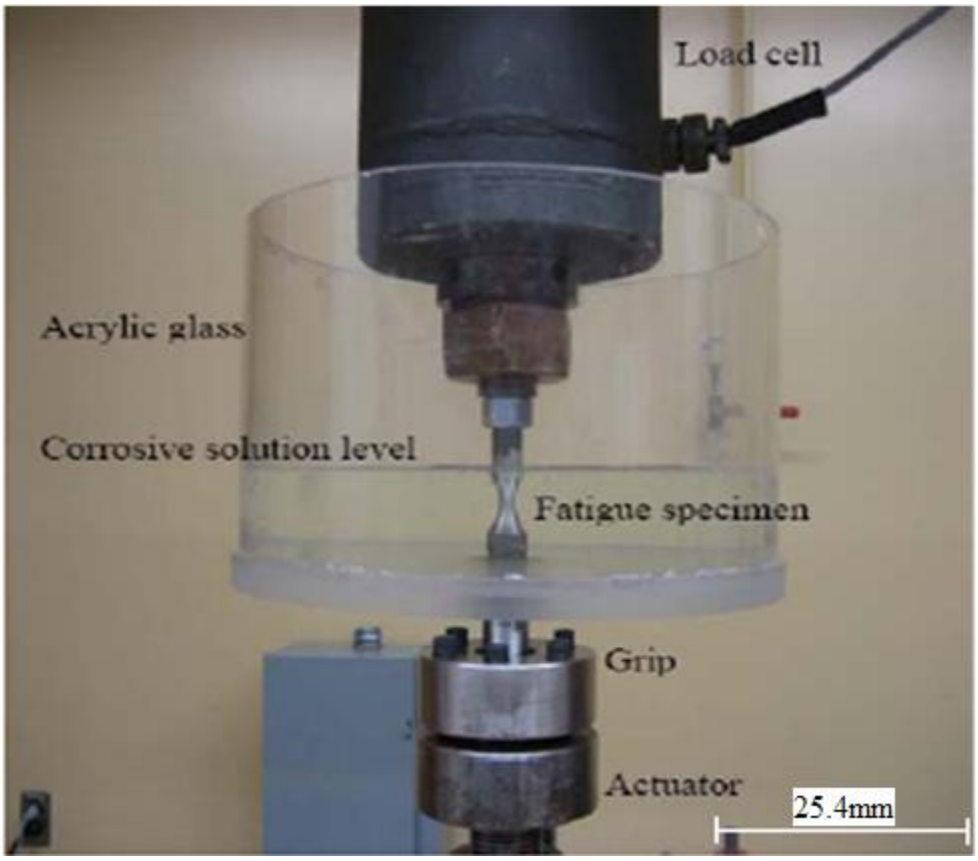

Figure 3.13 Corrosion fatigue test set up using INSTRON 1337 machine

The INSTRON 8500 programmable control unit was used to set up all the testing parameters. Furthermore, the INSTRON 8500 programmable control unit receives data from the displacement gauge and the load cell during fatigue testing. The data are then processed by the computer and, based on the programmed test parameters, feedback is sent back to the servo valve to control the hydraulic actuator.

3.5.2.2 Fatigue Tests

Details of the environmental cell configurations are shown in Figure 3.14 to Figure 3.16. An O-ring was installed at the bottom of the cell to permit transfer of force to the specimen while preventing leakage of the solution.

Fatigue tests were conducted on annealed specimens of the three alloys at a constant frequency of 10 Hz under axial tension-tension load. Fatigue tests in corrosive solutions were performed by enclosing the specimen within an “O” ring sealed, acrylic glass cylinder, as shown in Figure 3.17 and Figure 3.1.

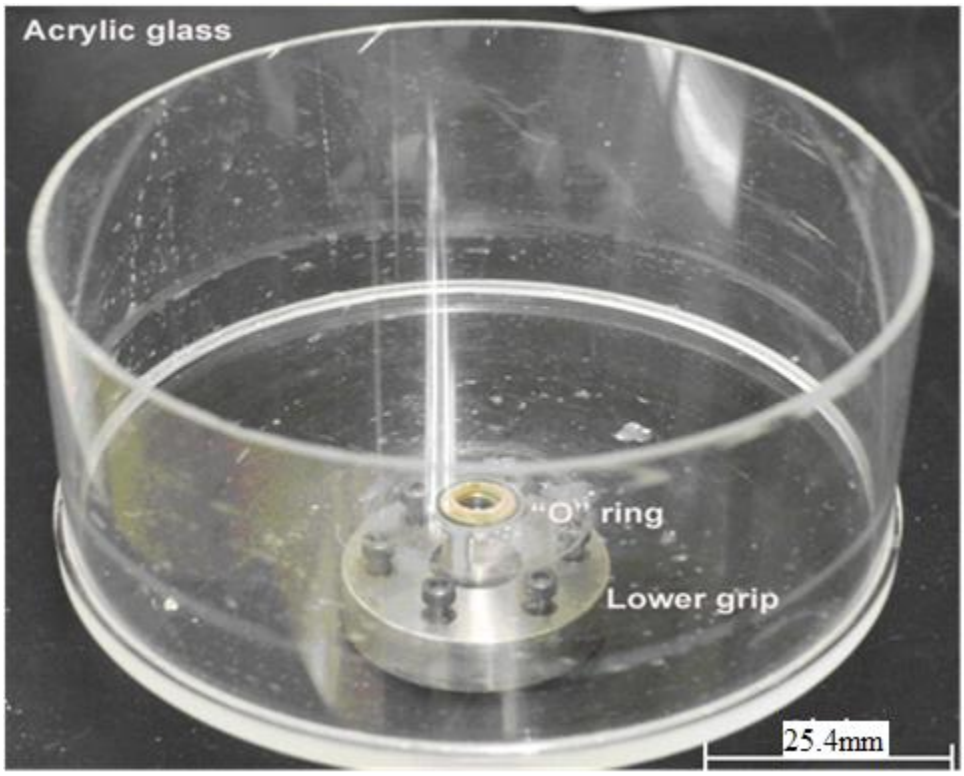

Figure 3.14 Photograph of acrylic glass showing “O” ring installed below

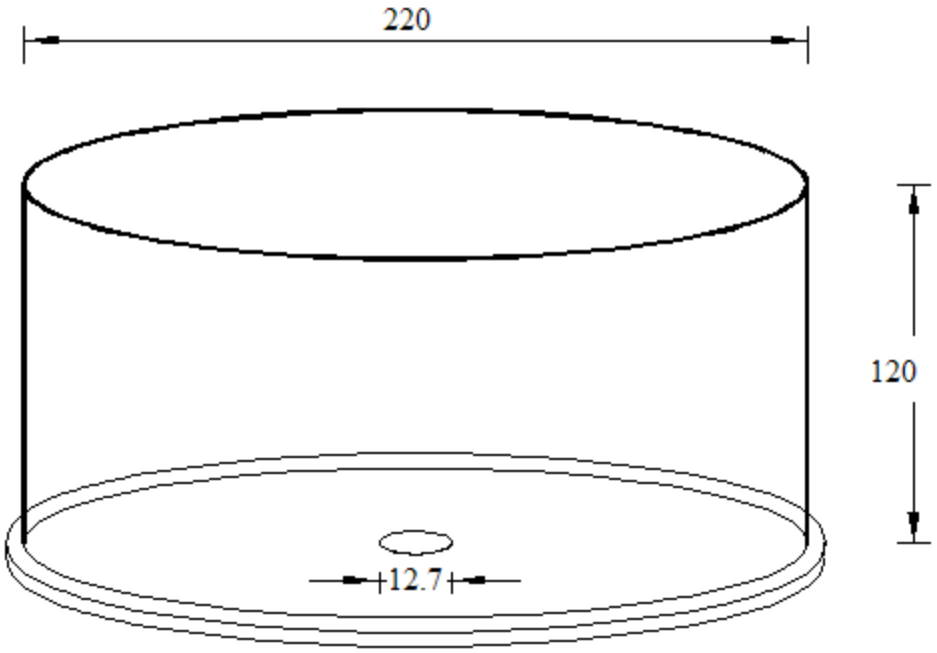

Figure 3.15 Dimensions of the acrylic cell [mm]

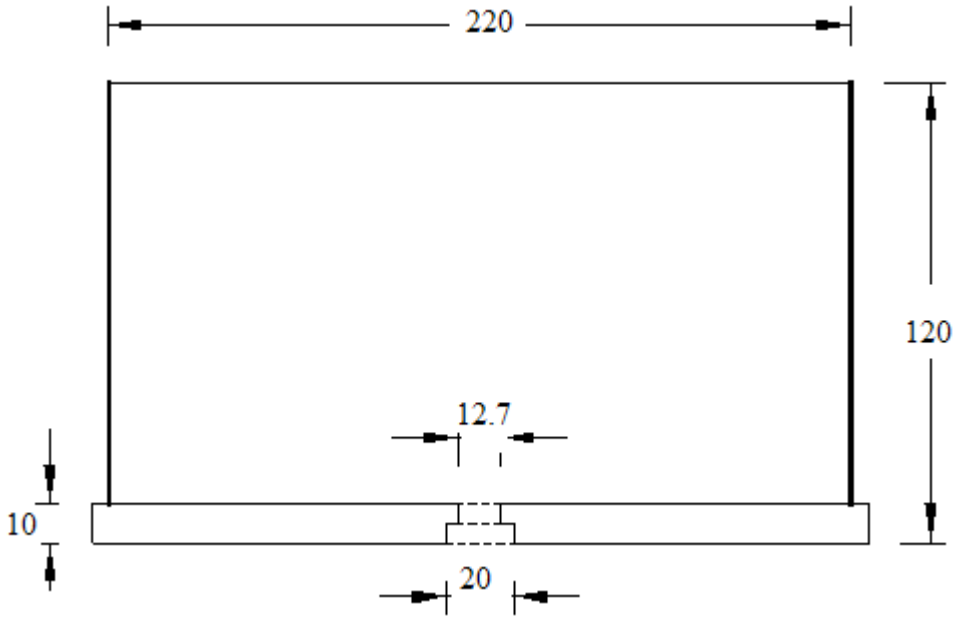

Figure 3.16 Cross section geometry of the acrylic glass cell [mm]

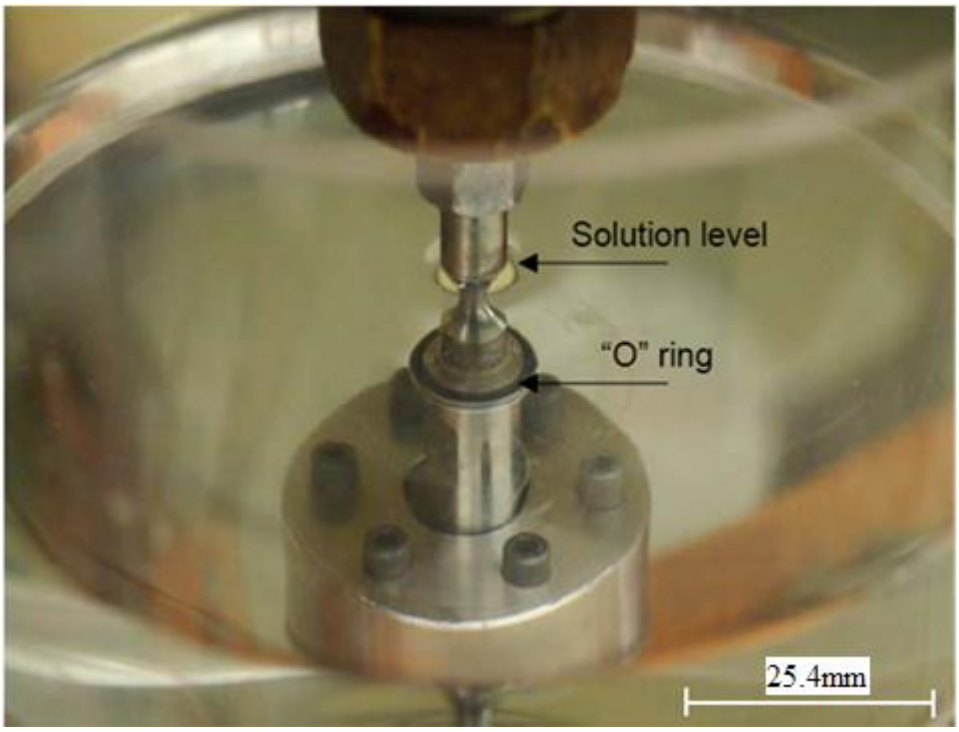

Figure 3.17 Specimen during corrosion fatigue test

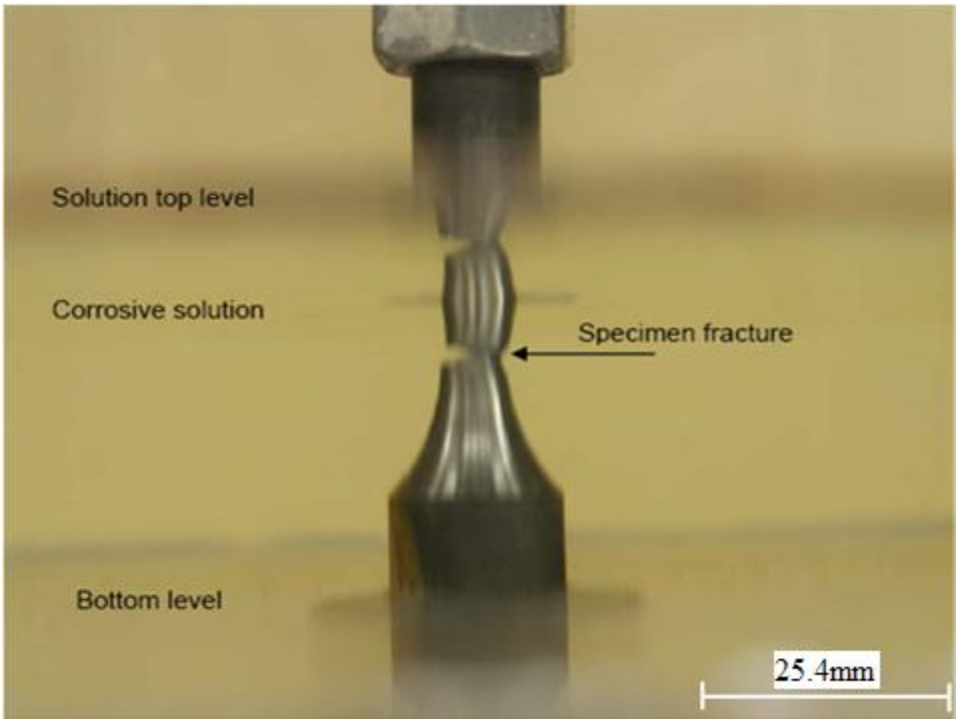

Figure 3.18 Specimen after failure and environmental cell configurations

3.6 Microstructural Characterization and Surface Analysis

More than 60 specimens were selected for microstructural analysis to determine crack initiation sites and crack propagation paths. Optical and scanning electron microscopy (SEM) was used for these studies. In an attempt to relate the corrosion behavior of these alloys to the nature of the surface oxide film, auger electron spectroscopy (AES) and secondary ion mass spectroscopy (SIMS) studies were conducted.

3.6.1 Auger Electron Spectroscopy

In Auger Electron Spectroscopy (AES), an electrically conducting sample is bombarded with an electron beam having an energy of 3-20 keV. These bombarding electrons cause a core electron from an atom in the sample to be ejected resulting in a photoelectron and an atom with a hole in a core electron shell. The atom then relaxes via an electron with a lower binding energy from an outer electron shell dropping into the core hole thus releasing some energy. The energy released results in the emission of an electron called an Auger electron after Pierre Auger who discovered this relaxation process. The energy of the Auger electron is characteristic of the element that emitted it and upon being measured can be used to identify the element. Since these ejected Auger electrons have very low energies and can escape only from the first few surface atomic layers, composition of the surface layers can thus be determined.

3.6.2 Secondary Ion Mass Spectroscopy (SIMS)

In secondary ion mass spectroscopy, a primary ion beam (eg. oxygen ions or cesium ions) having an energy of 1-30 KeV impinges upon the surface of the material as shown in Figure 3.19. This high energy beam ejects constituent ions from the surface of the

material. These ejected ions are then analyzed with mass spectrometers and the composition of the metal surface layer is therefore determined.

Cesium and oxygen ions in the primary beam bombarding the surface of specimens, a square crater with 200nm x 200nm was formed as shown in Figure 3.20. In order to give results as a function of depth rather than time, Alpha-Step (α-Step 500) techniques are used as shown in Figure 3.20. The specimen is located on the table and moved into position under the stylus and then the sample slowly approaches the stylus. Once the stylus has scanned a sample surface, it is then retracted. The image of the crater is brought into focus to measure its depth; the shape of the crater is a square 200nm x 200nm, (Four holes in the corners used to indicate position of square crater as shown in Figure 3.20). However, since the crater is square only a small round circle at the centre of the square crater was measured to avoid detect the edges of a profile artifact.

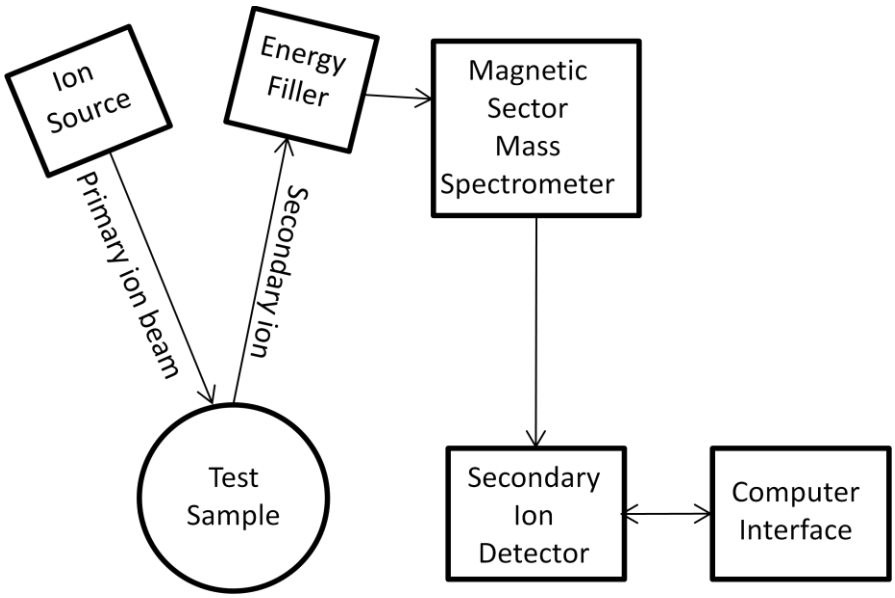

Figure 3.19 Diagram of SIMS-IMS-GEO Model (modified from [54])

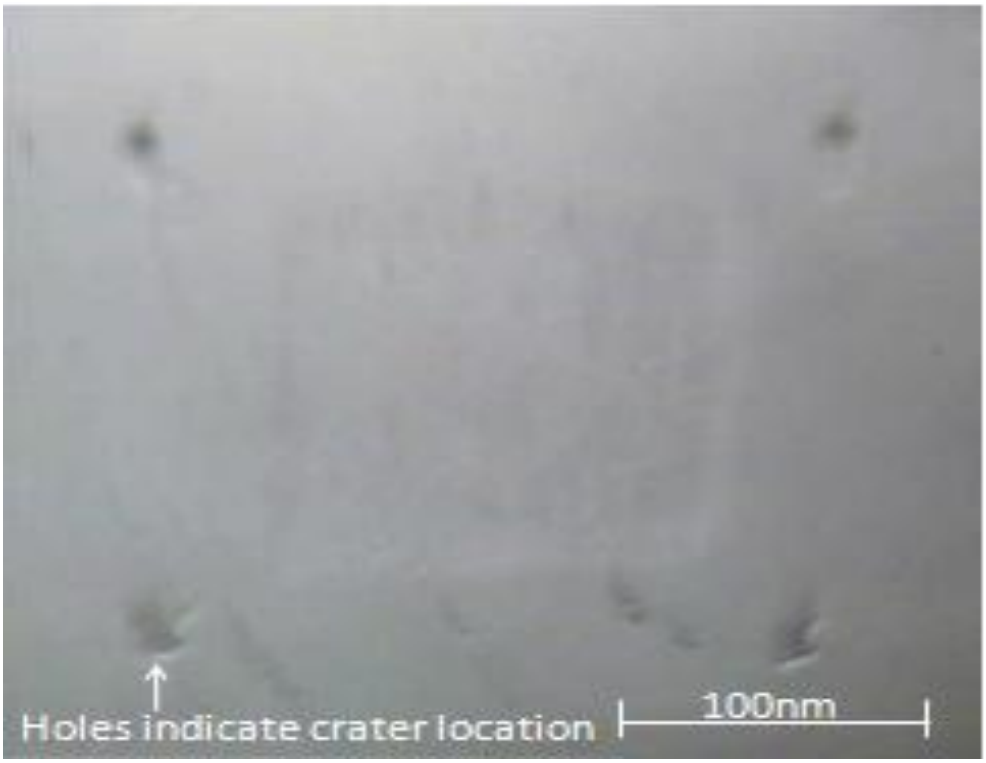

Figure 3.20 Alpha Step 500 Profiler micrograph after surface being bombarded by the primary beam using SIMS

4 Results and Discussion

Tensile, hardness, fatigue, corrosion-fatigue test data, microstructural characterization and surface analysis using several techniques such as Optical Microscopy, SEM, AES, and SIMS were obtained by the procedures outlined in Chapter 3. Results and discussions from these tests are included in the following sections. Notable trends and analysis of the data are included in this Chapter.

4.1 Tensile Strength

Tensile properties of the three nickel alloys were determined to provide data for establishing initial conditions for the fatigue tests and to ensure that the strength properties of various batches of material could be reproduced. Since different batches of as-received material could be supplied with various degrees of cold work, it was decided to develop an annealing procedure to ensure that the fatigue properties of the three materials could be both reproduced and better compared.

Specimens were annealed at 1000C^{o} for 1, 2, and 4 hours and the tensile properties determined. The stress strain curves for the as-received alloys and those for the alloy specimens annealed for 1, 2, and 4 hours are shown in Figure 4.1 to Figure 4.4 respectively. The tensile properties are summarized in Table 4.1 to Table 4.4.

Examination of Figure 4.2 to Figure 4.4, and Table 4.2 to Table 4.4 shows that the mechanical properties of the three alloys annealed for 1 hour were essentially identical to the properties of the alloys annealed for 2 and 4 hours. It was therefore decided to use a 1 hour anneal at 1000C^{o} as a standard heat treatment for all the test specimens.

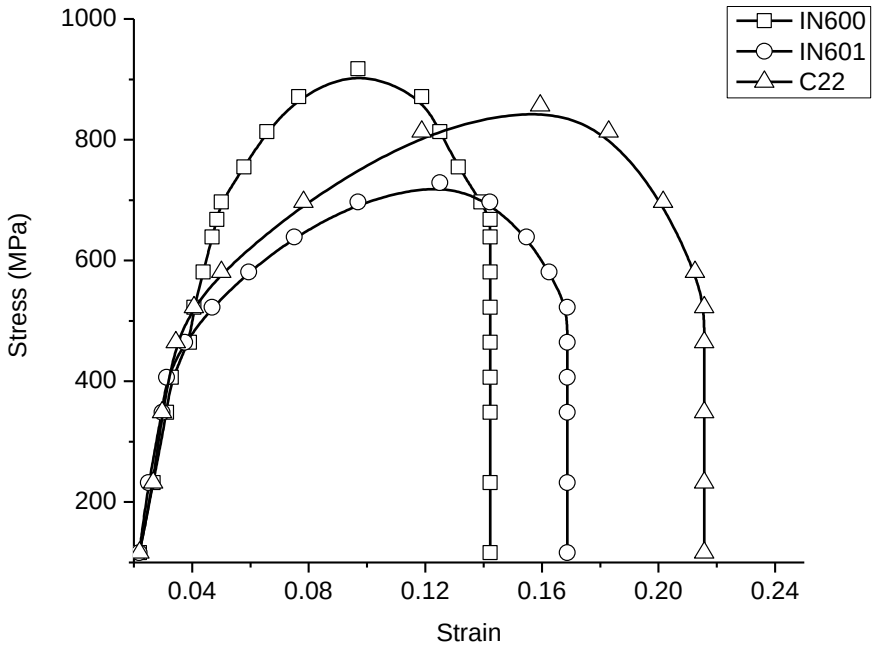

Figure 4.1 Stress strain curves of as-received alloys IN600, IN601 and C22

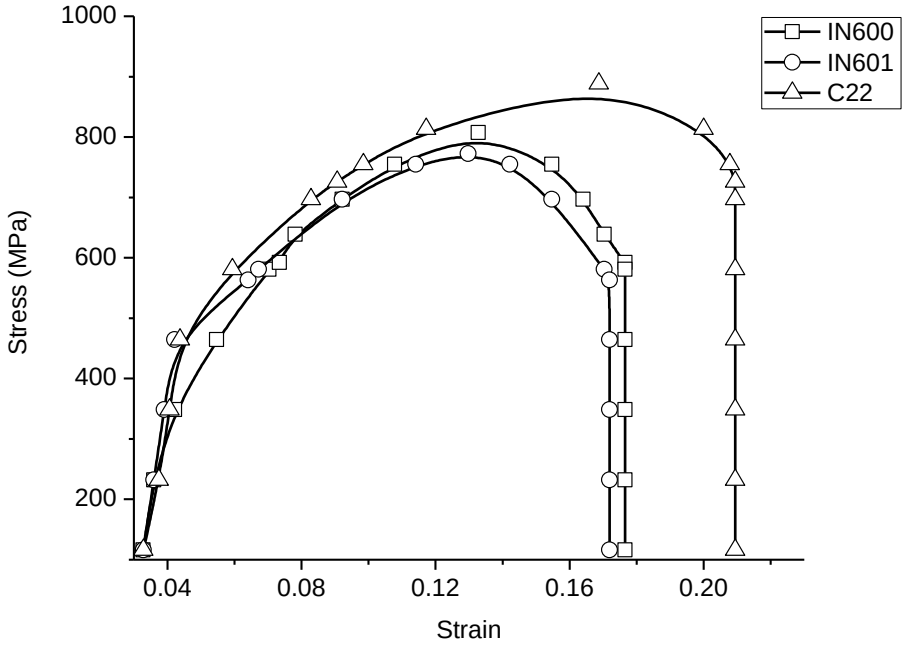

Figure 4.2 Stress strain curves of IN600, IN601 and C22 annealed for 1 hr at 1000C^{o}

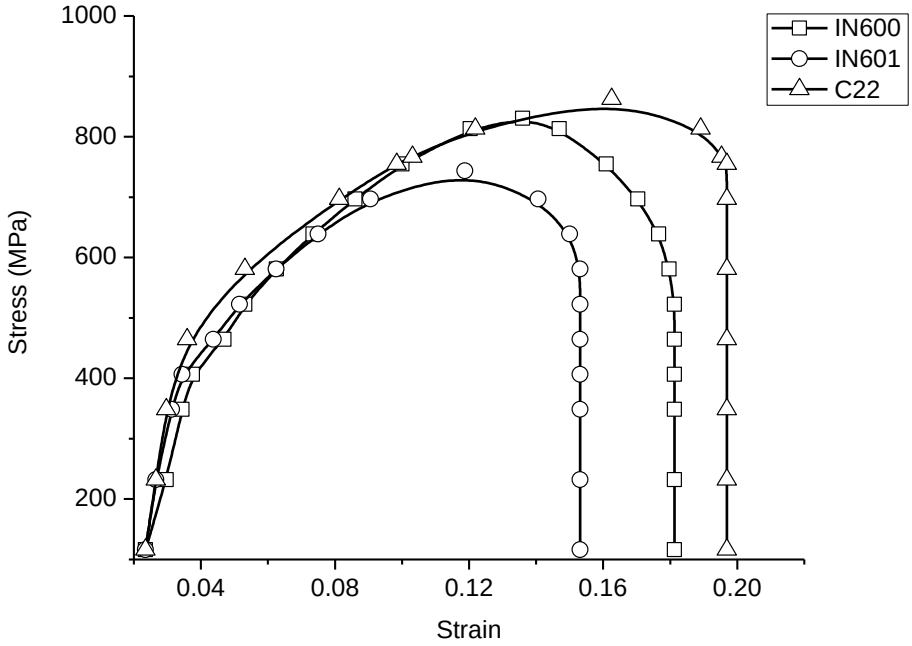

Figure 4.3 Stress strain curves of IN600, IN601 and C22 annealed for 2 hr at 1000C^{o}

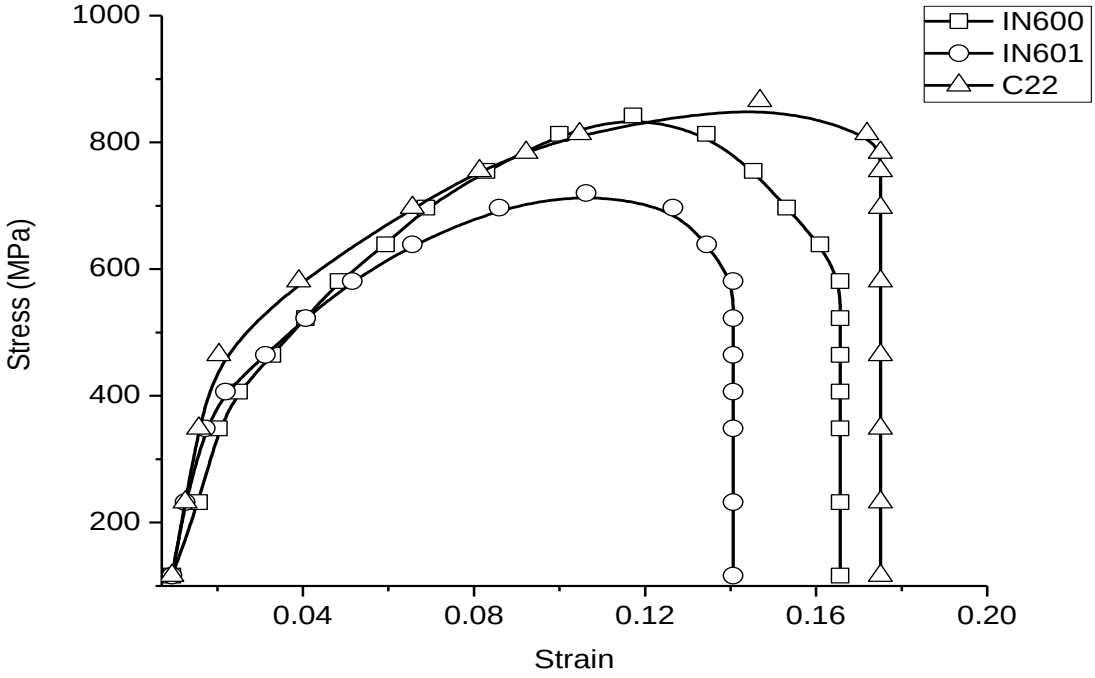

Figure 4.4 Stress strain curves of IN600, IN601 and C22 annealed for 4 hr at 1000C^{o}

Table 4.1 Mechanical properties of alloys in as received conditions

Alloy	σ_{YS} MPa	σ_{UTS} MPa	% Elongation
IN600	430	900	14
IN601	450	725	17
C22	450	850	22

Table 4.2 Mechanical properties of alloys annealed for 1h at 1000C^{o}

Alloy	σ_{YS} MPa	σ_{UTS} MPa	% Elongation
IN600	350	790	18
IN601	450	780	17
C22	450	850	22

Table 4.3 Mechanical properties of alloys annealed for 2 h at 1000C^{o}

Alloy	σ_{YS} MPa	σ_{UTS} MPa	% Elongation
IN600	400	825	18
IN601	400	725	16
C22	450	850	20

Table 4.4 Mechanical properties of alloys annealed for 4 hs at 1000C^{o}

Alloy	σ_{YS} MPa	σ_{UTS} MPa	% Elongation
IN600	400	825	17
IN601	400	700	14
C22	450	850	18

4.2 Electrochemical Behavior

4.2.1 Results

Cyclic potentiodynamic tests for the three Ni-Cr based alloys were conducted in three corrosive environments, 3.5 wt. % NaCl solution at pH = 7.0, concentrated HCl at pH = 0.0 and 10 wt. % $FeCl_3$ solution at pH = 0.0. Figure 4.5 to Figure 4.13 show nine potentiodynamic polarization scans of the three alloys grouped by the type of corrosive solution. Figure 4.5 to Figure 4.7 show the cyclic behavior of the three alloys in 3.5 wt. % NaCl solution. All of the alloys show a distinct passive region with a current density in the range 10^3 nA/cm^2 to 10^4 nA/cm^2. Both IN600 and IN601 exhibited a small amount of pitting and repassivation in the passive region as shown by the slight current increases as pitting initiates followed by a decrease in current as repassivation occurs (Figure 4.5 and Figure 4.6). The alloy C22 (Figure 4.7) showed no evidence of pitting during the passive region that started at -0.2 V followed by the initiation of oxide film breakdown and pitting at 0.6 V. The large hysteresis of the cyclic polarization curves for IN600 and IN601 (Figures. 4.5 and 4.6) indicate a susceptibility to crevice corrosion for these alloys in 3.5 % NaCl solution, whereas the complete absence of hysteresis for alloy C22 indicates resistance to crevice corrosion.

Figure 4.8 to Figure 4.10 show the three alloys tested in hydrochloric acid solution at pH = 0.0. Both IN600 and IN601 alloys exhibit active behavior with no indication of a passive region (Figures. 4.8 and 4.9).

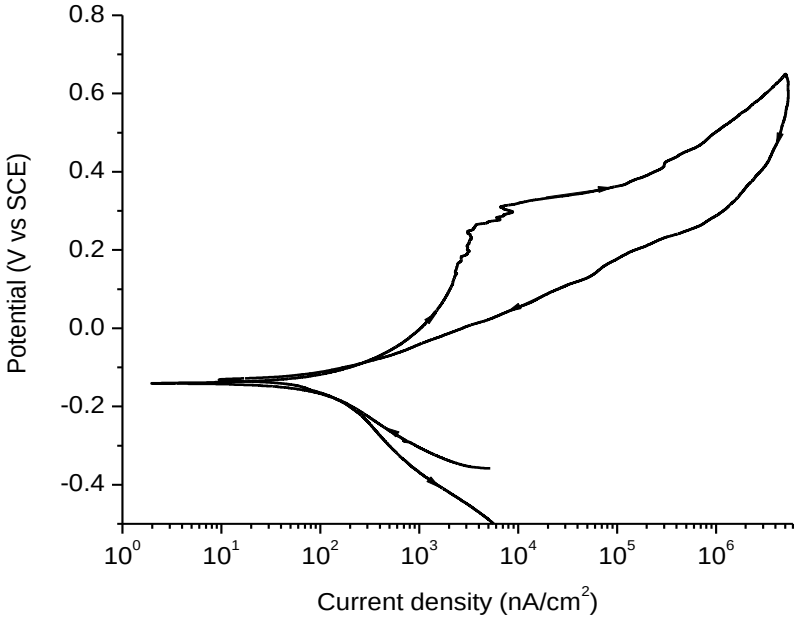

Figure 4.5 Potentiodynamic curve of IN600 in 3.5%NaCl solution at pH 7.0

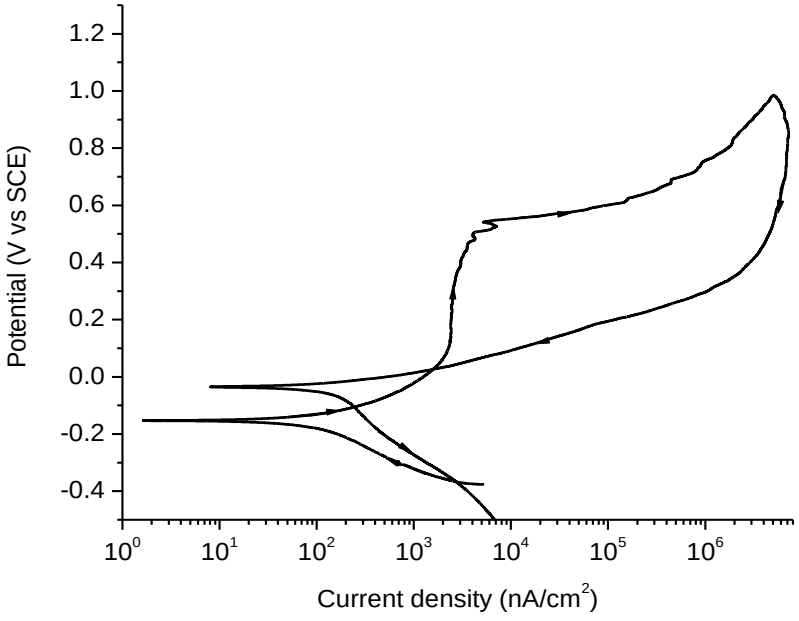

Figure 4.6 Potentiodynamic curve of IN601 in 3.5%NaCl solution at pH 7.0

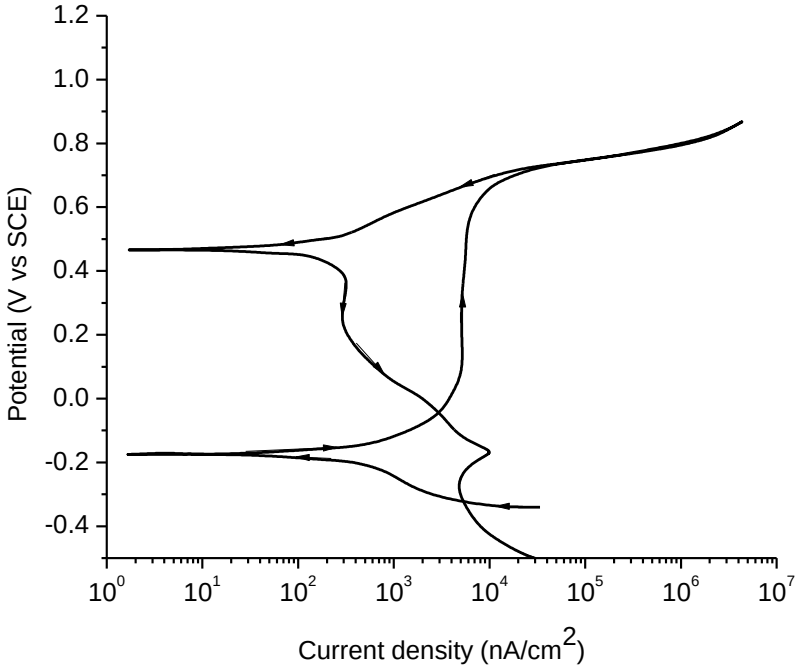

Figure 4.7 Potentiodynamic curve of C22 in 3.5%NaCl solution at pH 7.0

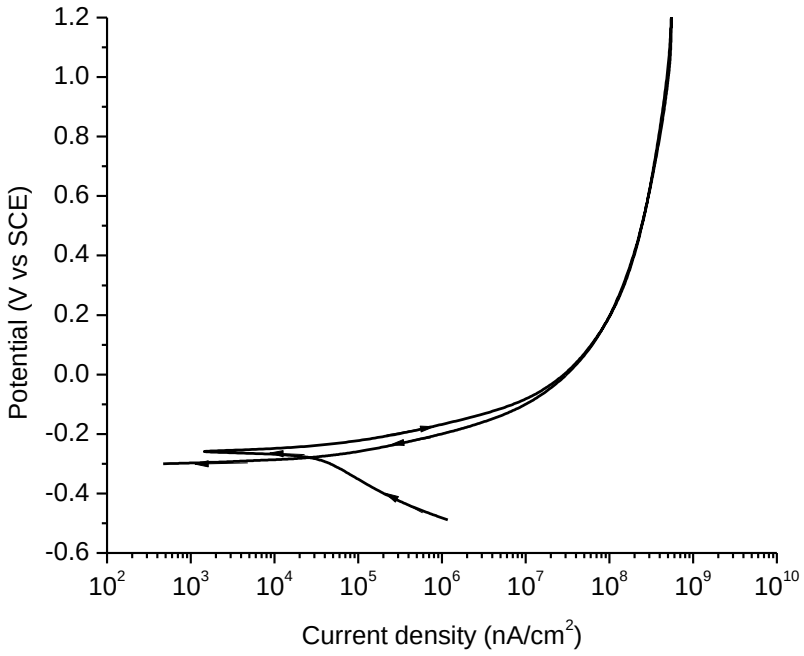

Figure 4.8 Potentiodynamic curve of IN600 in HCl solution at pH 0.0

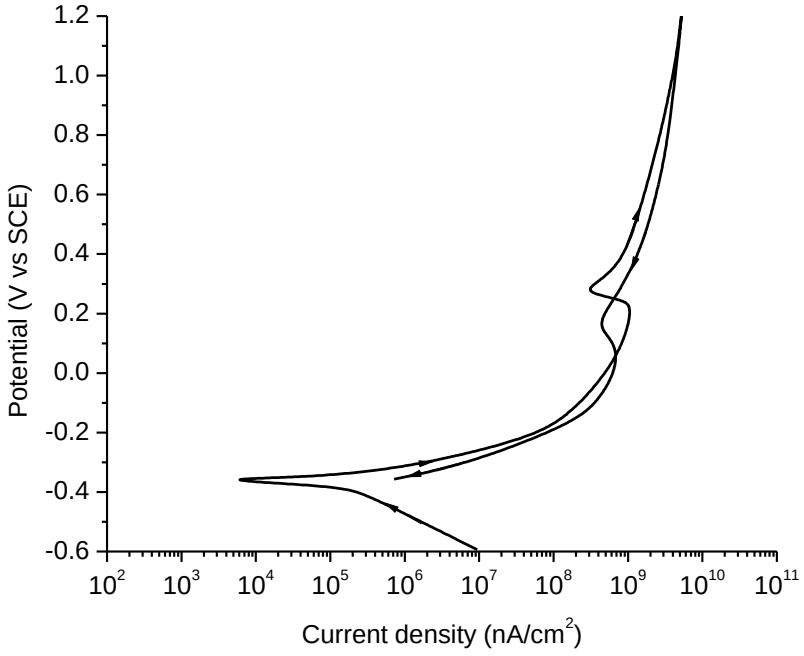

Figure 4.9 Potentiodynamic curve of IN601 in HCl solution at pH 0.0

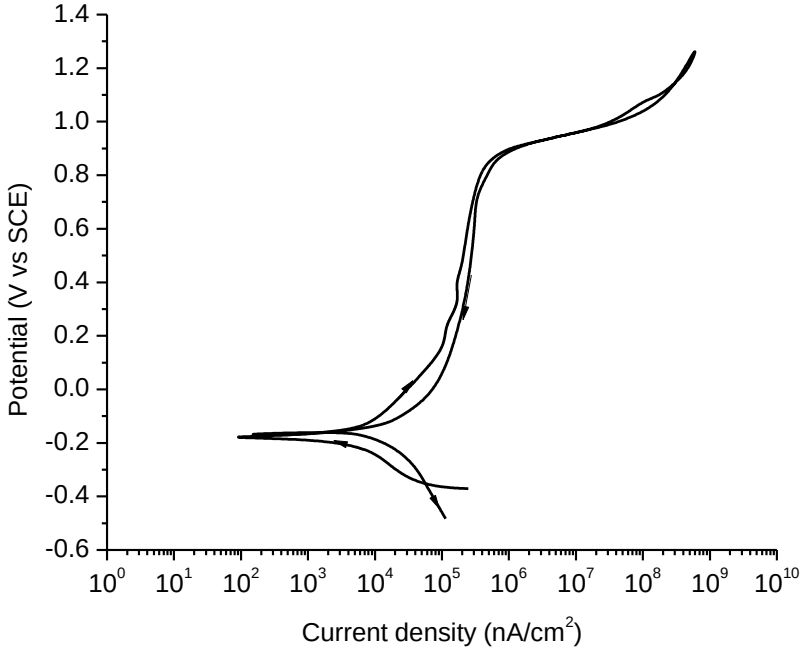

Figure 4.10 Potentiodynamic curve of C22 in HCl solution at pH 0.0

Alloy C22 in HCl at pH = 0.0 exhibited passive behavior with the passive region extending from 0.0 V to 0.8 V with breakdown occurring near 0.8 V (Figure 4.10). The cyclic polarization curve (Fig. 4.10) exhibited very small hysteresis indicating good resistance to crevice corrosion in concentrated HCl at pH = 0.0.

Figure 4.11 to Figure 4.13 show cyclic polarization curves for the three alloys tested in 10 wt % $FeCl_3$ solution. IN600 alloy (Figure 4.11) shows active behavior and no indication of a passive region. IN601 alloy (Figure 4.12) exhibits passive behavior with a passive current density of about 10^5 nA/cm^2 and the passive region extending from about 0.1 V to 0.6 V with breakdown occurring at about 0.6 V at slightly higher than, the passive region starting at 0.1 V and breakdown at 0.6 V. The polarization curve for IN601 in 10 wt % $FeCl_3$ solution exhibits film breakdown followed by repassivation in

the middle of the passive region at about 0.3 V. Further, the large amount of hysteresis in the cyclic polarization curve indicates a susceptibility to crevice corrosion for IN601 in in 10 wt % $FeCl_3$ solution.

Alloy C22 in 10 wt % $FeCl_3$ solution (Figure 4.13) exhibits passive behavior, the passive region extending from the rest potential of about -0.1 V to the breakdown potential of about 0.6 V. The passive current density was about 3×10^3 nA/cm^2.

The cyclic polarization curves for alloy C22 in 10 wt % $FeCl_3$ solution (Figure 4.13) exhibits a very small hysteresis indicating resistance to crevice corrosion in this solution.

Alloy C22 exhibited very little or no hysteresis when tested in all three solutions, as shown in Figure 4.7, Figure 4.10 and Figure 4.13, indicating that alloy C22 is resistant to crevice corrosion in all the solutions tested. By contrast, alloys IN600 and IN601, with no Mo content exhibited large hysteresis indicating a susceptibility to crevice corrosion when subjected to a 3.5 wt. % NaCl solution (Figure 4.5 and Figure 4.6). It should be noted that the 3.5 wt. % NaCl solution, the concentrated HCl and 10 wt. % $FeCl_3$ solutions represent extremes for corrosion solutions. The 3.5 wt. % NaCl solution is a mild corrodent whereas aluminum, copper and steel tested in 10 wt. % $FeCl_3$ solution showed corrosion rates of over 160 mm/year [55].

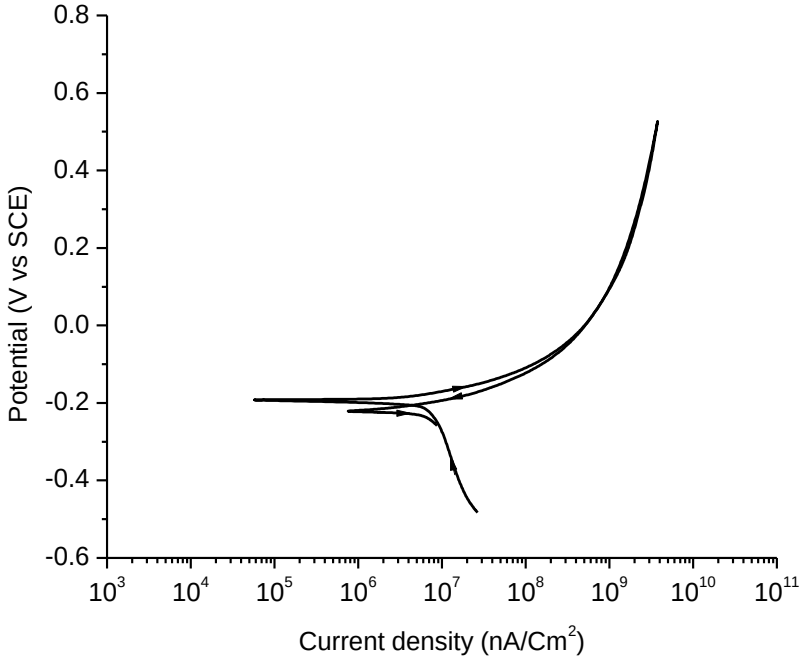

Figure 4.11 Potentiodynamic curve of IN600 in $FeCl_3$ solution at pH 0.0

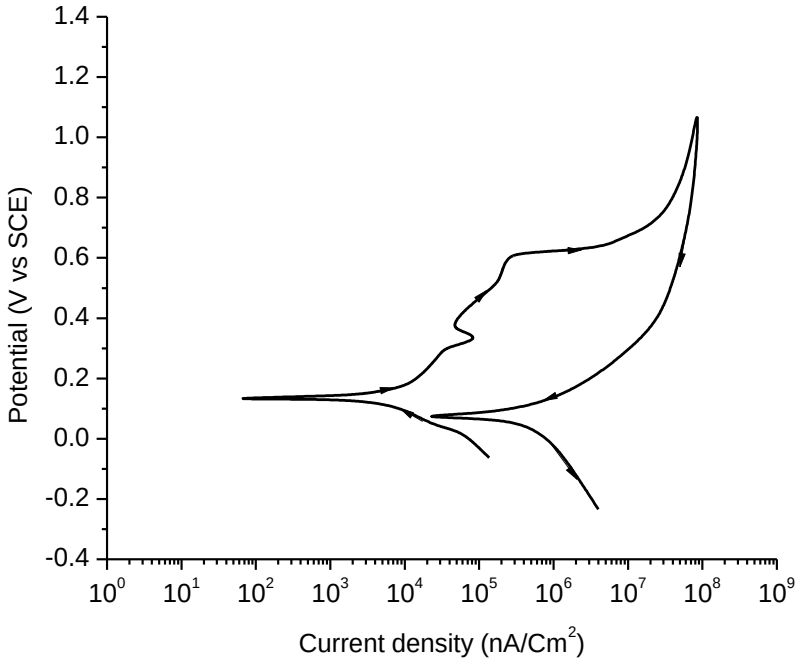

Figure 4.12 Potentiodynamic curve of IN601 in 10%$FeCl_3$ solution at pH 0.0

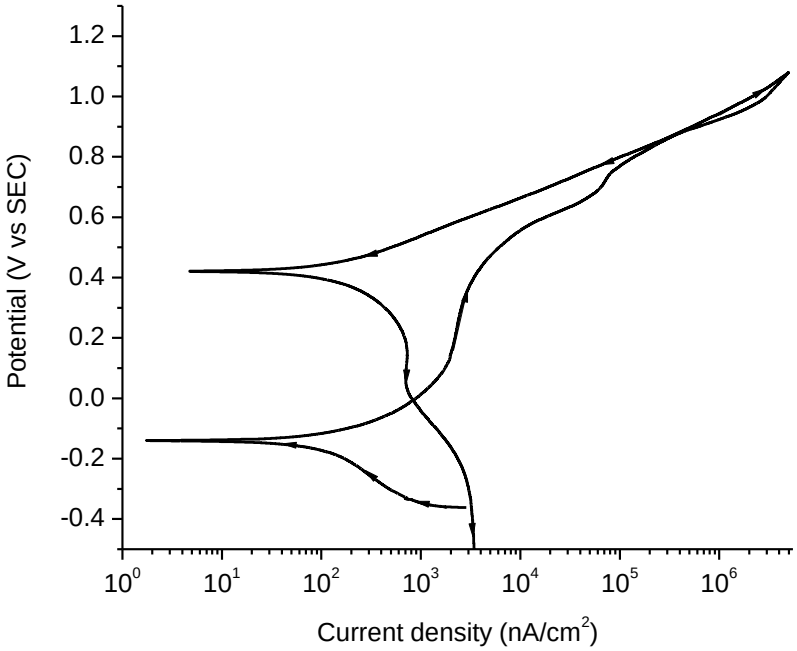

Figure 4.13 Potentiodynamic curve of C22 in 10%$FeCl_3$ solution at pH 0.0

The data from the cycle polarization curve for the three nickel based alloys in the three solutions are summarized in Table 4.5 to 4.7. The data for the calculation of corrosion rate and calculated corrosion rates are presented in Table 4.8 to 4.13.

4.2.2 Discussion

The main observations from this study are that Cr is responsible for the passive behavior and Mo is responsible for repassivation after breakdown occurs. This trend is illustrated in Figure 4.5 to Figure 4.13. The passive behavior of the chromium containing alloys indicates that passive corrosion behavior is primarily controlled by the presence of chromium, which forms a chromium oxide film that protects the surface. A minimum Cr concentration in the alloy, approximately 12% [56], is required before complete

passivation of the surface is seen. Above this threshold, chromium oxide completely passivates the surface. All three alloys in this study have Cr concentrations above 12%.

The formation of a passive film on the surface occurred in the three alloys tested in three corrosive solutions. When molybdenum precipitates on the surface as an oxide within a pit, this inhibits further pitting and hinders the intensification of the pit [56,57]. The molybdenum inhibits corrosion by forming a molybdonate [57,58]. Modification of the local solution occurs by reducing the concentration of the electrolytes. There is some evidence that molybdenum decreases the passive corrosion rate of the alloy [58] thus decreasing the amount of dissolved metallic ions that can lead to hydrolysis and acidification.

Table 4.5 Summary of electrochemical data for the three nickel base alloys in 3.5 % NaCl solution at pH = 7.0

Alloy	Rest Potential (V vs SCE)	Pitting Potential (Volts vs SCE)	Passive Current Density (nA/cm^2)	Corrosion Current (nA/cm^2)	Corrosion Rate (mm/Year)	Polyriz. Type	Amount of Hysteresis	Protect potential (V vs SCE)
IN600	- 0.24	0.23	1930	25	0.003	Passive	Large	-0.063
IN601	- 0.15	0.34	2000	102	0.001	Passive	Large	-0.003
C22	- 0.15	0.60	2300	250	0.003	Passive	None	0.60

Table 4.6 Summary of electrochemical data for the three nickel base alloys in concentrated HCl at pH = 0.0

Alloy	Rest Potential (V vs SCE)	Pitting Potential (Volts vs SCE)	Passive Current Density (nA/cm^2)	Corrosion Current (nA/cm^2)	Corrosion Rate (mm/Year)	Polyriz. Type	Amount of Hysteresis	Protect Potential (V vs SCE)
IN600	- 0.28	NA	NA	1.2×10^4	0.131	Active	NA	NA
IN601	- 0.28	NA	NA	1.1×10^4	0.12	Active	NA	NA
C22	- 0.11	0.84	4.8×10^3	9.0×10^2	0.010	Passive	None	0.84

Table 4.7 Summary of electrochemical data for the three nickel base alloys in 10 wt. % $FeCl_3$ at pH = 0.0

Alloy	Rest Potential (V vs SCE)	Pitting Potential (Volts vs SCE)	Passive Current Density (nA/cm^2)	Corrosion Current (nA/cm^2)	Corrosion Rate (mm/Year)	Polyriz. Type	Amount of Hysteresis	Protect potential (V vs SCE)
IN600	- 0.242	NA	NA	7.0×10^6	76.7	Active	NA	NA
IN601	- 0.091	0.314	3600	580	0.004	Passive	Large	0.14
C22	0.030	0.890	1.10×10^4	70	0.0008	Passive	None	0.830

Table 4.8 Properties of IN600 for the calculation of corrosion rates

Element	Composition (Wt.%)	Atomic Wt. (g/mole)	(At.%)	Composition (At.%)	(At. Wt.)	Density (g/cm^3)	Density Conc.	Oxidation state (Electrons)	Electron Contribution
Ni	75.72	58.93	1.2849	73.46	43.29	8.9	6.5380	2	1.47
Cr	15.50	52.00	0.2981	17.04	8.86	7.2	1.2270	2	0.34
Fe	8.00	55.85	0.1432	8.19	4.57	7.86	0.6437	2	0.16
Mn	0.50	54.94	0.0091	0.52	0.29	7.2	0.0375	2	0.01
Si	0.20	28.09	0.0071	0.41	0.11	2.33	0.0095	4	0.02
C	0.08	12.01	0.0067	0.38	0.05	2.25	0.0086	4	0.02
Total/Average	100.00	NA	NA	100	57.17	NA	8.46	NA	2.02

Table 4.9 Calculation of corrosion rates for IN600

Solution	$I_{Corr.}$ (nA/cm^2)	Corrosion rate (mm/year)
3.5 % NaCl at pH 7.0	25	0.0003
HCl at pH 0.0	1.20E+04	0.13
10%$FeCl_3$ at pH 0.0	7.00E+06	76.7

Table 4.10 Properties of IN601 for the calculation of corrosion rates

Element	Composition (Wt.%)	Atomic Wt. (g/mole)	(At.%)	Composition (At.%)	(At. Wt.)	Density (g/cm^3)	Density Conc.	Oxidation state (Electrons)	Electron Contribution
Ni	60.72	58.93	1.0304	57.25	33.73	8.9	5.0949	2	1.45
Cr	23.00	52.00	0.4423	24.57	12.78	7.2	1.7693	2	0.44
Fe	14.10	55.85	0.2525	14.03	7.83	7.86	1.1025	2	0.280
Mn	0.50	54.94	0.0091	0.51	0.28	7.2	0.0364	2	0.010
Al	1.40	26.98	0.0519	2.88	0.78	2.7	0.0778	3	0.086
Si	0.20	28.09	0.0071	0.40	0.11	2.33	0.0092	4	0.016
C	0.08	12.01	0.0067	0.37	0.04	2.25	0.0083	4	0.015
Total/Average	100.00	NA	NA	100	55.56	NA	8.10	NA	2.042

Table 4.11 Calculation of corrosion rates for IN601

Solution	$I_{Corr.}$ (nA/cm^2)	Corrosion rate (mm/ year)
3.5 % NaCl at pH 7.0	102	0.001
HCl at pH 0.0	1.1×10^4	0.12
10%$FeCl_3$ at pH 0.0	5.8×10^2	0.006

Table 4.12 Properties of C22 for the calculation of corrosion rates

Element	Composition (Wt.%)	Atomic Wt. (g/mole)	(At.%)	Composition (At.%)	(At. Wt.)	Density (g/cm^3)	Density Conc.	Oxidation state (Electrons)	Electron Contribution
Ni	50.69	58.93	0.8602	52.45	30.91	8.9	4.6684	2	1.05
Cr	21.50	52.00	0.4135	25.21	13.11	7.2	1.8153	2	0.50
Co	2.50	55.85	0.0448	2.73	1.52	8.9	0.2429	2	0.05
Mo	13.50	95.94	0.1407	8.58	8.23	10.2	0.8752	2	0.17
W	4.00	183.85	0.0218	1.33	2.44	19.3	0.2561	2	0.03
Fe	5.50	55.85	0.0985	6.01	3.35	7.86	0.4720	2	0.12
Mn	1.00	54.94	0.0182	1.11	0.61	7.2	0.0799	2	0.02
Si	1.00	28.09	0.0356	2.17	0.61	2.33	0.0506	4	0.09
C	0.01	12.01	0.0008	0.05	0.01	2.25	0.0011	4	0.00
V	0.30	50.94	0.0059	0.36	0.18	5.96	0.014	2	0.01
Total/Average	100.00	NA	NA	100	60.98	NA	8.48	NA	2.04

Table 4.13 Calculation of corrosion rates for C22

Solution	$I_{Corr.}$ (nA/cm^2)	Corrosion rate (mm/year)
3.5 % NaCl at pH 7.0	250	0.003
HCl at pH 0.0	900	0.010
10%$FeCl_3$ at pH 0.0	70	0.0008

This, in turn, increases the time it takes to reach a critical pH to break down the passive film. In stainless steels, it has been found that Mo can complex with sulfur removing it from the surface, thus preventing pit formation, and there is some evidence for the interaction of Mo and Cl, which can form a film protecting the surface and prevent the breakdown of the passive film due to the aggressive Cl^- ion [59-61]. It has been suggested that this takes place by Mo enriching at nucleation sites on the metal surface and slowing the propagation of the pits, or by forming an enriched alloy at the stainless steel surface after the preferential dissolution of iron in stainless steels [41,62,63]. Preferential dissolution of one alloy component can also lead to a restructuring of the surface into an alloy with increased corrosion resistance [1,57,58]. This suggests that molybdenum has very little effect on the breakdown of the passive film, and thus localized pitting resistance is due to chromium. This agrees with finding by Wanklyn [61] in a study of stainless steels 431, 316, and alloy 625 in KCl and HCl solutions. It was found that only Mo inhibited pitting, either by shifting the potential of the crevice or pit negatively, or by competing with the diffusion of the Cl^- ion. In stainless steels, the pitting potential is well below the potential for the formation of molybdate. However, [52] showed that for nickel-based alloys, the pitting potential was such that this species could form during pit initiation when the pitting solution was still relatively neutral. Once the pit formed, and began to acidify, the pH of the solution made molybdate thermodynamically unstable, and it would form MoO_2 by the reaction $MoO_4^{2-} + 4H^+ + 2e^- \rightarrow MoO_2 + 2H_2O$.

As the alloy dissolved further, releasing more Cr ions into solution for hydrolysis, the pH would push the reaction to $MoO_2 + 4H^+ + e^- \rightarrow Mo^{3+} + 2H_2O$. Thus, the Mo would inhibit corrosion by reducing the amount of acid in solution, but only temporarily until more hydrolysis occurred. Furthermore, MoO_2 formed in the pit can serve as a physical barrier to pit propagation and

diffusion of species in and out of the pit [58]. Molybdenum oxide formation has been observed in crevices during crevice corrosion experiments on various Ni-Cr-Mo alloys [39]. A specific driving potential must be applied to the alloy to maintain a dissolution rate such that the hydrolysis of chromium exceeds the inhibiting effect of Mo. This driving force would depend on the amount of Mo in the alloy. C22 repassivates as soon as the driving force is removed. This alloy shows variation in its repassivation behavior (Figure 4.7), (Figure 4.10) and (Figure 4.13), suggesting that this is due to a difference of severity of the aggressive solutions. This suggestion is reinforced by the behavior of the alloys in different aggressive solutions. A study comparing IN625 to C276 and C22 with different amount of Cr and Mo found that alloys with more Mo content had a lower passive current density, and were less susceptible to pitting [64]. These results agree with the current study, that the passive current density and susceptibility to pitting depend on Cr and Mo contents. This suggests that the addition of chromium beyond a critical threshold does not significantly improve the corrosion resistance as measured by corrosion rates or breakdown potential. However, addition of the Mo content significantly improves the corrosion resistance and repassivation behavior. Once pitting occurs, the high breakdown potential of nickel alloys allows the formation of an inhibiting molybdate, which slows the propagation of the pit.

In summary, the electrochemical behavior of the three alloys IN600, IN601 and C22 was examined in detail in three electrolyte solutions: 3.5%NaCl, HCl and 10%$FeCl_3$ solutions. Results indicate that Cr is responsible for the passive behavior and Mo is responsible for repassivation after breakdown occurs. The main effect of adding Mo to the alloy is to inhibit the pitting from further propagation as well as to modify the local solution environment by

consuming H^+ ions, thus decreasing the acidity of the pit. The alloy C22 with Mo content exhibited excellent corrosion resistance in the three aggressive solutions.

4.3 Fatigue Behavior

Fatigue testing was first conducted in air to provide a baseline for further fatigue testing. The initial testing in aqueous solutions was done with 3.5 % NaCl solution at pH = 7.0 because of ease of preparation and handling. The results of the initial fatigue testing are presented in Figure 4.14 to Figure 4.16 which are S-N curves. These show that fatigue in 3.5 % wt. NaCl solution had little effect on the fatigue strength of any of the alloys compared to the results for fatigue in air. Further, the fracture surfaces for specimens tested in air showed little difference compared to those specimens tested in air, as shown in Figure 4.17 to Figure 4.22. These are all typical of ductile failure showing no evidence of corrosion. It was therefore concluded that all three alloys had excellent corrosion resistance in 3.5 % NaCl solution even though the cyclic polarization curves for alloys IN600 and IN601 exhibited a large hysteresis indicating a susceptibility to crevice corrosion. A similar study on corrosion fatigue tests for annealed type 316 stainless steel showed the maximum stress level for failure in 0.5 M sodium chloride aqueous solution at pH = 4.2 was one-third lower than in air after a similar number of cycles [65]. These results showed crack initiation resulting from pit formation and crack coalescence was suggested to explain the decrease in the maximum stress level for corrosion fatigue of austenitic, which exhibited passive behavior and generally good corrosion resistance in 0.5 M NaCl solution at pH = 4.2 [65].

This larger difference between corrosion potential and pitting potential for the nickel-based alloys indicates a greater inherent resistance to pitting than for type 316 stainless steel and therefore a comparatively greater inherent resistance to crevice corrosion and reduced fatigue strength [65]. To gain further insight into the corrosion fatigue of nickel-based alloys, fatigue

tests were conducted using more aggressive solutions, concentrated HCl at pH = 0.0 and 10 wt. % $FeCl_3$ solution at pH = 0.0.

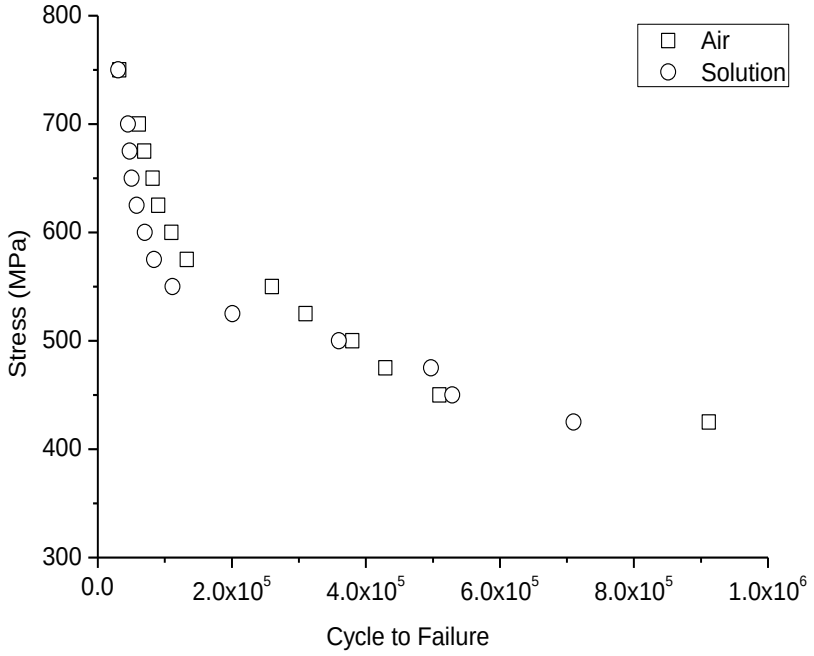

Figure 4.14 Fatigue test of alloy IN600 in air and in 3.5%NaCl at pH 7.0

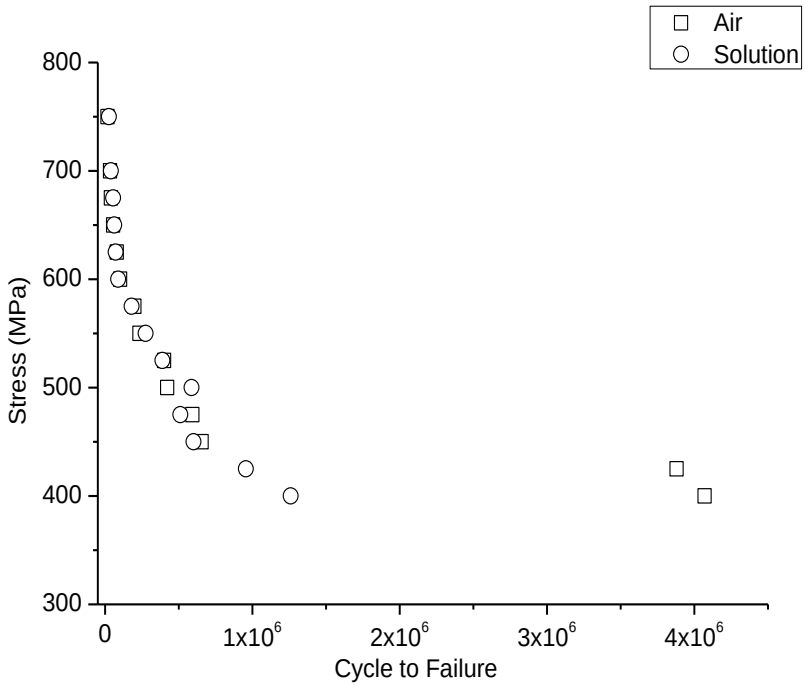

Figure 4.15 Fatigue test of alloy IN601 in air and in 3.5%NaCl at pH 7.0

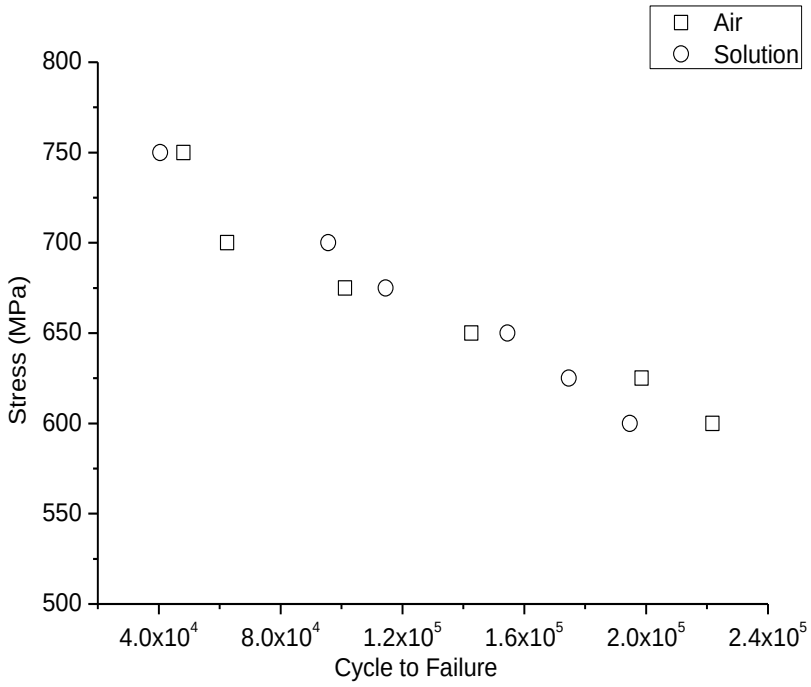

Figure 4.16 Fatigue test of alloy C22 in air and in 3.5%NaCl at pH 7.0

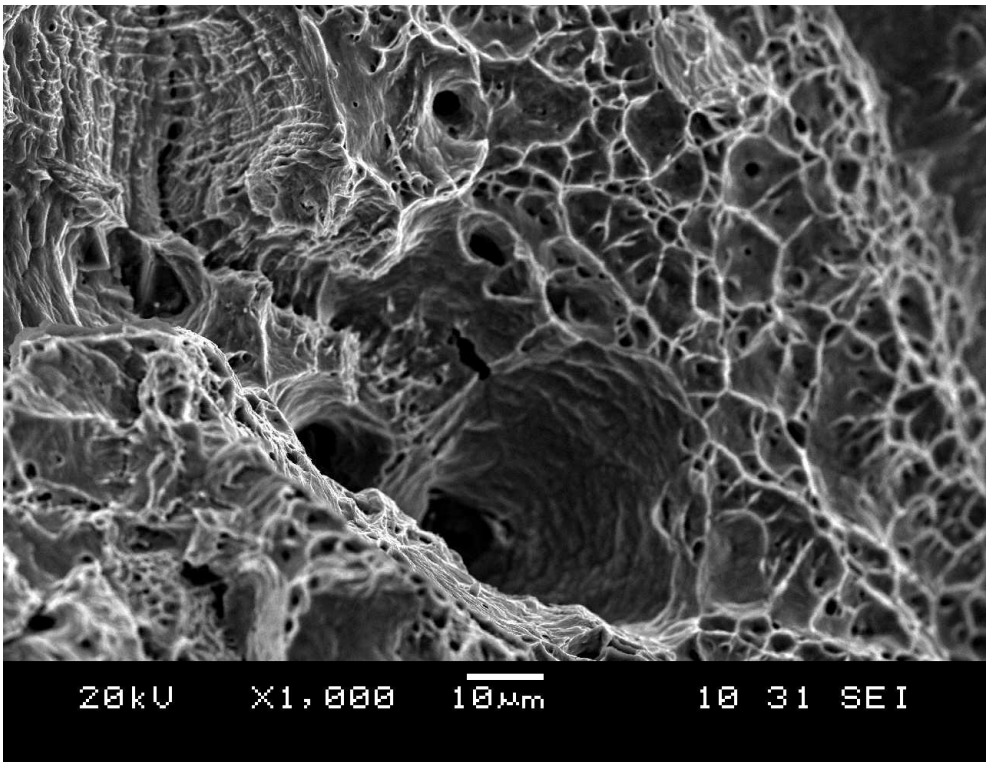

Figure 4.17 Fatigue fracture surface of IN600 in air

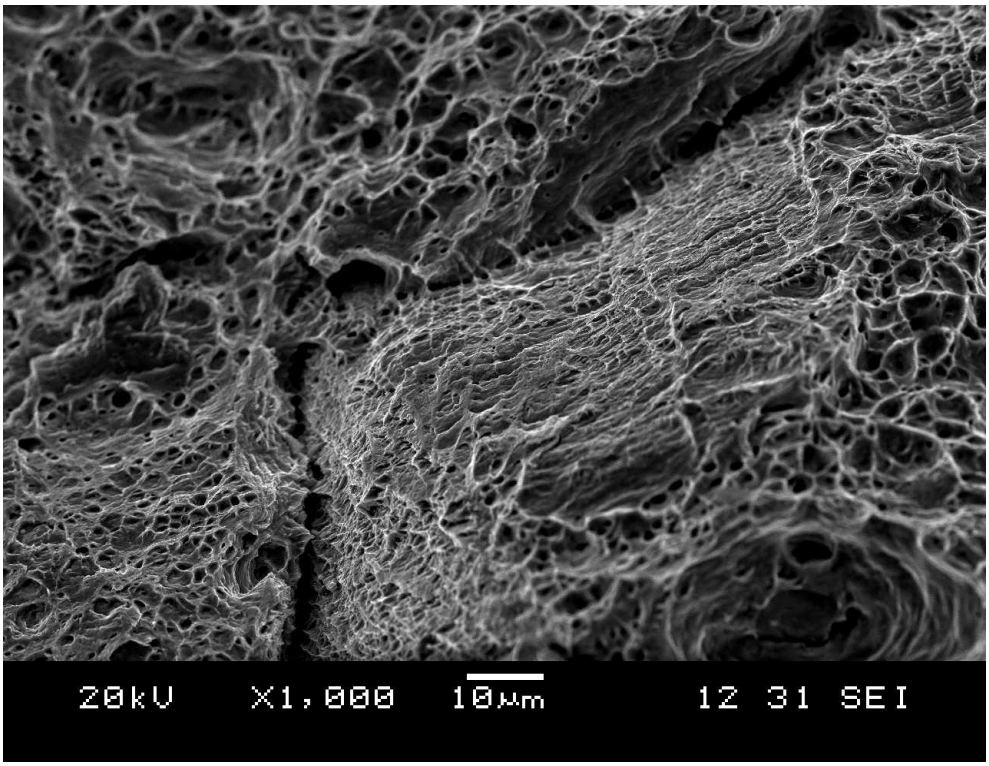

Figure 4.18 Fatigue fracture surface of IN600 in 3.5%NaCl solution at pH = 7.0

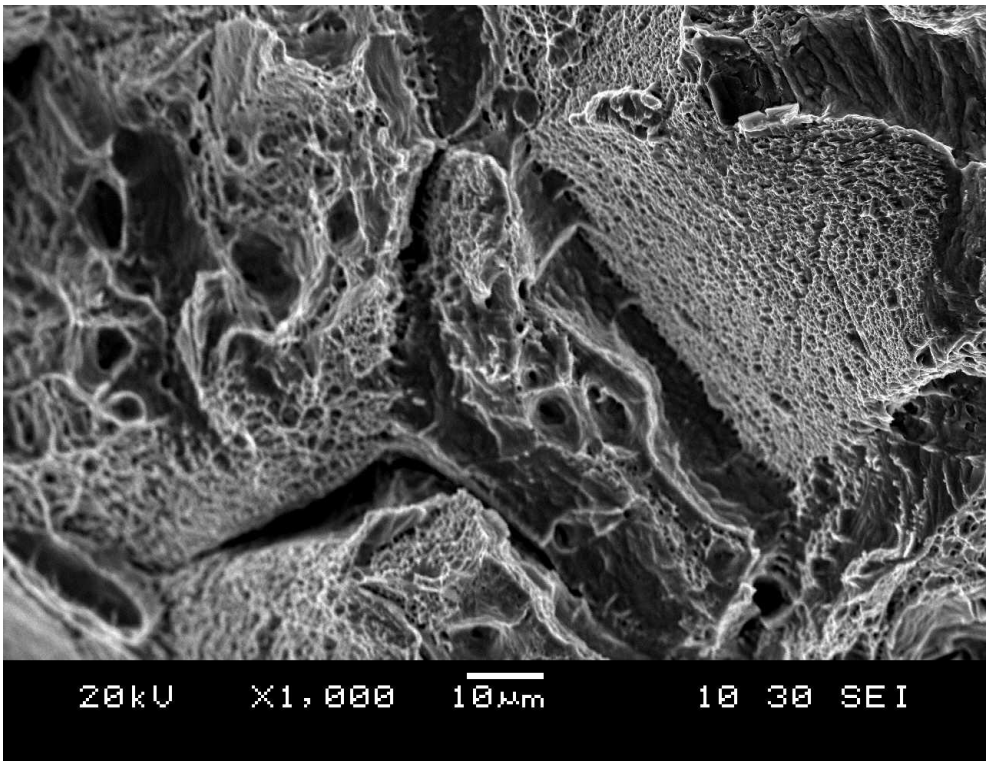

Figure 4.19 Fatigue fracture surface of IN601 in air

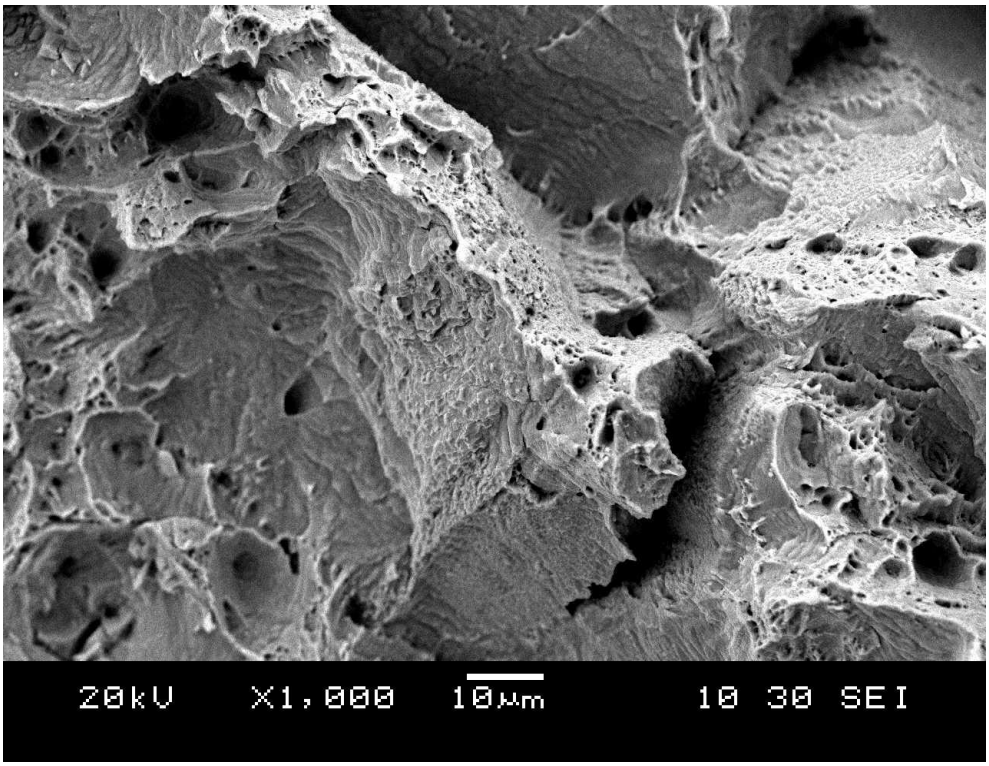

Figure 4.20 Fatigue fracture surface of IN601in 3.5%NaCl solution at pH = 7.0

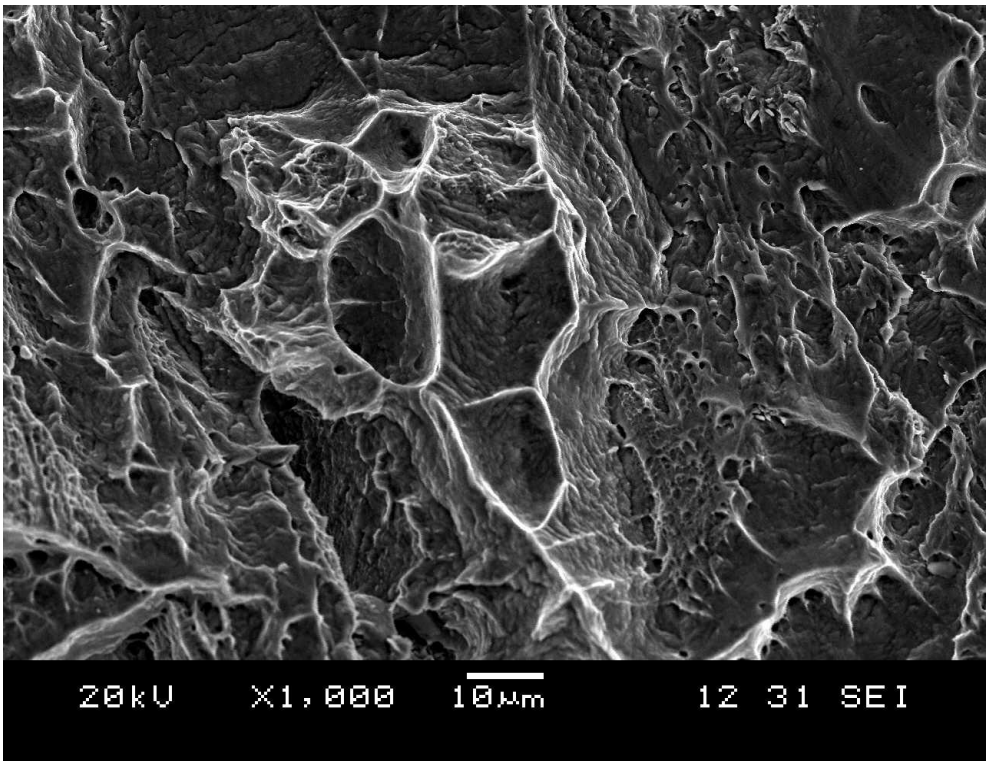

Figure 4.21 Fatigue fracture surface of C22 in air

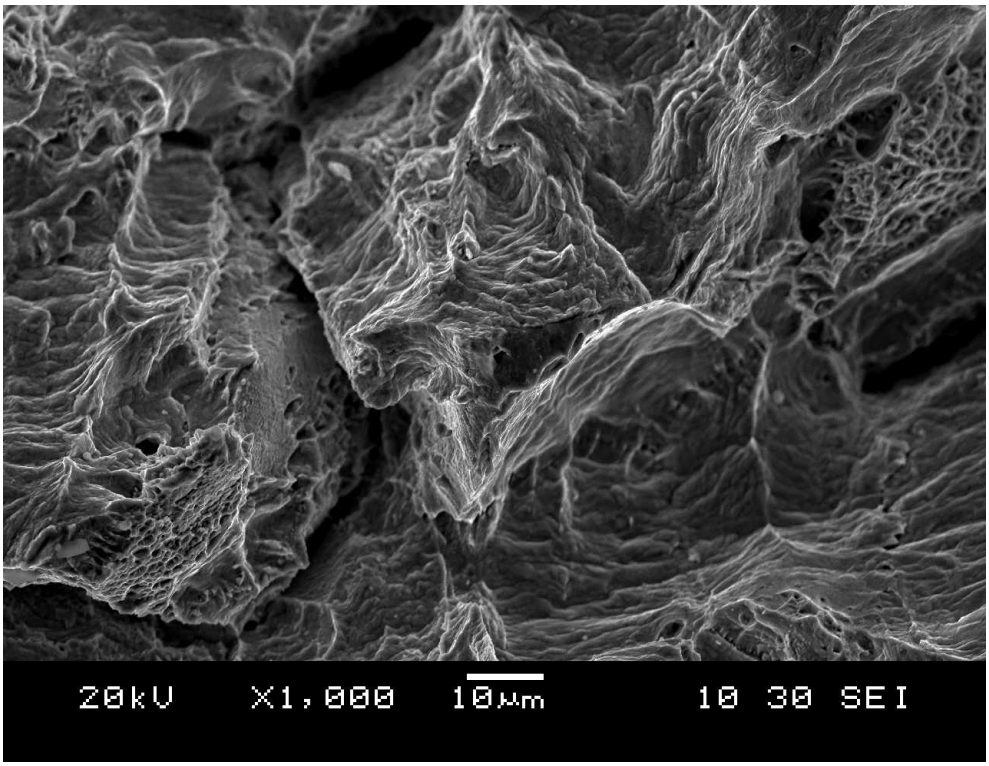

Figure 4.22 Fatigue fracture surface of C22 in NaCl solution at pH = 7.0

Establishment of S-N curves for the three alloys for all aggressive environments would have consumed an inordinate amount of time. Therefore, tests were selected at constant stress level to provide failure in a reasonable amount of time, ranging from several hours to a few days. The stress levels selected were 480 MPa for the IN600 alloy and 532 MPa for the IN601 and C22 alloys. Tests duplicated for each alloy in air and in each environment were conducted to ensure consistency.

Any reduced fatigue strength due to a corrosive environment could be a result of one of two factors or a combination of both. Firstly, a corrosive environment would likely cause damage and would lower the fatigue life. Secondly, the generally held view of corrosion fatigue is that surface pits are generated at crevices where slip bands exit on the specimen surface and thus fatigue is a mandatory precursor for corrosion fatigue failure. Therefore, tests were conducted on specimens that had been pre-corroded in the aqueous environment and then fatigued in air. These results were then compared with results for fatigue in air alone and for results obtained by fatigue testing in the corrosive aqueous environments. The results of these fatigue tests are presented in Tables 4.14 to 4.15 and Figure 4.23 to Figure 4.28.

The fatigue results for IN600 show that in general, the fatigue life for specimens fatigued in solution is less than that of pre-corroded specimens fatigue tested in air. This suggests that, for IN600, there is an interaction between the environment and the propagating fatigue crack. Pre-corrosion does, however, reduce the fatigue life of specimens tested in air without preceding corrosion.

Table 4.14 shows fatigue results of the three alloys IN600, IN601, and C22 tested at constant stress in air, precorroded and in HCl solution at pH = 0.0, as shown in Figures 4.23, 4.24, and 4.25.

Table 4.14 Corrosion fatigue data cycles to failure in HCl for IN600, IN601 and C22

IN600	Air	PreCorr	Solution	IN601	Air	PreCorr	Solution	C22	Air	PreCorr	Solution
1	808882	128483	85766	1	131463	125110	112400	1	175570	516495	364570
2	393612	91111	75097	2	190753	127112	102535	2	609387	440000	255441
3	1460000	76885	65787	3	132895	142432	133421	3	416000	443220	336431
4	1790000	553278	81288	4	232412	154140	112535	4	176000	617779	251457
5	887000	562586	89927	5	111342	124553	101342	5	528270	335534	155351
6	957654	98676	89762	6	198332	125247	125211	6	610074	367635	300532
7	488866	-	-	-	-	-	-	7	532200	-	-
8	188700	-	-	-	-	-	-	8	645000	-	-
9	201100	-	-	-	-	-	-	9	523000	-	-
10	877551	-	-	-	-	-	-	10	481000	-	-
-	-	-	-	-	-	-	-	11	565000	-	-
-	-	-	-	-	-	-	-	12	687000	-	-
Average	805300	251837	81271		166199	133099	114574		495708	453444	277297

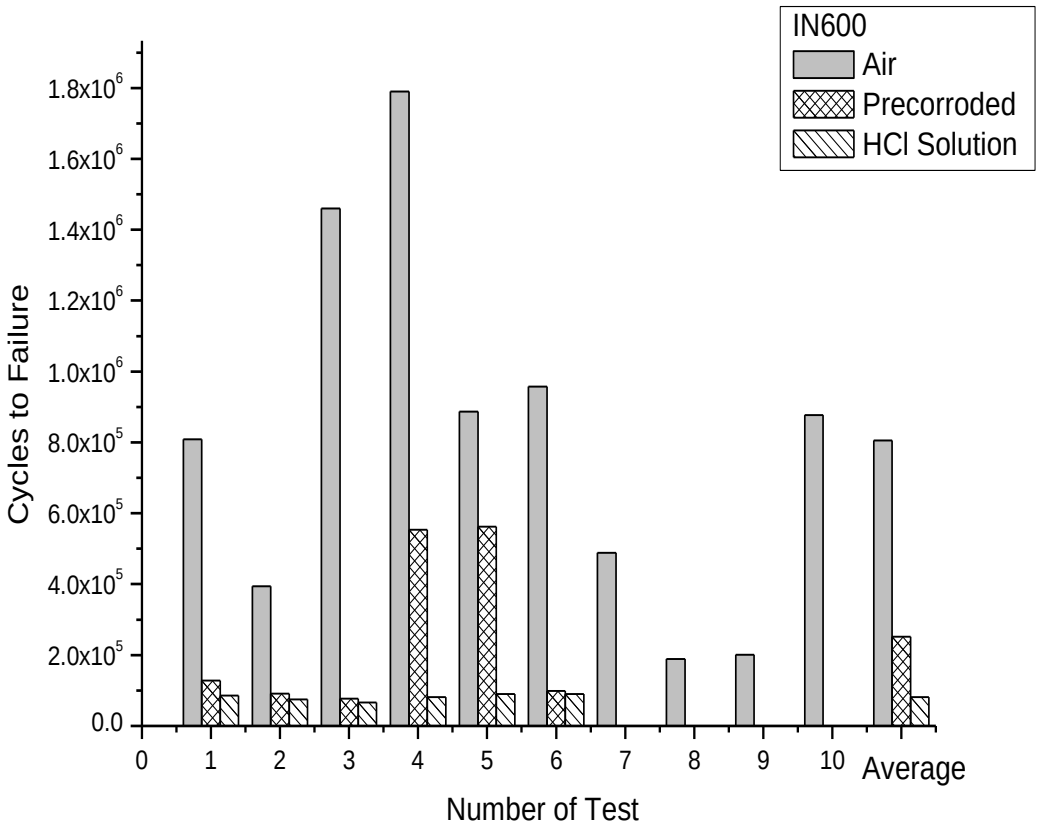

Figure 4.23 Effect of pre-corrosion and a concentrated HCl at pH = 0.0 environment on the fatigue behavior of IN600 at 480 MPa

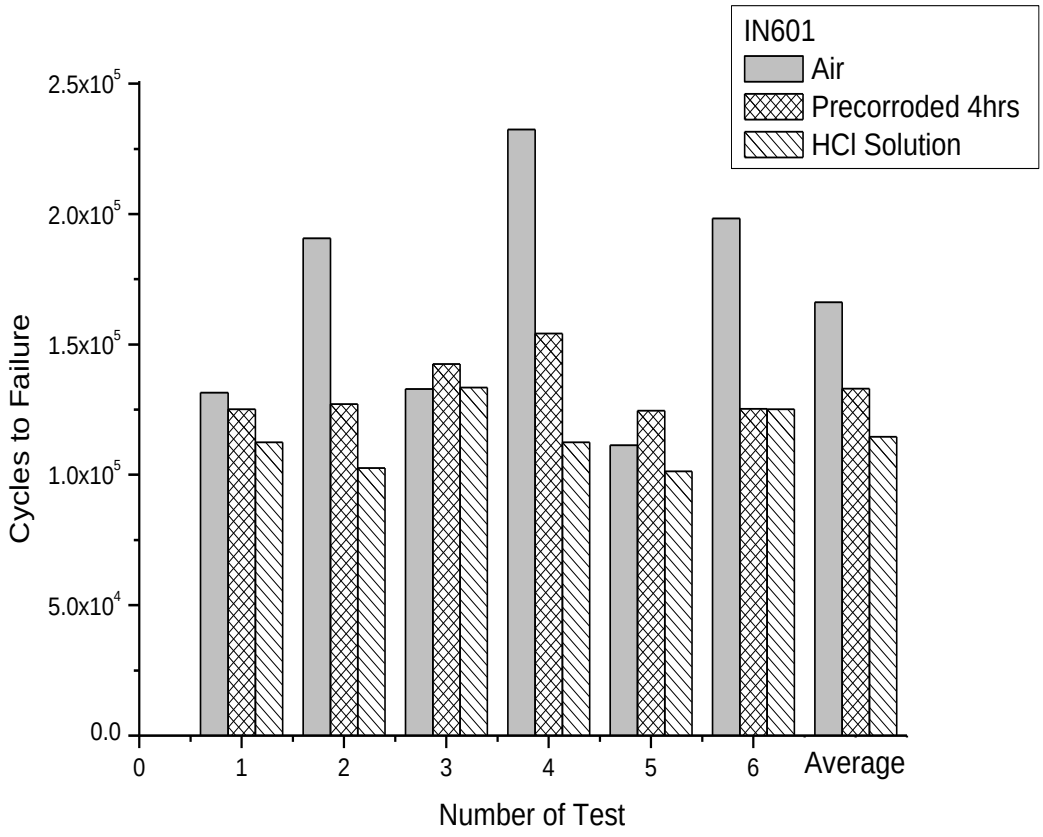

Figure 4.24 Effect of pre-corrosion and a concentrated HCl at pH = 0.0 environment on the fatigue behavior of IN601 at 532 MPa

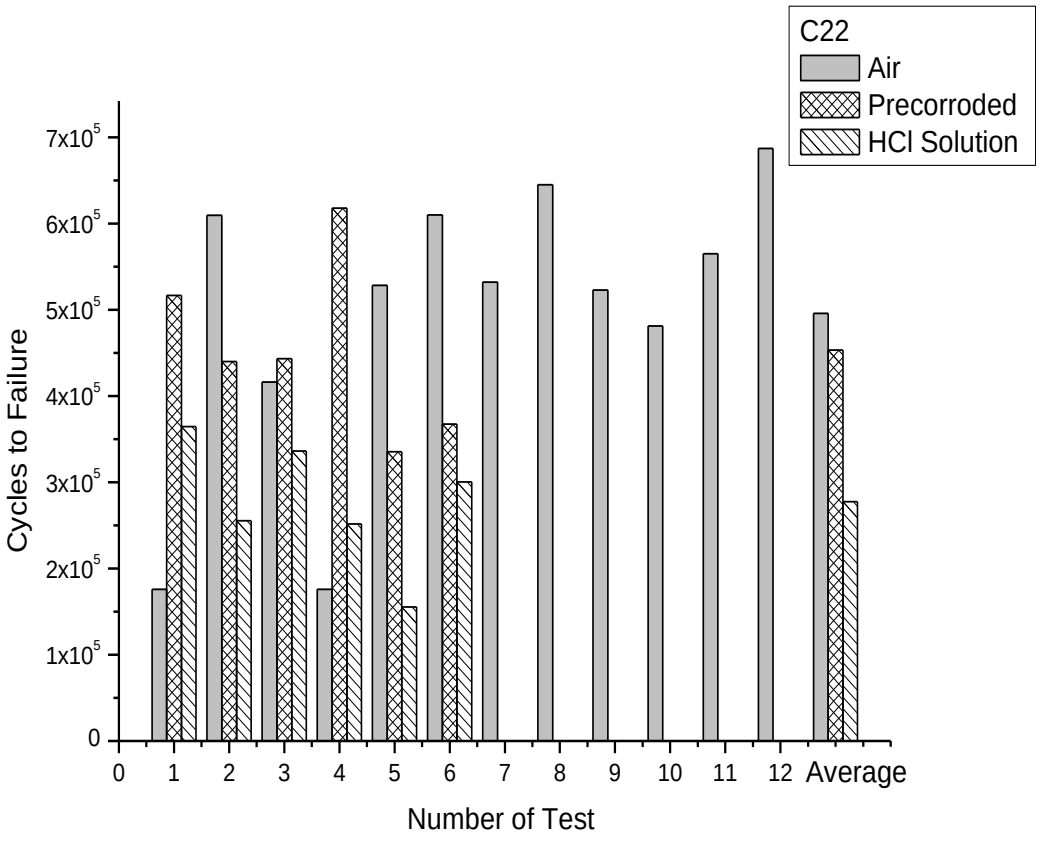

Figure 4.25 Effect of pre-corrosion and a concentrated HCl at pH = 0.0 environment on the fatigue behavior of C22 at 532 MPa

Table 4.15 show fatigue results of three alloys IN600, IN601, and C22 tested at constant stress in air, precorroded and in 10% $FeCl_3$ solution at pH = 0.0, as shown in Figures 4.26, 4.27, and 4.28.

Table 4.15 Corrosion fatigue data in 10%$FeCl_3$ for IN600, IN601 and C22

IN600	Air	PreCorr	Solution	IN601	Air	PreCorr	PreCorr	Solution	C22	Air	PreCorr	Solution
1	808882	569496	251181	1	131463	582491	133392	211372	1	175570	316495	97457
2	393612	1380000	364657	2	190753	116106	285456	112301	2	609387	190000	67262
3	1460000	649315	308534	3	132895	181551	130548	101797	3	416000	152227	98456
4	1790000	346910	268809	4	232412	221311	142314	115404	4	176000	317779	71457
5	887000	929144	101851	5	111342	79544	137702	342791	5	528270	136734	99357
6	957654	775932.6	281502	6	198332	254247	-	111342	6	610074	167635	-
7	488866	-	-	-	-	-	-	-	7	532200	-	-
8	188700	-	-	-	-	-	-	-	8	645000	-	-
9	201100	-	-	-	-	-	-	-	9	523000	-	-
10	877551	-	-	-	-	-	-	-	10	481000	-	-
-	-	-	-	-	-	-	-	-	11	565000	-	-
-	-	-	-	-	-	-	-	-	12	687000	-	-
Average	805337	775133	265071		166199	239208	-	165835		495708	213434	86798

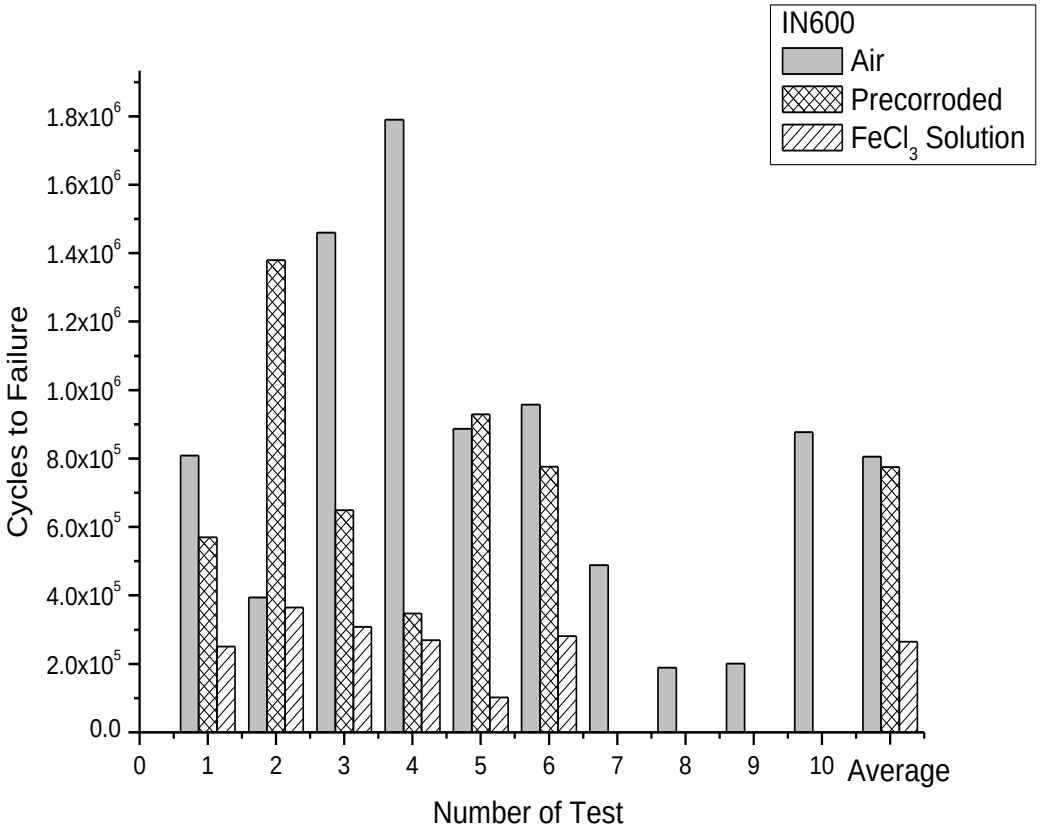

Figure 4.26 Effect of pre-corrosion and 10 % $FeCl_3$ solution at pH = 0.0 environment on the fatigue behavior of IN600 at 480 MPa

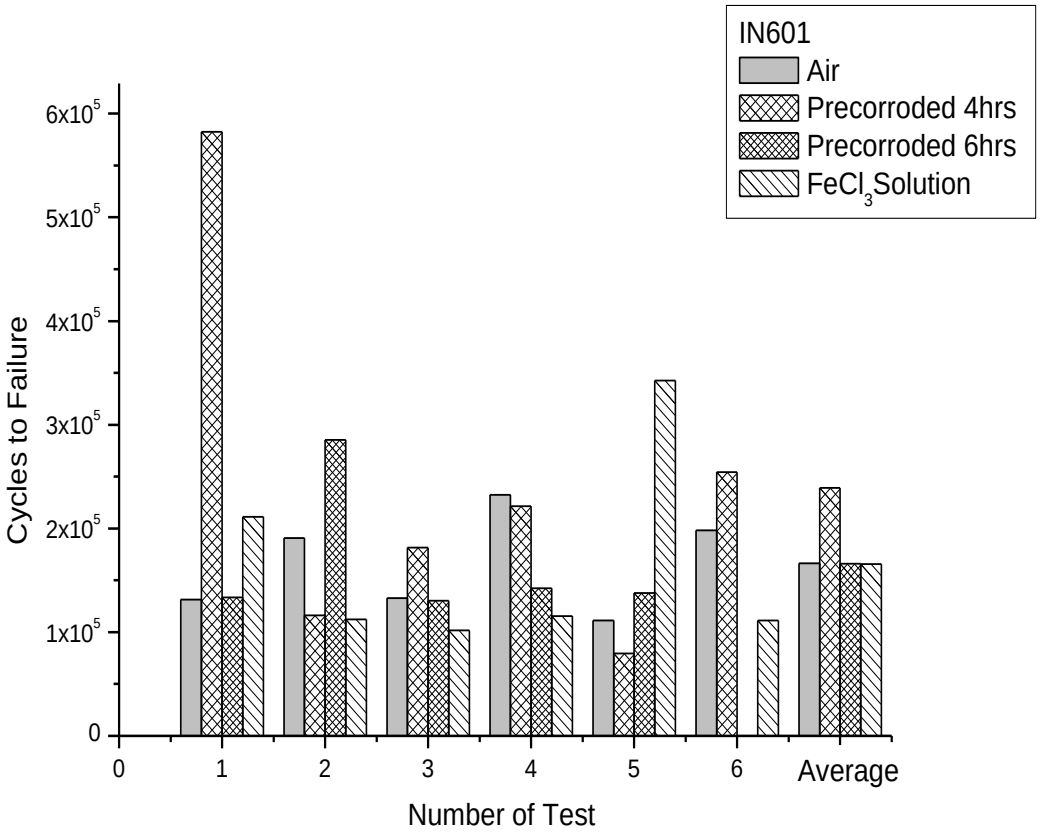

Figure 4.27 Effect of pre-corrosion and 10 % $FeCl_3$ solution at pH = 0.0 environment on the fatigue behavior of IN601 at 532 MPa

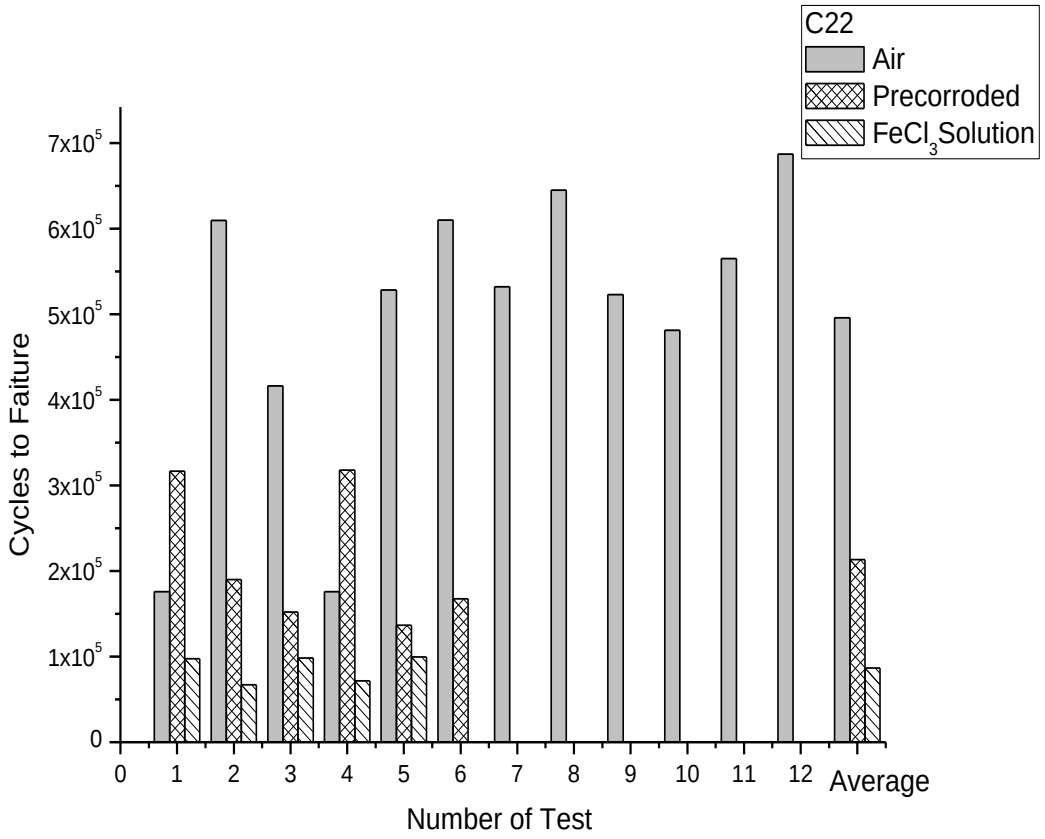

Figure 4.28 Effect of pre-corrosion and 10 % $FeCl_3$ solution at pH = 0.0 environment on the fatigue behavior of C22 at 532 MPa

Table 4.16 providing a summary of statistical data analysis of corrosion fatigue in both corrosion environments HCl and 10%$FeCl_3$ solutions for the three alloys IN600, IN601 and C22. These data include number of tests for each alloy and in each condition, % errors, average, weighted value were calculated and the over all average of these alloys in both conditions are given. Figures 4.29, 4.30 and 4.31 show the standard deviation of these results.

Table 4.16 Summary of Statistic data analysis of corrosion fatigue in HCl and 10%$FeCl_3$ for alloys IN600, IN601 and C22

Summary HCl						Summary 10%$FeCl_3$					
IN600	Value	Std. Dev.	Number of Test	% Error	Weighted	IN600	Value	Std. Dev.	Number of Test	% Error	Weighted
Air	805300	522000	10	64.82056	648.20564	Air	805300	522000	X	64.82056	X
Precorr	251800	238000	6	94.51946	567.11676	Precorr	775100	355000	6	45.80054	274.803251
Solution	81300	9400	6	11.56212	69.372694	Solution	265000	98400	5	37.13208	185.660377
IN601						IN601					
Air	166200	47600	6	28.64019	171.84116	Air	166200	47600	X	28.64019	X
Precorr	133100	14100	6	10.59354	63.561232	Precorr	239200	180200	6	75.33445	452.006689
Solution	114574	12627	6	11.02082	66.12495	Precorr	165900	67000	6	40.38577	242.314647
						Solution	165200	95800	5	57.99031	289.951574
C22						C22					
Air	495700	166300	12	33.54852	402.58221	Air	495700	166300	X	33.54852	X
Precorr	453400	102500	6	22.60697	135.64182	Precorr	213500	82200	6	38.50117	231.007026
Solution	277300	74400	6	26.83015	160.98089	Solution	86800	16000	6	18.43318	110.599078
			64		2285.4273				40		1786.34264
Average 39.15163											

X = Tests are all included in data for HC

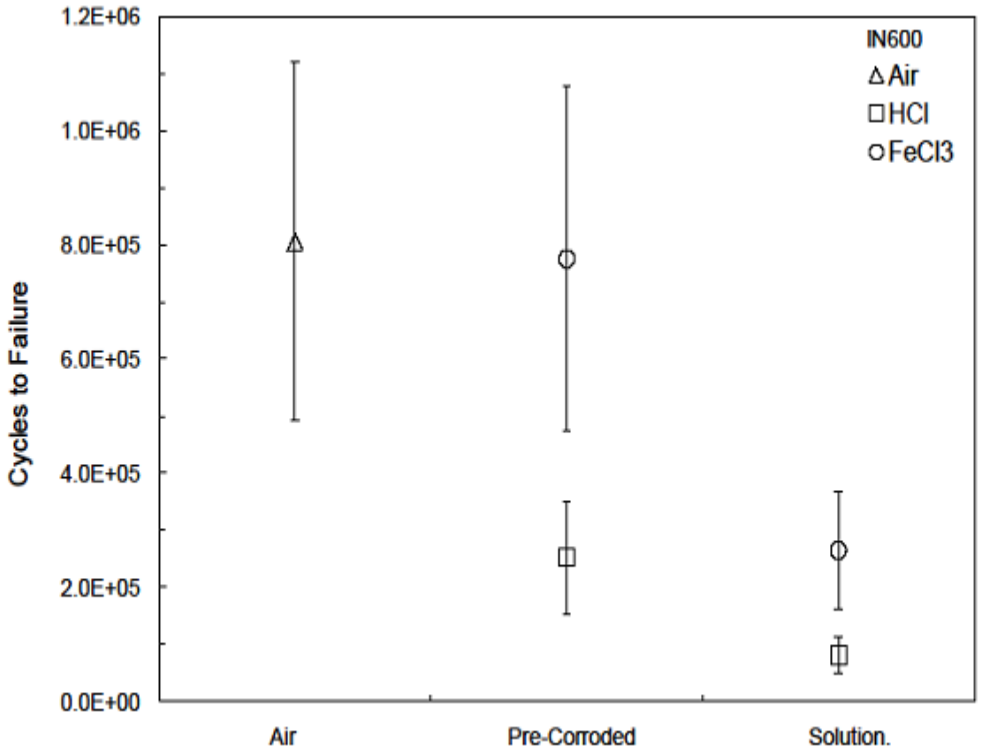

Figure 4.29 Standard deviation of IN600 fatigue data at pH = 0.0

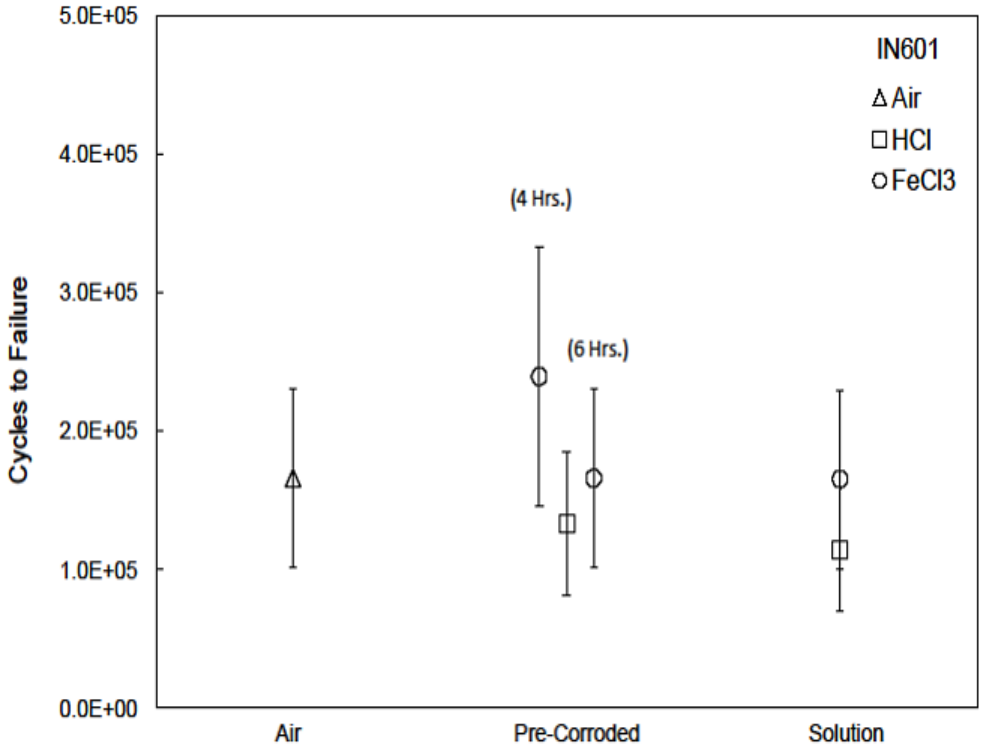

Figure 4.30 Standard deviation of IN601 fatigue data at pH = 0.0

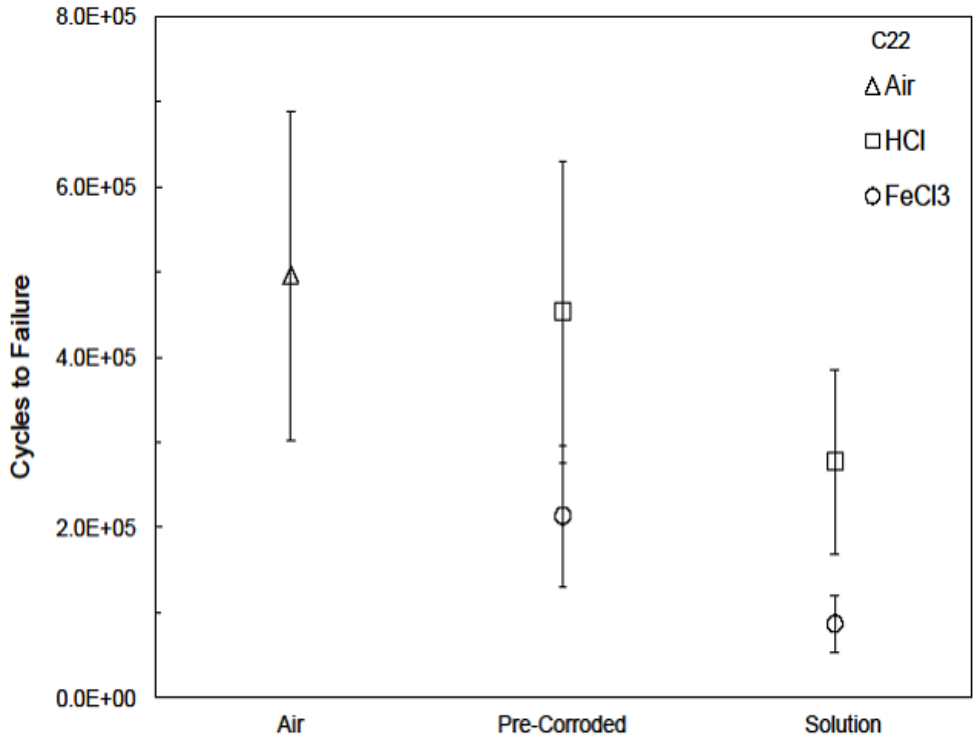

Figure 4.31 Standard deviation of C22 fatigue data at pH = 0.0

4.4 Effect of Corrosion on Fatigue

More corrosion fatigue tests were conducted to examine the effect of surface corrosion on fatigue behavior of the three alloys. Tests were carried out at constant stress in two different aggressive environments, concentrated HCl at pH = 0.0 and 10%$FeCl_3$ solutions at pH = 0.0, and under three different conditions: in air without pre-corrosion, in air with pre-corrosion, and in solution without pre-corrosion. Figures 4.23 to 4.28 show that, in general, the number of cycles to failure for all the alloys tested was highest for fatigue testing in air without pre-corrosion, lower for pre-corroded specimens fatigue tested in air, and lowest for specimens fatigue tested in a corrosive environment without pre-corrosion. However, these generalizations are qualified in the following.

The fatigue results for IN601for HCl at pH = 0.0 presented in Figure 4.24 showed that the corrosive environment has an effect on the fatigue life of the specimen. The specimens pre-corroded for 4 hours actually exhibited the largest (average) life and the fatigue specimens tested in air has higher fatigue life than in the corrosive environment.

The fatigue results for alloy C22 given in Figure 4.25 show that the corrosive environment does reduce the fatigue life of this alloy and that the fatigue life of specimens tested in air after 6 hours of pre-corrosion are higher than the results for the specimens fatigue tested in the HCl solution. In both cases fatigue tests ran for an average of about 6 hours (200, 000 cycles at 36,000 cycles per hour).

The fatigue results for IN600 tested in 10 wt. % $FeCl_3$ solution at pH = 0.0 given in Figure 4.26 show that the fatigue life for the specimens fatigue tested in this solution is shorter than that for specimens pre-corroded for 7 hours prior to testing in air. This is particularly significant because these fatigue tests lasted about 7 hours, similar to the time required for fatigue failure in solution (about 250,000 cycles at 36,000 cycles per hour).

For IN600, the corrosion rate in 10 wt. % $FeCl_3$ solution at pH = 0.0 is very high, 27 mm/year as given in Table 4.8 and Table 4.9. It is obvious that such a high corrosion rate would greatly affect the fatigue life if tests were conducted over a time frame of weeks or months instead of the tests of a few hours conducted here.

This fatigue results for IN601 in 10 wt. % $FeCl_3$ solution at pH = 0.0 presented in Figure 4.28 show that pre-corrosion in solution has a great effect on the fatigue life of IN601.

This is similar to the corrosion results for IN601 in HCl solution at pH of 0.0 and is indicative of both the toughness and the corrosion resistance of this alloy.

The fatigue results for alloy C22 in 10 wt. % $FeCl_3$ solutions at pH = 0.0 presented in Figure 4.28 show that pre-corrosion for 7 hours followed by fatigue testing in air has about the same effect as fatiguing in solution. (The fatigue life in solution is about 200,000 cycles / second). It may therefore be conducted that for alloy C22 in 10 wt. % $FeCl_3$ solution at pH = 0.0 there is an interaction between the solution and the alloy at the crack tip.

In summary, the results indicate that for both alloys IN600 and C22 there is an interaction between the corrosive HCl and $FeCl_3$ solution and the alloy at the fatigue crack tip which shortens the fatigue life over the specimens pre-corroded for a similar length of time.

Further, the fatigue life of IN601 is not greatly affected by the presence of HCl solution or 10 wt. % $FeCl_3$ solution at pH of 0.0 either diverging pre-corrosion or corrosion in solution.

4.4.1 Surface Morphology

Figure 4.32 shows a representative surface of IN600 sample prior to any fatigue environment test. The surfaces for IN600 fatigued in air after pre-corrosion in HCl solution at pH of 0.0 revealed many large surface pits as shown in Figure 4.33. For IN601 Figure 4.34, shows smaller and fewer pits and alloy C22 exhibits only a few small pits as shown in Figure 4.35. These results are consistent with the fatigue test results which show a large effect of corrosion for IN600 and much smaller effect for IN601 and alloy C22.

The specimen surface for IN600 fatigued in air after pre-corrosion in 10 wt. % $FeCl_3$ solution at pH = 0.0 exhibited extensive pitting as shown in Figure 4.36.

Fewer pits were observed for IN601 (Figure 4.37) and almost no pits for alloy C22 (Figure 4.38). This again indicates the inherent toughness (Table 4.1 to Table 4.4) and corrosion resistance for both IN601 and alloy C22. Also, for alloy C22 the reduction in fatigue strength must result from

an interaction between the metal and the $FeCl_3$ solution at the fatigue crack tip since there is little surface pitting to initiate the fatigue crack.

The resistance to corrosion fatigue for the alloys studied here is in proportion to the amount of alloying elements, particularly Cr, Mo, Co and W. Alloy IN600, with the least corrosion fatigue resistance has only 25 % alloying elements (Table 3.1). IN601 with 40% alloying elements has better resistance and alloy C22 with 49 % alloying elements has the best resistance.

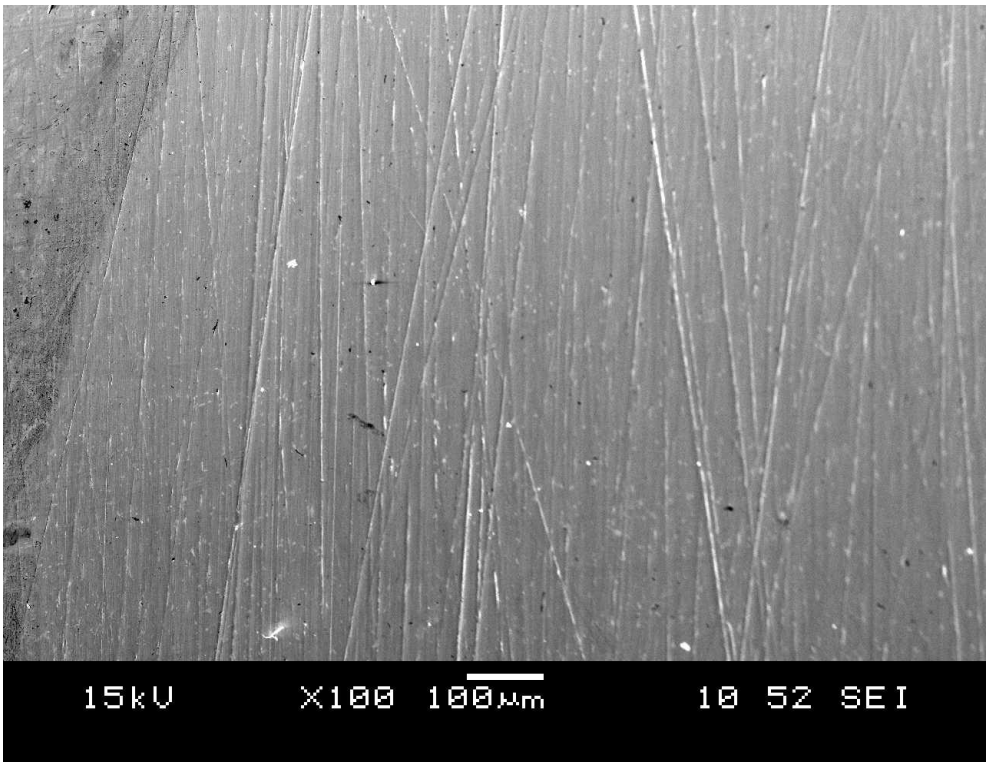

Figure 4.32 A representative test sample of IN600 prior to any fatigue environment

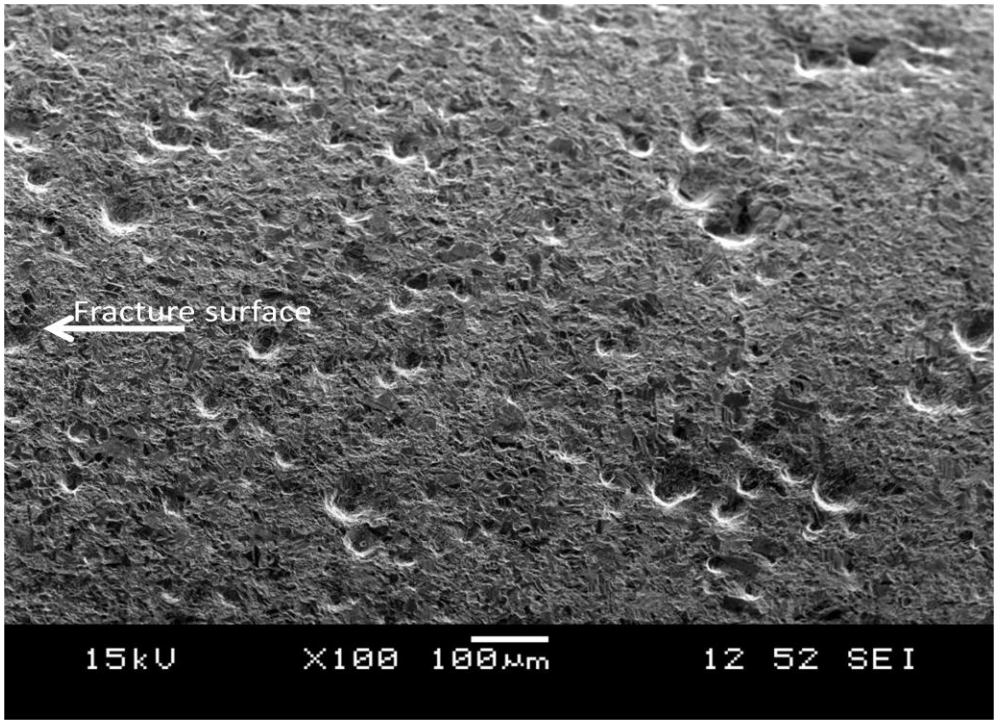

Figure 4.33 Pits near the fracture surface of IN600 after pre-corrosion of 13 hours HCl at pH = 0

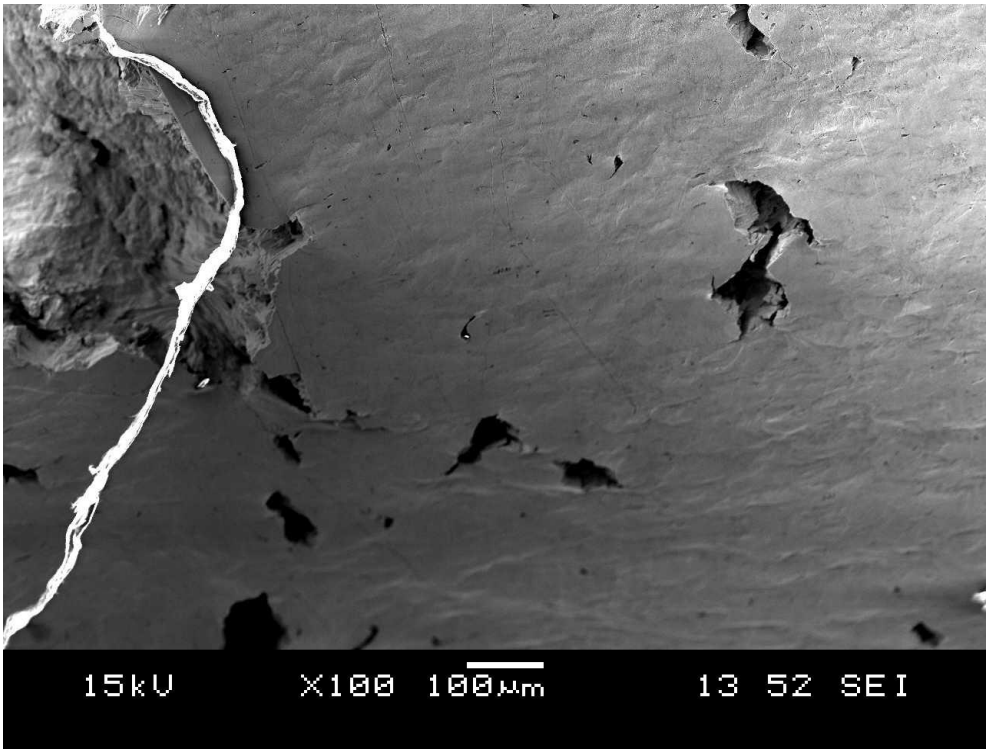

Figure 4.34 Pits near the fracture surface of IN601 after pre-corrosion of 4 hours in concentrated HCl solution at pH = 0

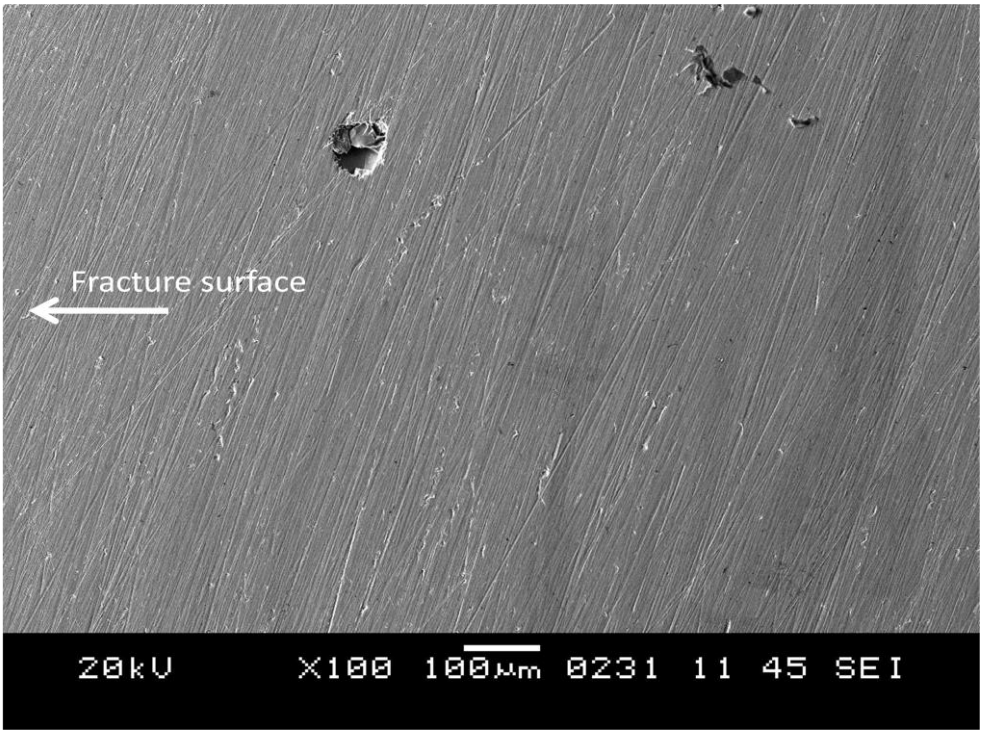

Figure 4.35 Pits near the fracture surface of alloy C22 after pre-corrosion formed by concentrated HCl solution at pH = 0

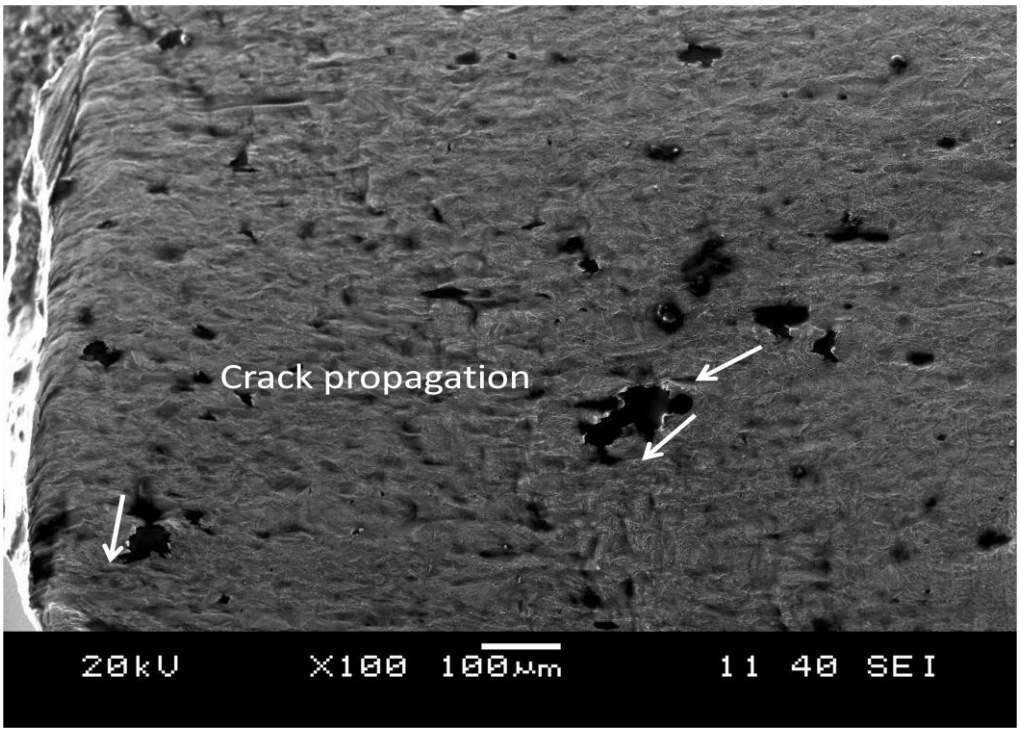

Figure 4.36 Pits near the fracture surface of alloy IN600 after pre-corrosion formed by 10%$FeCl_3$ solution at pH = 0

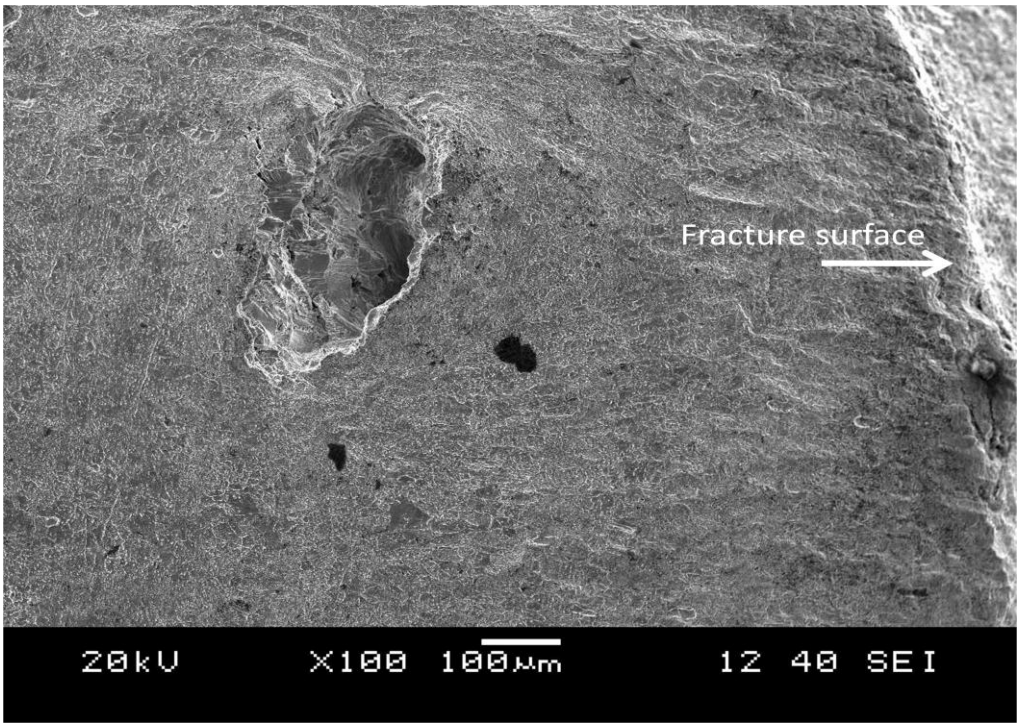

Figure 4.37 Pits near the fracture surface of IN601 after pre-corrosion formed by 10%$FeCl_3$ solution at pH = 0

Figure 4.38 No evidence of pits near the fracture surface of alloy C22 after pre-corrosion formed by 10%$FeCl_3$ solution at pH = 0

The beneficial effects of alloying elements added to type 316L stainless steel were also observed by Cahoon and Bandy [66] who studied the effect of additions of Cr, Ni and Mo on the polarization behaviour of the stainless steel. They reported that increases in the amounts of any of these alloying elements increased the critical pitting potential when tested in Ringers solution, a saline solution simulating tissue fluid. This increase in pitting potential decreases the propensity towards pitting and therefore renders the alloy more suitable for use as prosetheses and surgical implants.

The specimen surface for these alloys fatigue tested in concentrated HCl solution at pH of 0.0 and $FeCl_3$ solution at pH of 0.0 are shown in Figure 4.36 to Figure 4.41. The results are similar to those for the pre-corroded specimens. IN600 exhibits numerous pits (Figure 4.36), IN601 fewer pits (Figure 4.37), and alloy C22 very minor pits (Figure 4.38).

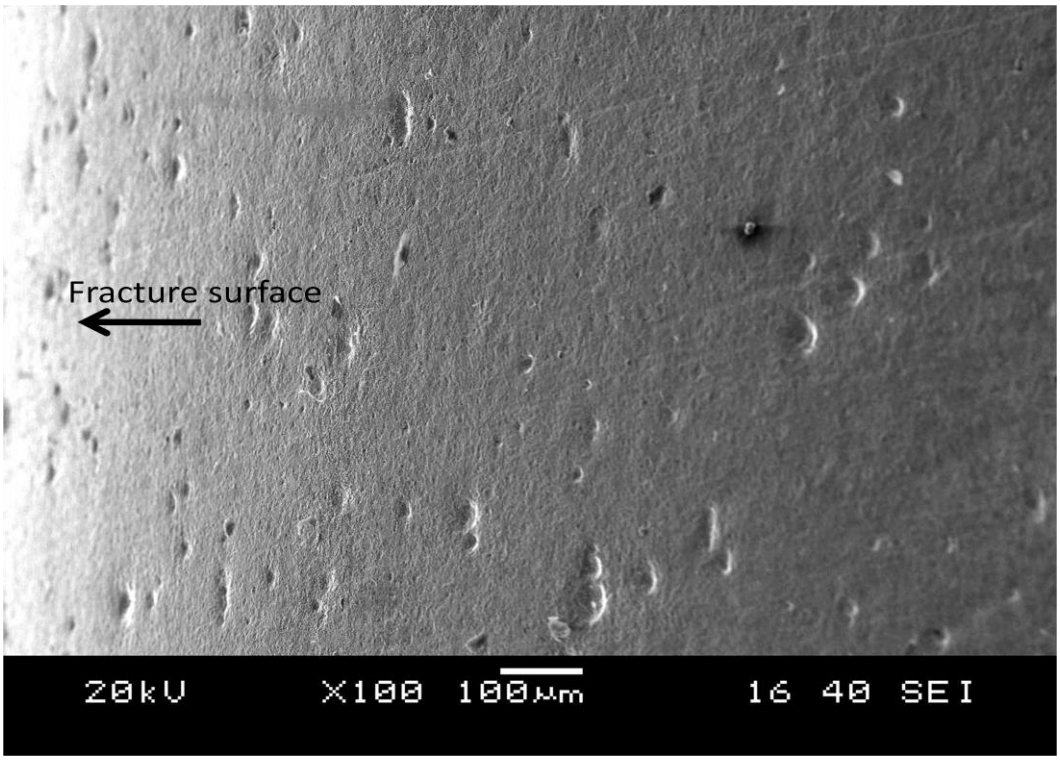

Figure 4.39 Corrosion pits near the fracture surface of IN600 after being fatigued in concentrated HCl solution at pH = 0.0

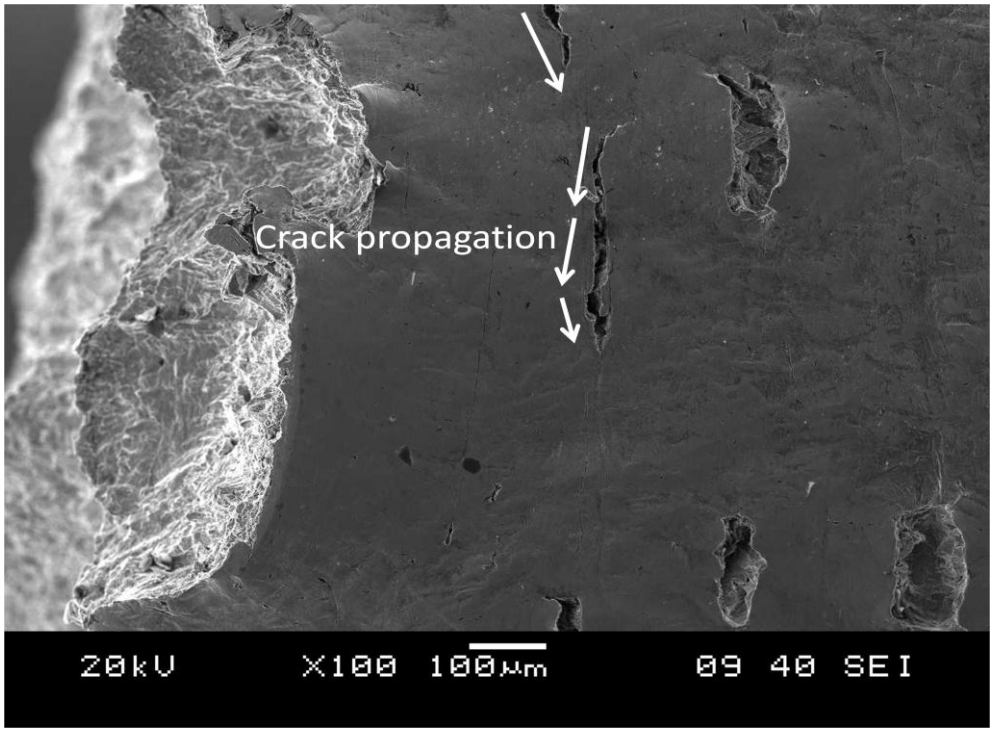

Figure 4.40 Corrosion pits near the fracture surface of IN601 after being fatigued in concentrated HCl solution at pH = 0

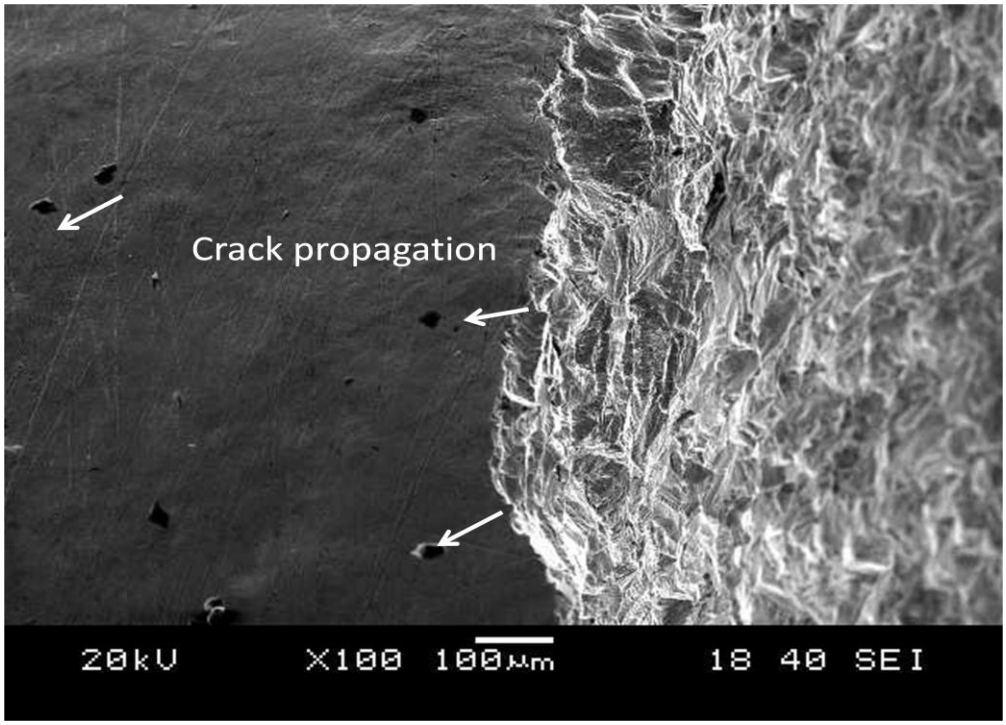

Figure 4.41 Corrosion pits near the fracture surface of C22 after being fatigued in concentrated HCl solution at pH = 0

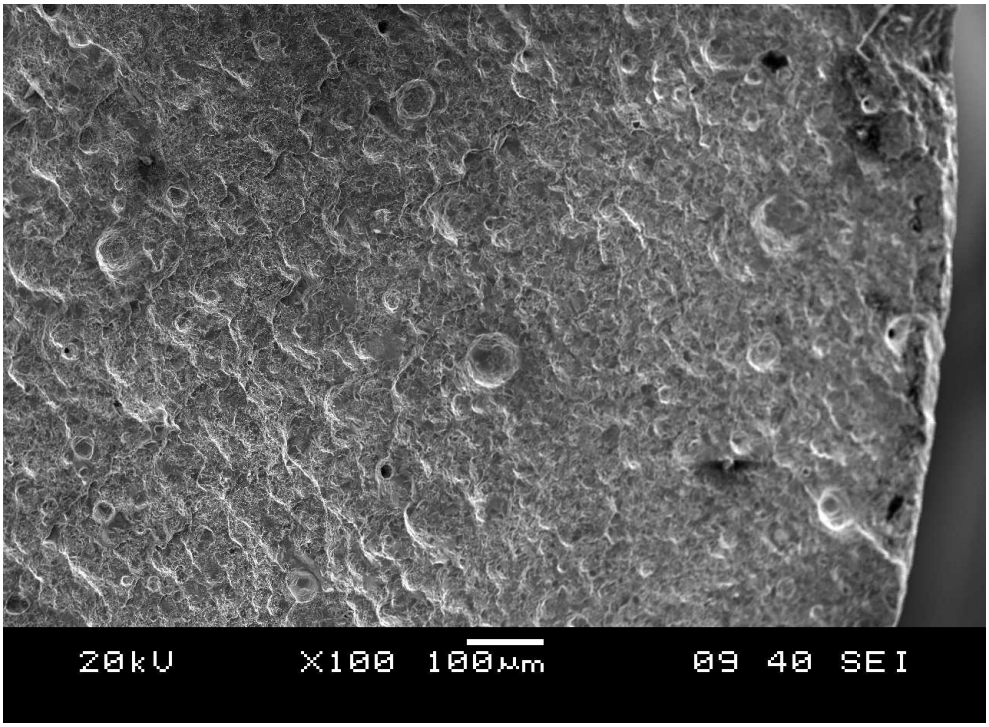

Figure 4.42 Corrosion pits near the fracture surface of IN600 after being fatigued in 10 % $FeCl_3$ solution at pH = 0

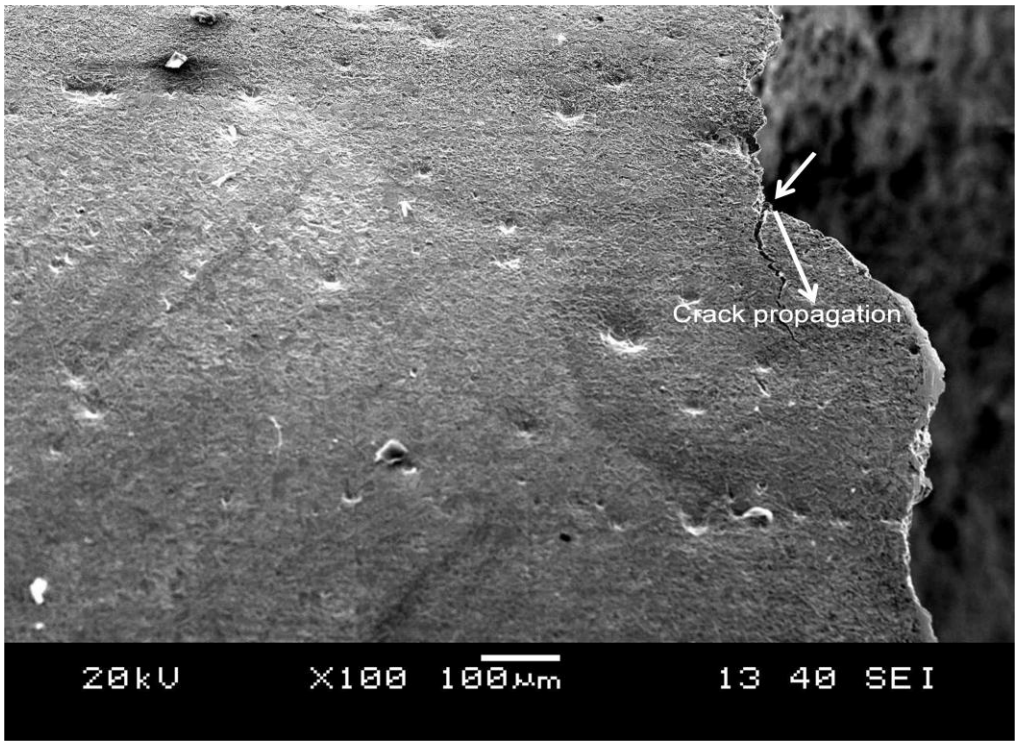

Figure 4.43 Corrosion pits near the fracture surface of IN601 after being fatigued in 10 % $FeCl_3$ solution at pH = 0

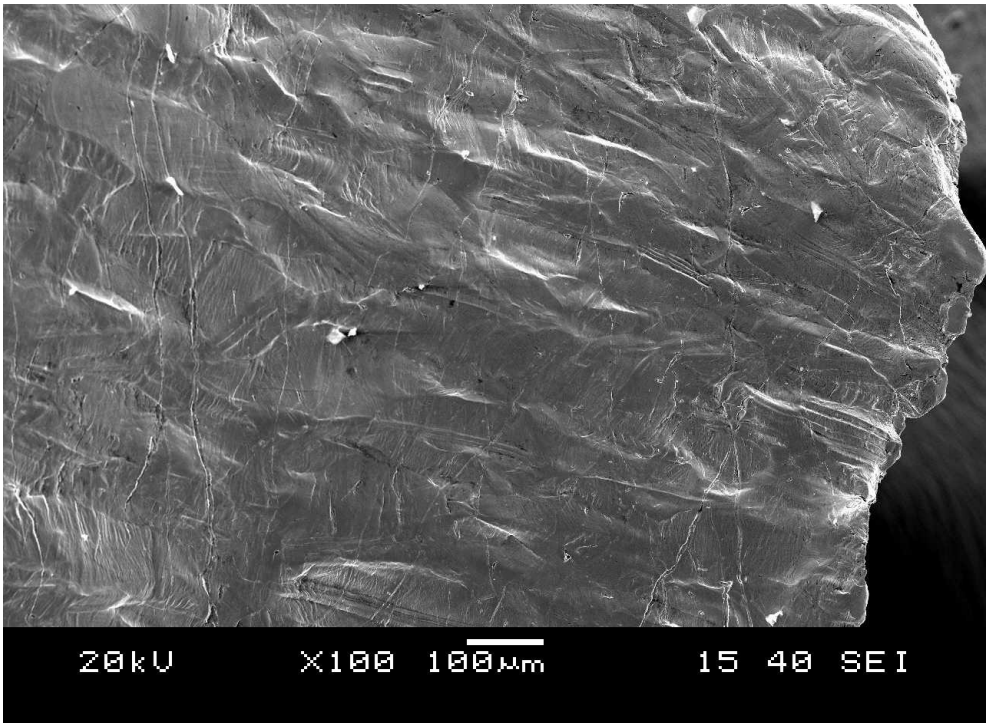

Figure 4.44 No pits near the fracture surface of C22 after being fatigued in 10 % $FeCl_3$ solution at pH = 0

For $FeCl_3$ solution at pH of 0.0, IN600 exhibits numerous pits (Figure 4.39), IN601 fewer pits (Figure 4.40) and alloy C22 almost no pits (Figure 4.41).

The corrosion resistance of IN601 is likely due to its high chromium content (23%, Table 3.1) since it is well known that Cr forms a very protective, corrosion resistant Cr_2O_3 oxide layer.

Extensive corrosion pits formed by aggressive environments (HCl) and (10%$FeCl_3$), such as those in Figure 4.37 and Figure 4.40, respectively, may occur at carbide sites or inclusions and appear to be larger closer to the fracture zone (plastic zone). One can observe pits adjacent to fracture zone pits extended from one pit to another adjacent pit while specimens were undergoing fatigue. Each pit becomes a site of crack nucleation and propagates to the next pit and so on, one after the other, until final fracture (Figure 4.40). IN600 has the lowest amount of Cr (15.5%Cr) as compared to the other two alloys IN601 and C22. This might explain the shorter

fatigue life of IN600. Generally, pitting corrosion was most severe when specimens were fatigued in solution and less than those fatigued in air or even less than those specimens that contained pits but were fatigued in air.

The main reason for adding Mo to an alloy is to enhance repassivation behavior. This behavior can be attributed to the formation of Mo oxide during pitting or the enrichment of Mo metal at the alloy surface. The Mo-containing oxide film formed at the specimen surface can prevent the further growth of the pit, thus decreasing the acidity within the pits.

It can be concluded that pits which formed on specimens fatigued in 10 wt. % $FeCl_3$ solution are more severe than those formed in HCl solution in affecting fatigue life. Hence, when these three alloys are considered for fatigue applications in aggressive corrosive environments, alloy C22 would be considered superior.

4.5 Surface Analysis

A few studies on the composition of passive oxide films have been reported for Ni–Cr–Mo based alloys [49-51]. These were studies based on results from surface sensitive techniques such as Auger electron spectrometer (AES) and secondary ion mass spectrometry (SIMS) as illustrated in Table 4.17.

The three alloys in the present study, IN600, IN601 and C22 show that the presence of a chromium oxide layer is a primary factor in creating passivity. The mechanism by which Mo enhances the corrosion resistance of C22 is not yet understood and a variety of possible mechanisms have been suggested. It has been postulated that Mo on C22 alloy surface preferentially locates at pits, which otherwise would act as dissolution sites [52] and [36] and slows anodic dissolution because of its higher metal–metal bond strength [65-68]. An alternative hypothesis is that MoO_4^{2-} is formed in the exterior layer of the film. This MoO_4^{2-} layer is cation

selective, and resists the incorporation of anions such as Cl^- and OH^-, allowing for the growth of a Cr oxide inner barrier layer.

Table 4.17 Surface techniques used in this study

Technique	Measured particle	Process	Information	Probing depth	Spatial resolution
Auger electron spectroscopy (AES)	AES excited by incident electron beam	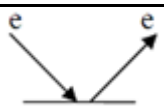	-Elemental analysis -Depth profiles	1-3 nm	50 nm
Secondary ion mass spectrometry (SIMS)	Ion ejected from surface by primary ion	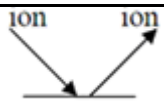	-Elemental trace analysis -Depth profiles	1 nm	40 nm

4.5.1 Auger Electron Spectroscopy (AES)

Ni-Cr-Mo based alloys are widely used in aggressive environment industries due to their excellent corrosion properties. Auger electron spectroscopy (AES) is a surface sensitive analytical technique used mainly to determine elemental compositions of materials and in certain cases to identify the chemical states of surface atoms [50-52]. If a scanning primary electron beam is used, electron images yield information related to surface topography [36].

Auger electron spectroscopic studies on the surface of different austenitic stainless steels with different Cr and Mo contents revealed that the surface composition of the surface which had been formed in Ringer's physiological solution was almost independent of the bulk composition of the three alloys reported [69].

The aim of the present surface analysis is to provide analysis of the surface composition of IN600, IN601 and alloy C22.

4.5.2 Auger Results and Discussion

Auger analysis for IN600, IN601 and alloy C22 before sputtering and after sputtering are presented in Figure 4.45 to Figure 4.50. Sputtering involves removal of surface layers using an argon ion beam so that before-sputtering results are indicative of the surface composition whereas after-sputtering results represent the bulk composition of the alloy.

Both IN600 (Figure 4.45) and alloy C22 (Figure 4.49) show the presence of C on the surface but not in the bulk alloys (Figure 4.46 and Figure 4.50).

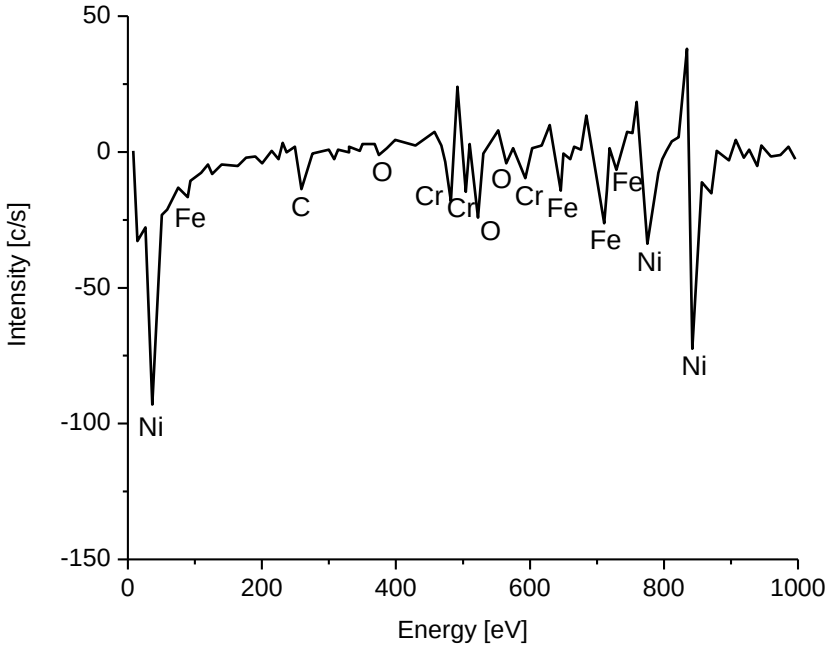

Figure 4.45 Surface Auger results for IN600 before sputtering

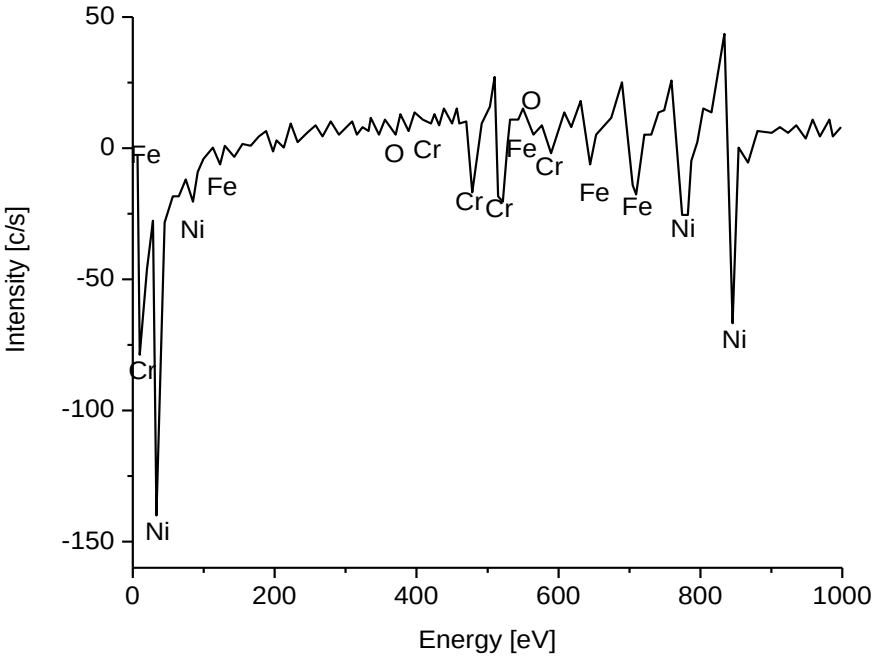

Figure 4.46 Surface Auger results for IN600 for bulk after sputtering

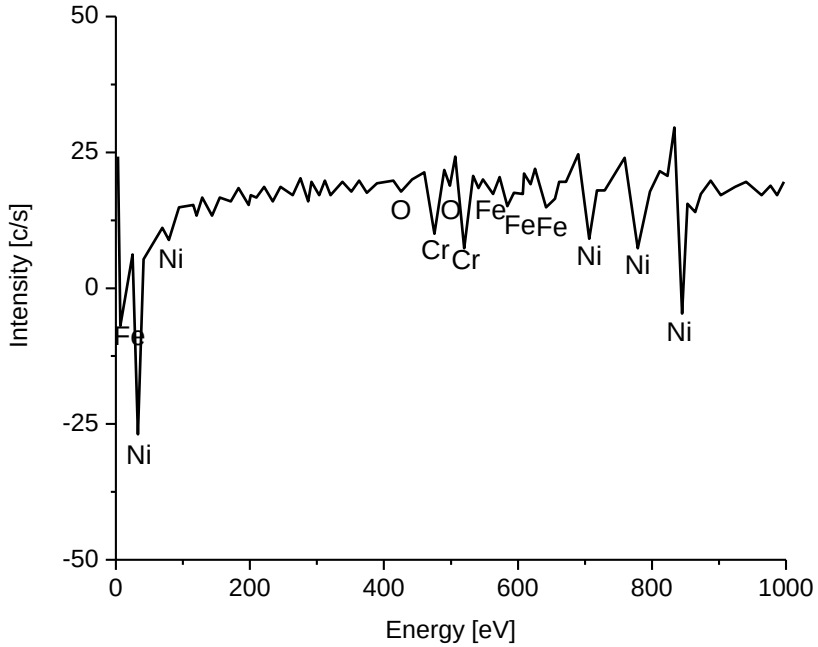

Figure 4.47 Auger result for surface of IN601 before sputtering

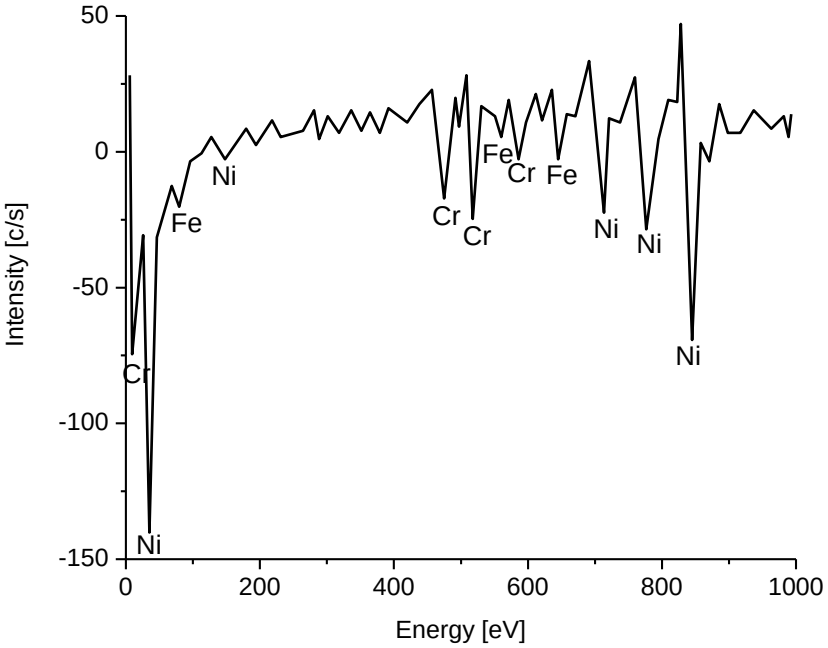

Figure 4.48 Auger results for IN601 bulk after sputtering

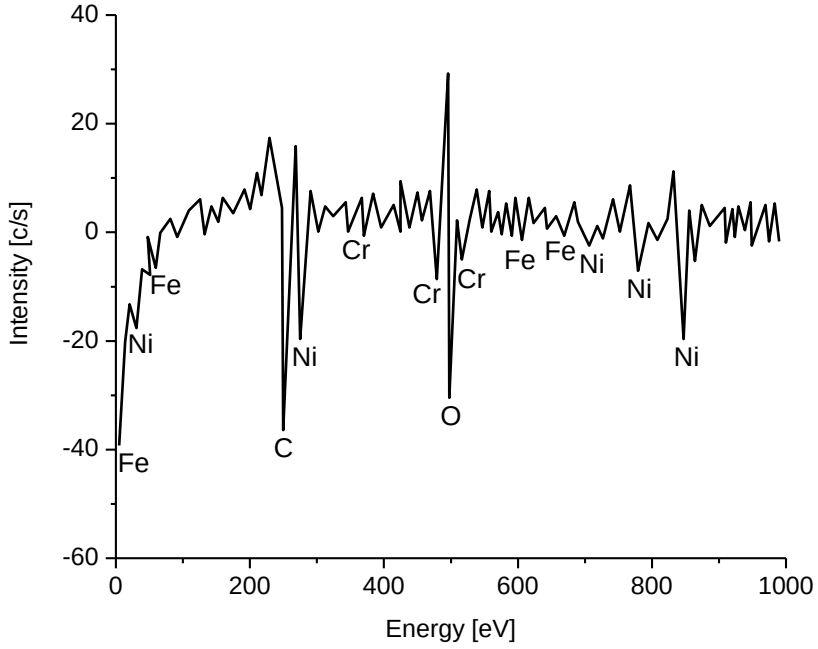

Figure 4.49 Auger results for surface of C22 before sputtering

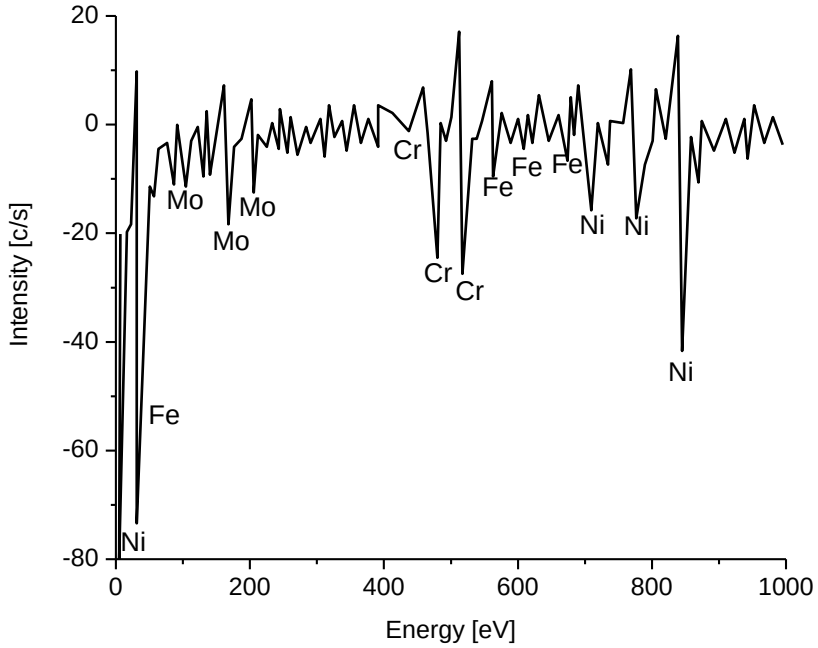

Figure 4.50 Auger result for C22 bulk after sputtering

Since these alloys contain very little carbon it is highly probable that the presence of C on the surface results from CO_2 in the atmosphere.

The most interesting result of these analyses is that the surface of alloy C22 does not exhibit any Mo (Figure 4.49) even though the bulk contains considerate Mo (Figure 4.50).

This is puzzling since Mo supposedly enhances corrosion resistance. The absence of Mo on the surface of austenite stainless steel was also reported by [69]. Figure 4.35 to Figure 4.44 show the micrographs of sample surfaces obtained by the SEM method. Auger electron spectra were recorded. Each alloy was examined as-received for oxides as in Figure 4.45, Figure 4.47 and Figure 4.49. Clean surfaces of the samples were obtained by removing C and O atoms as in Figure 4.46, Figure 4.48 and Figure 4.50 by means of an Argon (Ar^+) ion beam etching to

remove the top 200 nm to 250 nm. Figure 4.51 to Figure 4.53 show Auger depth profile results for IN600, IN601 and C22 respectively.

Auger depth profiles obtained by simultaneous sputtering and analysis are presented in Figure 4.51 to Figure 4.53. These show that for each alloy Cr and O presumably in the form of Cr_2O_3 tend to replace Ni and Fe on the surface.

The Mo depth profile for alloy C22 shows an absence of Mo on the surface as noted previously. Figure 4.51 to Figure 4.53 also show that the thickness of the oxide film is typically about 3 nm ($30A^o$).

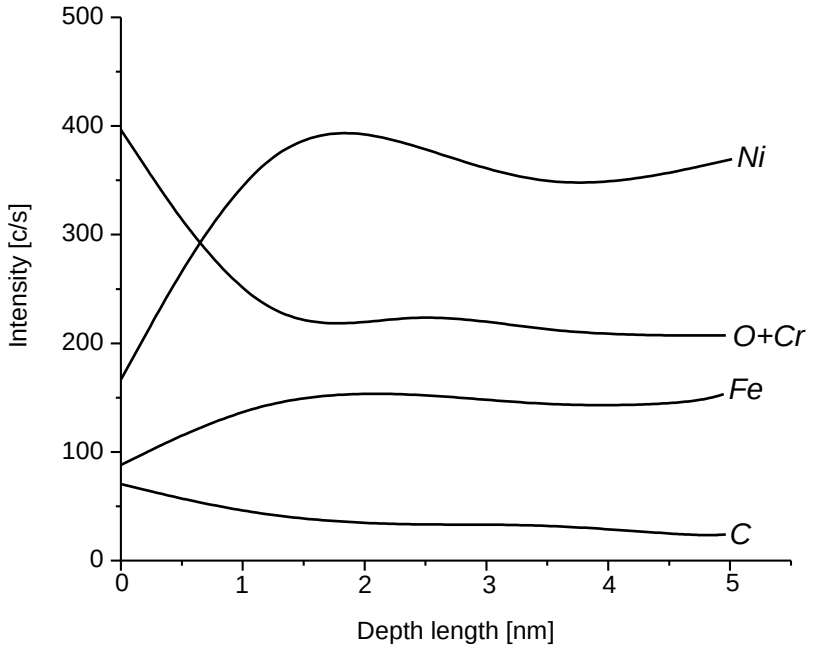

Figure 4.51 Auger depth profile for IN600

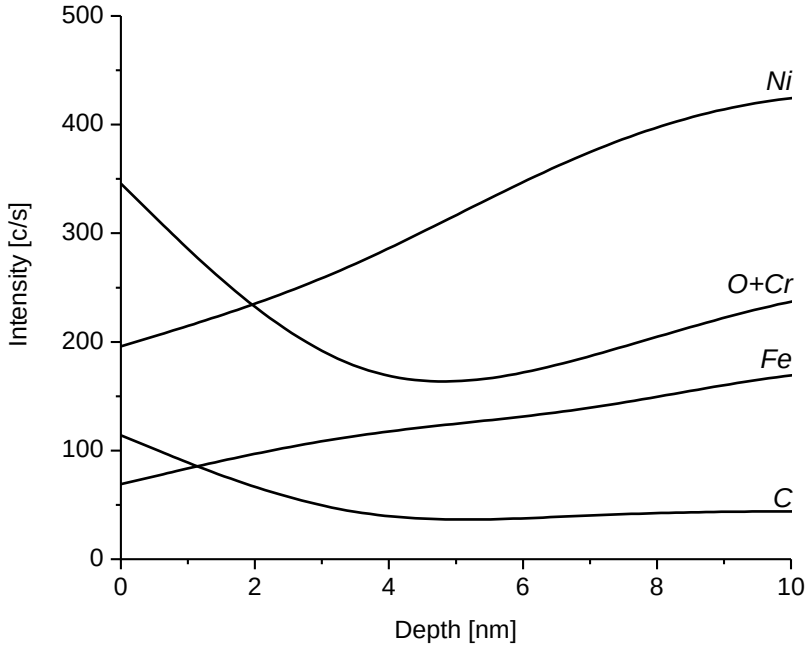

Figure 4.52 Auger depth profile for IN601

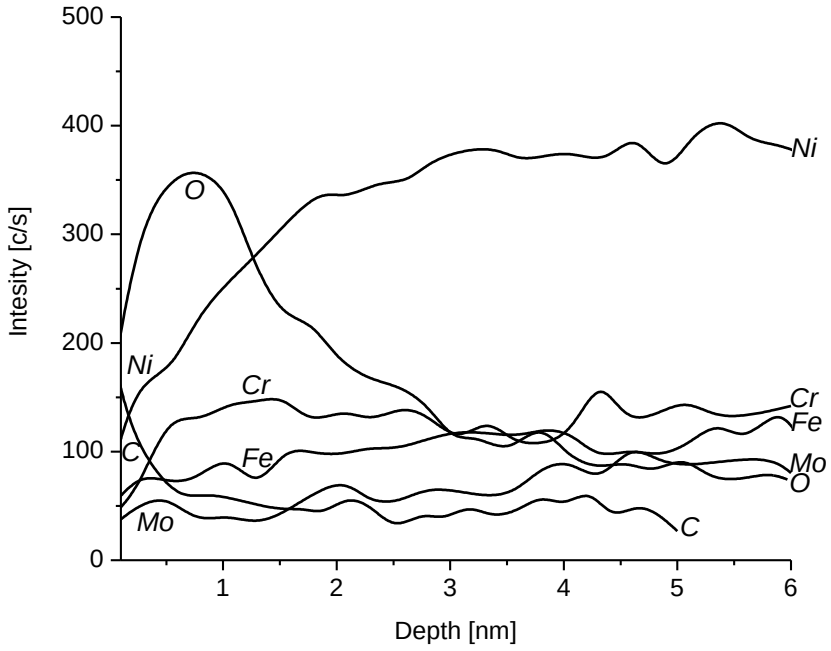

Figure 4.53 Auger depth profile for alloy C22

4.5.3 Secondary Ions Mass Spectrometry (SIMS)

Secondary ion mass spectrometry (SIMS) is one of the most powerful and versatile techniques for characterizing surface oxides of alloys. Amongst other applications, SIMS in the "dynamic mode" is commonly used as a high sensitivity depth profiling tool when investigating oxide films of materials. This capability of the SIMS technology is of particular interest for characterizing the three alloys IN600, IN601 and C22 oxide films. Since SIMS is a destructive technique, the (non-destructive) Auger electron spectrometer analysis was carried out prior to performing the SIMS depth analysis on the same three alloys IN600, IN601 and C22.

4.5.3.1 Background:

A typical SIMS instrument consists primarily of an ion source, a mass spectrometer and a secondary ions detection unit as shown in Figure 3.19. The ion source is used to produce a highly focused ion beam. The ion beam is directed towards the sample to be analyzed resulting in sputter removal of particles from the sample surface.

This high energy bombardment may ionize some of the sputtered material/particles [70]. These charged particles or secondary ions are separated using an energy filter and directed towards a mass spectrometer. The ionized particles, filtered by the difference in their masses, are measured to determine the elemental composition of the sample surface. In a SIMS depth profile analysis, a primary ion beam is used to continuously raster a selected region on the sample surface and etches a crater that may be used for SIMS analysis. The ionized particles are mass analyzed to obtain chemical information as a function of depth.

4.5.3.2 Procedure:

A Cameca IMS-7f Universal Magnetic Sector SIMS instrument was used to perform depth profiling of the three alloys IN600, IN601 and C22. Tests were run using two types of ion

sources - cesium primary negative secondary (Cs^+) with atomic number of 55 and oxygen primary positive secondary (O_2^+) with atomic number of 32. Thus, (10keV) primary cesium ion beam and (15keV) primary oxygen ion beam were used to characterize the reactively sputtered IN600, IN601 and C22. The Cameca IMS-7f employs magnets to separate the secondary ions. The secondary ions (with different masses), accelerated to the same kinetic energy, have a different resultant velocity. When these accelerated secondary ions are directed through a magnetic field, they experience a deflection force. The amount of deflection will depend on the mass (m) and charge (q) of the secondary ion [70]. For an applied magnetic field, secondary ions with the right mass/charge ratio amount will be directed towards the secondary ion detector. The secondary ion current for other elements can be detected by varying the magnetic field. Thus, the mass/charge ratio can be used to identify elements present in an analysis sample.

4.5.3.3 Test Feedback:

Both primary (10keV) cesium ion beam and (15KeV) oxygen ion beam, focused to a fine spot with a diameter of 60 μm, were used to raster a 200 nm^2 square crater on the sample surface. The secondary ions, originating only from 60 μm region in the centre of the crater, were directed towards the mass spectrometer. The vacuum was maintained at 1×10^{-9} torr. The secondary ions for the key elements (nickel, chromium, molybdenum, iron, carbon, and oxygen) in the three alloys IN600, IN601 and C22 were monitored and detected in the depth profiles. During the depth analysis, test samples were rotated at one rpm to obtain a uniformly sputtered crater for analysis. After the completion of the depth analysis, the crater depth was measured using a surface profilometer (α-Step 500) as shown in Figure 3.20.

4.5.4 SIMS Results and Discussion

Secondary ion mass spectrometry (SIMS) profiles were obtained for each of the three alloys using (Cs^+) primary ion as shown in Figure 4.54 to Figure 4.56.

These results are puzzling in that the concentration of all the elements increase towards the surface.

The SIMS unit used was a very recent acquisition and the results reflect the inexperience of all concerned. The results do tend to confirm the Auger results in that the surface layer extends about 3nm into the material.

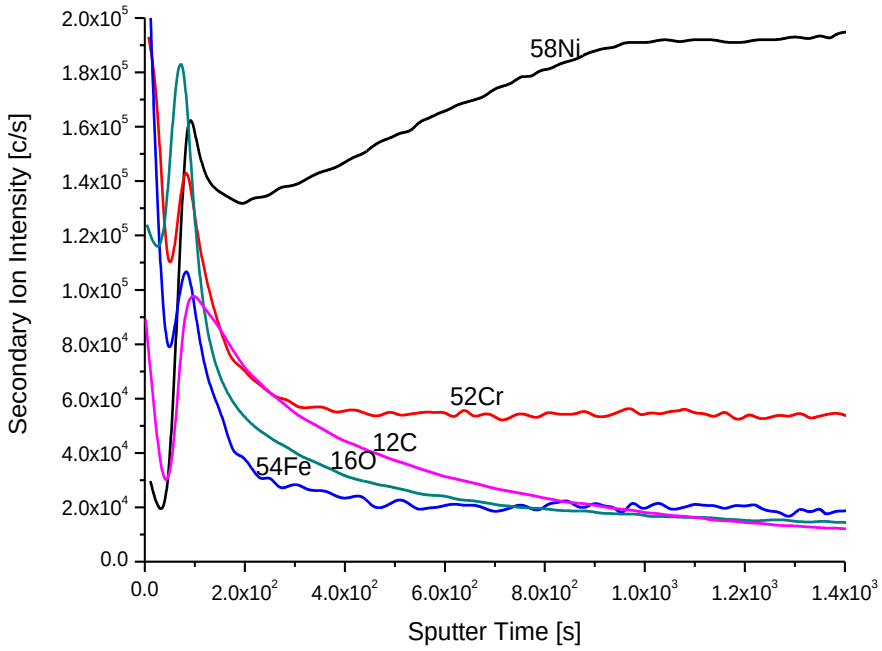

Figure 4.54 Alloy IN600 SIMS results for primary ion cesium (Cs^+)

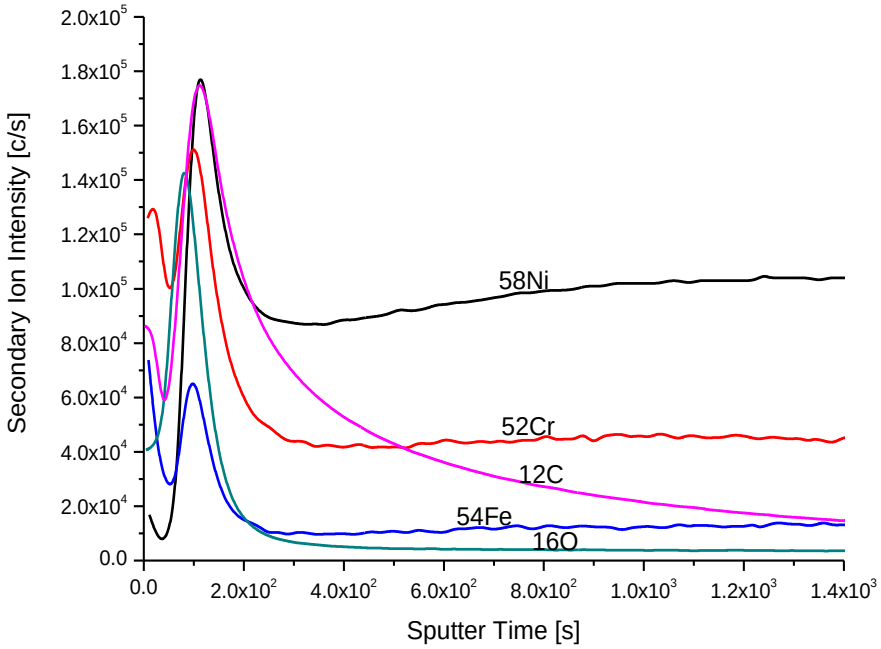

Figure 4.55 Alloy IN601 SIMS results for primary ion cesium (Cs^+)

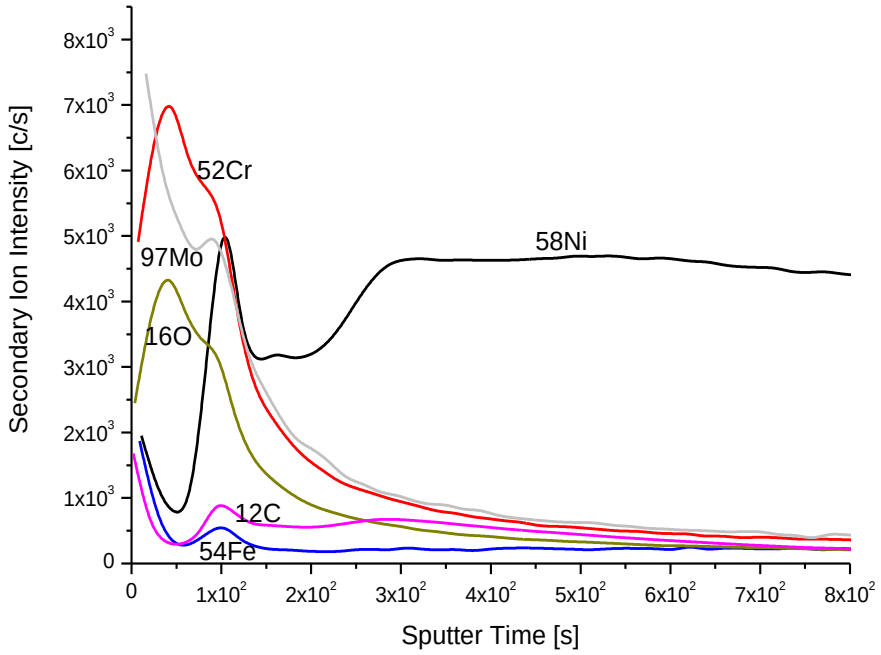

Figure 4.56 Alloy C22 SIMS results for primary ion cesium (Cs^+)

5 Summary and Conclusions

- The electrochemical behavior of the three alloys IN600, IN601 and C22 was examined in detail in three electrolyte solutions: 3.5%NaCl, concentrated HCl at pH = 0.0, and 10%$FeCl_3$ solution at pH = 0.0. Results indicate that Cr is responsible for the passive behavior and Mo is responsible for stabilization of the surface oxide film and causing repassivation after breakdown occurs. The main effect of adding Mo to the alloy is to inhibit the pitting from further propagation as well as to modify the local solution environment by consuming H^+ ions, thus decreasing the acidity of the pit. The alloy with Mo content exhibited excellent corrosion resistance in all three solutions.
- The 3.5% NaCl solution at pH = 7.0 had no effect on the fatigue life of any of the three alloys tested.
- IN600 exhibited the least corrosion resistance of the three alloys studied. In 10 % $FeCl_3$ solution at pH = 0.0, the corrosion rate was 77 mm / year compared to slightly under 1.0 mm / year for both alloys IN601 and C22.
- For the IN600, exposed to pre-corrosion in HCl and $FeCl_3$ solution at pH = 0.0 a considerable decrease in fatigue life over the non pre-corroded specimens was noted. However, the fatigue life for specimens tested in these solutions was even lower suggesting that there is an interaction between the metal and the solution at the fatigue crack tip.
- IN601 did not experience a decrease in fatigue life for either pre-corroded or tested in solution specimens over these fatigued only in air. This result provides evidence of the inherent corrosion resistance of IN601. IN601 is also inherently “tough“since surface damage due to corrosion has low effect on the short term high cycle fatigue life.

- Pre-corroded and fatigued-in-air alloy C22 specimens exhibited a decrease in fatigue life over specimens fatigued only in air. This indicates some surface damage as a result of pre-corrosion even though pitting was minimal. All C22 specimens fatigued in solution exhibited a fatigue life similar to that for pre-corroded specimens. This same indication between the corrosive environments and the alloy at the fatigue crack tip reduces the fatigue life of the alloy.
- Auger analysis indicated that Cr and O are present on the surface of all three alloys and is likely in the form of a Cr_2O_3 layer. Further, the layer extends about 3 nm into the alloys.
- Auger results did not show any Mo on the surface of alloy C22. However, a bulk, Mo content of 13.5% was noted. This is a puzzling result in that Mo supposedly enhances the pitting resistance of an alloy.
- Secondary ion mass spectrometry SIMS results were inconclusive. More testing is required to validate the SIMS results. These results did, however, confirm that the surface layer extends about 3 nm into the alloys from the surface.

6 Suggestions for Future Work

The goal of the …presented in this thesis was to determine the effect of corrosive environment on fatigue behavior of three Ni-based alloys, IN600, IN601, and C22, tested in three corrosive environments, namely, 3.5%NaCl solution at pH of 7, HCl acid solution at pH of 0 and 10%$FeCl_3$ acid solution at pH 0. Tests were conducted at constant pH, load frequency, and temperature. The research results raised several questions that have not been answered during this work and therefore we concluded two main recommendations for future research:

The first recommendation is to study the effect of load frequency and temperature to provide designers with a more comprehensive knowledge of the corrosion-fatigue behavior of these three alloys. Such as investigation could include varying the pH and determining the effects associated with pH level. It could be also include the influence of these variables (load, pH, temperature) on fracture surface and microstructural characterization.

The second recommendation relates to the research findings of the Auger analysis which indicated the presence of Cr and O on the surface of all three alloys, likely in the form of a Cr_2O_3 layer. Interestingly enough, Auger results did not show any Mo on the surface of alloy C22 although a bulk Mo content of 13.5% was noted. This is a puzzling result in that Mo supposedly enhances the pitting resistance of an alloy. Further analysis should focus on how Mo softening and prolong the surface oxides from premature film breakdown this could play a role in enhancing pitting resistance.

References

1. Rebak, R.B. and Estil, J.C.A, *"Study of Corrosion Behavior of Ni-22Cr-13Mo-3W alloy under Hygroscopic Salt Deposits on Hot Surface"*, MRS Fall Meeting, Boston, MA, Report # UCRL-JC-148826. December 2–6, 2002, pp. 1-20.

2. Kehler, B.A., "*Crevice CorrosionStabilization and Repassivation Behavior of Alloys 625"*, Corrosion Journal, Vol. 57, 2001, pp. 1042-1065.

3. Gorhe, D.D., "*Development of an Electrochemical Reactivation Test Procedure for Detecting Microstructural Hetrogeneity inNi-Cr-Mo-W Alloy Weld"*, Journal of Materials Science, Vol. 39, 2004, pp. 2257-2261.

4. Gorhe, D.D., "*Electrochemical Methods to Detect Susceptibility of Ni-Cr-Mo-W Alloy 22 to Intergranular Corrosion"*, Metallurgical and Materials Transactions A, Vol. 36, 2005, pp. 1153-1167.

5. Ilevbare, G.O., *"The Effect of Welding on the Crevice Breakdown and Repassivation Potentials of Alloy 22 in 5M $CaCl_2$ between 45 and 120^oC"*, The Electrochemical Society, Inc, ABS. 464, 204th Meeting, 2003, pp. 464-465.

6. Lloyd, A.C., Noël, J.J., McIntyre, N.S., and Shoesmith, D.W., "*The Open-Circuit Ennoblement of Alloy C-22 and Other Ni-Cr-Mo Alloys"*, Journal of the Minerals, Metals and Materials Society, Vol. 57, No. 1, January, 2005, pp. 31-35.

7. Fuchs, H.O., and Stephens, R.S. "*Metal Fatigue in Engineering"* New York, John Wiley and Sons, 1980, pp. 26-74.

8. Hertzberg, W.R., "*Deformation and Fracture Mechanics of Engineering Materials"* Forth Edition. New York, John Wiley, 1996.

9. Fontana, Mars G., "*Corrosion Engineering",* John Wiley & Sons, 1996, pp. 130-140.

10. El-Madhoun, Y., Mohamed, A., and Bassim, M.N.*"Cyclic Stress-Strain Response and Dislocation Structures in Polycrystalline Aluminum"*, Material Science and Engineering A, Vol. 359, No. 1-2, 25, October 2003, pp. 220-227.

11. El-Madhoun, Y., Mohamed, A., and Bassim, M.N. *"Cyclic Stress-Strain Response and Dislocation Structures in Polycrystalline Nickel"*, Materials Science and Engineering A, Vol. 385, 2004, pp. 140–147.

12. Mohamed, A., El-Madhoun, Y., and Bassim, M.N. *"Dislocation Boundary Width Changes due to Cyclic Hardening"*, Journal of Metallurgical and Materials Transactions A, Vol. 37A, December 2006, pp. 3440- 3441.

13. Mohamed, A., El-Madhoun, Y., and Bassim, M.N. *"A Comparative Study of Fatigue Properties of Two Face-Centered-Cubic"*, Journal of Metallurgical and Materials Transactions A Volume 37A, December 2006, pp. 435-437.

14. Dieter., "*Mechanical Metallurgy"* Second Edition, John Wily & Sons, 1976, pp. 404-407.

15. Lin, X., and Cheng, X., "*Laser Ablation Rates of Inconel and Aluminum with Femo and Nanosecond Pulses"*, San Francisco, Conference Proceedings of CLEO, 1998.

16. Vasudevan, A.K., and Sadananda, K., "*Classification of Fatigue Crack Growth Behavior"*, Journal of Metallurgical and Materials Transactions A, Vol. 26A, 1995, pp. 1221-1234.

17. Oliferuk, W., Korbel, A., and Grabsk, M., "*Slip Behavior during uniaxial Tensile of Austenitic Steel"*, Journal of Mateial Science and Engineering A, Vol. 234, 1997, pp. 1122- l 125.

18. Speidel, PR., and Sahn. MO., "*High Temperature Materials in Gas Turbines"*. New York, John Wiley & Sons. 1974.

19. Akio, H., Kentaro, S., and Koboyashi, K.F., "*Microstructure and Mechanical Properties of Laser Beam Welded IN718"*, 1-2, Journal of Material Processing Technology, Vol. 13, 1998, pp. 28-44.

20. Fronva, J.G., and Gonzalez Rodriguiez. I., "*Effect of Structural Evolution in IN601 on Intergranular Corrosion"*, Material Chemical Physics, Vol. 56, 1998, pp. 70-73.

21. Rack, V., J., Vankahtesh. H., and Vankahtes, V., "*Elevated Temperature Hardening of IN690"*, Journal Mech. Material, Vol. 30, 1998, pp. 69–81.

22. Pandey, M.C., and Satyanarayana, D.V., "*Effect of Gamma Pprime Depletion on Creep Behavior of Ni Base Aloy"*, Journal Material of Science, Vol. 19, June, 1996, pp. 1009-1015.

23. Hicks, V.P., Swaminathan. H.B., and Owens. N., *"Evaluation of Gas Turbine Inter", GCologne"*, Germany, Aerospace Congress and Exposition Conference. 1992.

24. Clavel, M., and Pineau, A, *"Frequency and Wave-Form Effects on the Fatigue Crack Growth Behavior of Alloy 718 at 298K and 823K"*, Journal of Metallurgical Transactions A, (Physical Metallurgy and Materials Science), Vol. 9A, April 1978, pp. 471-480.

25. Worthem, D.W., Robertson, I.M., and Altstetter, C., "*Inhomogeneous Deformation in INCONEL 718 during Monotonic and Cyclic Loadings"*, Metallurgical Transactions A, Vol. 21, 1990, pp. 3215-3220.

26. Juvinall, Robert C., "*Engineering Consideration of Stess, Strain and Strength"*, New York, McGraw-Hill Book Company, 1967.

27. Pourbaix, M., "*Atlas of Electrochemical Equilibria iin Aqueous Solutions"*, New York, Pergamon Press, 1974, pp. 329-333.

28. Jones, Denny A., "*Principle and Prevention of Corrosion"*, Prentice Hal, 1996, pp. 9-10.

29. Grimal, J.M., and Marcus, P. *"The Anodic Dissolution and Passivation of Ni-Cr-Fe Alloys Studied by ESCA", (*PNC UK), Corrosion Science, Vol. 33, No. 5, May 1992, pp. 805-814.

30. Hashimoto, K., and Asami, K., "*XP Study of Surface Film on Nickel Alloys in Hot Concentrated NaOH"*, Corrosion Science, Vol. 19 , June, 1979, pp. 427-435.

31. McIntyre, N.S., Zetaruk, D.G., and Owen, D., *"X-Ray Photoelectron Studies of the Aqueous Oxidation of Inconel-600 Alloy"*, J. Electrochemical Society, Vol., 126, No.5, May, 1979, pp. 750-760.

32. Marcus, P., and Grimal, J.M., *"Anodic Dissolution and Passivation of Ni-Cr-Fe Alloys Studied by ESCA"*, Corrosion Science, Vol. 33, May 1992, pp. 805-814.

33. Grimal, J.M., and Marcus, P., "*Corrosion Behaviour of Inconel 600 and 601 in Orthophosphoric Acid Solutions"*, Corrosion 88 and Euro Corr, Vol. 3, 1988, pp. 2-5.

34. Gilli, G., Borea, P., Zucchi, F., and Trabanelli, G., "*Passivation of Ni Caused by Layers of Salts in Concentrated H2SO4"*, Joournal of Corrosion Science, Vol. 9, No. 9, 1969, pp. 673-681.

35. Worthem, D.W., Robertson, I. M., Leckie, F. A., Socie, D. F., and Altstetter, C. J., *"Inhomogeneous Deformation in INCONEL 718 during Monotonic and Cyclic Loadings"* Metallurgical Transactions A, Vol. 21, No. 12, 1990, pp. 3215-3220.

36. Newman, R.C., *"Dissolution and Passivation Kinitics of Stainless Steel Alloys containing Molybdenum II: Dissolution Kinetics in Artificial Pits"*, Corrosion Science, Vol. 25, No. 5, 1985, pp 341-350.

37. Lillard, R. S., Jurinski, M.P., and Scully, J. R., *"Crevice Corrosion of Alloy 625 in Chlorinated ASTM Artificial Ocean Water"*, Corrosion Science, Vol. 50, No. 4, 1994, pp. 251-260.

38. Abdallah, M.M.A., *"Impedance measurements on Inconel and Monel alloys in Dead Sea water and sulphate solution"*, British Corrosion Journal, Vol. 31, N 3, 1996, pp. 213-217

39. Rebak, R., Koon, N. and Cotner, J., "*Localized Corrosion"*, Electchemical Society, Vol. 99, No. 27, 1999, pp. 470-473.

40. NASA., "*Candidate Alloys for the Construction of Metal Flex Hoses in the STS Launch Environment"*, Testing Branch MTB-325-87A, 1988.

41. Stout, D. A., Lumsden, J. B., and Staehle, R. W., *"Investigation of Pitting Behavior of Iron-Molybdenum Binary Alloys"*, Corrosion Science, Vol. 35, No. 4, April 1979, pp. 141-147**.**

42. Taylor, D., and Knott, J.F., "*Effects of High Frequency on Fatigue Crack Propagation Rate"*, Proceedings of International Conference on Fracture, New Delhi-India, Vol. 3, 1984, pp. 1759-1766.

43. ASM. "*Metal Hand Book",* ASM International 10. OH 44073, Vol. 1, 1990.

44. Pan, Y.M., and Dunn, D.S., "*Topologically Close-Packed Phase Precipitation and Thermal Stability in Alloy 22"*, Metallurgical and Materials Transactions A (Physical Metallurgy and Materials Science), Vol. 36A, May 2005, pp. 43-51.

45. Pelloux, F. and Gabrielli, R. M., *"Effect of Environment on Fatigue and Creep Crack Growth in IN-X-750 at Elevated Temperature"*, Springer Boston, Metallurgical Transactions A, Vol. 13, June 11, 1982, pp. 1083-1090.

46. Estill, J. C., Hust, G. A. and Rebak, R. San Diego.,"*NACE Corrosion Meeting"*, NACE Corrosion Meeting, 2003, pp. 3680-3688.

47. Wekken, C. J., and Janssen, M., "*Solute Transport in Corrosion Fatigue Cracks"* Electrochemical Society, Vol. 138, 1991, pp. 2891-2896.

48. Turnbull, A., "*The Solution Composition and Electrode Potential in Pits, Crevices, and Cracks"*, Corrosion Science, Vol. 23, 1983, pp. 833-870.

49. Boudin, S., Vignes, J.L., Lorang, G., Da Cunha Belo, M., Blondiaux, G., Mikhailov, S. M., Jacobs, J. P., Brongersma, H. H., *"Analytical and Electrochemical Study of Passive Films Formed on Nickel - Chromium Alloys: Influence of The Chromium Bulk Concentration"*, Surface Interface Analysis, Vol. 22, No. 1-12, 1994, pp. 262-466.

50. Jabs, T., Borthen, P., and Strehblow, H. H., *"X-Ray Photoelectron Spectroscopic Examinations of Electrochemically Formed Passive Layers on Ni-Cr-Alloys"* Journal of Electrochemical Society, Vol 144, No.4, April1997, pp.1231-1243.

51. Lorang, G., Jallerat, N., Quang, K. Vu., and langeron, J.-P., "*AES depth profiling of passive overlayers formed on nickel alloy"* Journal of Surface and Interface Analysis, Vol. 16, No. 1-12, July 1990, pp 325-330.

52. Lillard, R.S., Jurinski, M.P., Scully, J.R., *"Crevice Corrosion of alloy 625 in Chlorinated ASTM Artificial Ocean Water"*, Corrosion, Vol. 50, No. 4, April 1994, pp. 251-265.

53. Amy C. Lloyd, James J. Noël, Stewart McIntyre, and David W. Shoesmith., "*Cr, Mo and W Alloying Additions in Ni and their Effect onPpassivity"*, Electrochimica Acta, Vol. 49, January 2004, pp. 3015–3027.

54. Vickerman, J. C., Brown, A., and Reed, N. M, *"Secondary Ion Mass Spectrometry: Priciples and Applications"*, Oxford University Press, 1989, pp. 1-10.

55. Cahoon, J. R., Bassim, M. N., and Gennelle Oman, E., *"Acoustic Emission during Corrosion"* Canadian Metallurgical Quarterly, Vol. 25, No.1, 1986, pp. 73-77.

56. Sedriks, A. John., "*Corrosion of Stainless Steel"*, Nnew York, John Wiley and Sons, Inc. 1996.

57. Moriya, M., and Ives, M. B.,*"Surface Segregation of Molybdenum during Pitting Corrosion of Nickel-Molybdenum Alloy",* Corrosion Science, Vol. 40, 1984, pp. 105-109.

58. Moriya, M., and Ives, M. B., *"The Structure of Anodic Films Formed on Nickel and Nickel-13 w/o Molybdenum Alloy in pH 2.8 Sodium Sulfate Solution"*, Corrosion Science Vol. 40, 1984, pp. 62-72.

59. Qvarfort, R., *"Some Observations Regarding the Influence of Molybdenum on the Pitting Corrosion Resistance of Stainless Steel"*, Corrosion Science, Vol. 40, No. 2-3, February 1998, pp. 215-223.

60. Lemaitre, C., Moneim, A.A., Djoudjou, R., Baroux, B., and Beranger, G., *"A statistical Study of the Role of Molybdenum in the Pitting Resistance of Stainless Steels"*, Corrosion Science, Vol. 34, No. 11, November 1993, pp. 1913-22.

61. Wanklyn, J. N., *"The Role of Molybdenum in the Crevice Corrosion of Stainless Steels"* Corrosion Science, Vol. 21, No. 3, 1981, pp. 211-225.

62. Galvele, J. R., Lumsden, J.B., and Staehle, R.W., *"Effect of Molybdenum on the Pitting Potential of High Purity 18%Cr Ferritic Stainless Steel"*, Journal of the Electrochemical Society, Vol. 125, No. 8, August 1978, pp. 1204-1208.

63. Bastidas, J. M., Torres, C. L., Cano, E., and Polo, J. L., *"Influence of Molybdenum on Passivation of Polarized Stainless Steels in a Chloride Environment"* , Corrosion Science, Vol. 44, No. 3, 2002, pp. 625-633.

64. Oldfield, J.W., "*Corrosion Initiation and Propagation of Nickel-Base Alloys in Severe Seawater Applications",* 266 Houston, TX., NACE International Corrosion, 1995.

65. Qian, Y., and Cahoon, J. R.,*"Crack Initiation Mechanisms for Corrosion Fatigue of Austenitic stainless Steel",* Corrosion Science, Vol. 53, 1997, pp. 129-135.

66. Cahoon, J. R., and Bandy, R., "*Effect of Composition on the Electrochemical Behavior of Austenitic Stainless Steel in Ringer's Solution",* Corrosion Science, Vol. 33, June 1977, pp. 204-208.

67. Marcus, P., Maurice, V., and Schutze, M., "*Corrosion and Environmental Degradation".* New York, Wiley-VCH, 2000, Chapter 3.

68. Sadough, A., Audouard, J. P., and Marcus, P., *"The Role of Nitrogen in the Passivity of Austenitic Stainless Steel",* Corrosion science, Vol 36, No 11, 1994, pp.1825-1834.

69. Bandy, R., and Cahoon, J. R., "*Auger Electron Spectroscopic Studies on Oxide Film of Some Austenitic Stainless Steels",* National Association of Corrosion Engineers, Vol. 38, June 1982, pp. 299-305.

70. Vickerman, J. C., Brown, A., and Reed, N. M., "*Secondary Ion Mass Spectrometry: Principles and Applications",* Oxford University Press,1989.